# Calretinin neurons in the primate prefrontal cortex

**Sedmak, Dora**

**UNIVERSITY OF ZAGREB**
**SCHOOL OF MEDICINE**

**Dora Sedmak**

# Calretinin neurons in the primate prefrontal cortex

**DISSERTATION**


**Zagreb, 2019**

This dissertation was made at the Department of Anatomy and Clinical Anatomy and Croatian Institute for Brain Research University of Zagreb School of Medicine and INSERM, Institut de Neurosciences des Systèmes, Aix Marseille Université.

Mentors: Zdravko Petanjek, MD, PhD
Professor of Anatomy and Neuroscience,
University of Zagreb School of Medicine

Monique Esclapez, PhD, DR1
Research Director INSERM,
Aix-Marseille University Medical School,
Institute de Neurosciences de la Timone

This work was supported by the Croatian Science Foundation grant number HRZZ5943 "*Microcircuitry of higher cognitive functions"*, PI Zdravko Petanjek, MD, PhD.

Contents

Abbreviations

CR calretinin

PV parvalbumin

CB calbindin

SOM somatostatin

NeuN neuronal nuclear protein

PFC prefrontal cortex

BA Brodmann area

OM orbito-medial

DL dorso-lateral

GABA gamma-aminobutyric acid

PBS phosphate-buffered saline

KPBS potassium-phosphate-buffered saline

VGAT vesicular GABA transporter

GAD glutamic acid decarboxylase

NGS normal goat serum

NHS normal horse serum

# 1. Introduction

The question of superior human abilities remains one of the main interests in evolutionary biology. The cerebral cortex is believed to be the primary location of human thought, ideas and feelings. In mice, monkeys and humans, its basic building blocks (neurons) are the same, and it has a similar six-layer structure. The most obvious difference in the mammalian order is the variability in size. As the brain size is determined by body size, experts have tried to link brain size beyond the mass related to body size, e.g. Jerison's 'encephalization' quotient (EQ) to the increase in cognitive capacities (Jerison, 1985; Lefebvre, 2012). Although the general size is not the answer to why humans possess superior cognition it shed the light onto possible selective expansion within the cortex. Since the prefrontal cortex is the origin of all of the cognition making us human its size and structure is still in the center of evolutionary neuroscience.

## 1.1 Prefrontal cortex

The prefrontal cortex (PFC) is the cerebral cortex which covers the front part of the frontal lobe and is divided into medial, orbital, dorsolateral and ventrolateral cortex. The prefrontal cortex contains the Brodmann areas 8, 9, 10, 11, 12, 13, 14, 24, 25, 32, 44, 45, 46, and 47. Prefrontal cortex is defined as the part of the cerebral cortex that receives reciprocal projections from the mediodorsal nucleus of the thalamus (Barbas, 2015; Fuster, 1980; Uylings and van Eden, 1990). The ontogenetic development of the prefrontal cortex reflects its phylogeny. Orbitomedial areas mature earlier than lateral ones. Furthermore, it seems likely that most mammals have a gross subdivision of the frontal areas into an "orbital-like" region involved especially with the control of socio-affective behaviors, a "dorsolateral-like" area involved especially in working memory, and an "anterior cingulate-like" area concerned primarily with visceromotor behaviors and some forms of motor sequencing. According to not only functional but also cytoarchitectonic criteria that include granular cortex and magnocellular layer IIIC, the dorsolateral and ventrolateral prefrontal cortex have no clear correlate in the rodent brain (Uylings et al., 2003; Uylings and van Eden, 1990)

The primate dorsolateral prefrontal cortex (dlPFC) has long been implicated in higher cognitive functions, such as switching attention, working memory, maintaining abstract rules, and inhibiting inappropriate responses. As much as intelligence is manifested and tested by performance of logical goal-directed tasks and sequences of behavior and language, it is reasonable to assume that the dorsolateral prefrontal cortex is an important component of the neural substrate of intelligence. Indeed, it has been argued on the basis of empirical data from the human, that this cortex is the foundation of general intelligence, as measured by

Spearman (Duncan et al., 1996). The medial prefrontal cortex (mPFC) is involved in feedback categorization, performance monitoring, and task monitoring, and may contribute to the reinforcement learning that would affect decision-making processes in the lateral prefrontal cortex (lPFC). The medial prefrontal cortex also is a premotor area that projects to the rostral ventrolateral medulla, a major source of cardiovascular sympatho-excitatory neurons involved in emotional responses (Etkin et al., 2011).

Areas of interest for this study were hierarchically and structurally different parts of the prefrontal cortex, all involved in the higher cognitive functions. Area 9 is located in the dorsolateral prefrontal cortex, extending medially to the paracingulate sulcus of humans and the cingulate sulcus of macaque monkeys (Petrides and Pandya, 1999; Rajkowska and Goldman-Rakic, 1995b). This cortical area is expanded in anthropoids (i.e. monkeys, apes, and humans) with no obvious homologue in other mammals (Goldman-Rakic, 1991). For this study, the part of area 9 sampled was located on the dorsal portion of the superior frontal gyrus in humans, and corresponded to area 9 in macaque monkeys as designated by Paxinos et al. (Paxinos et al., 2000). Based on functional imaging studies of humans, this area has been shown to be involved in several cognitive processes, including inductive reasoning and theory of mind (ToM) (Goel and Grafman, 1995) as well as the retrieval phase of episodic and working memory (Marklund et al., 2007).

Area 32 is in human defined as the portion of the paralimbic cortex around limbic areas surrounding the genu of the corpus callosum (Carmichael and Price, 1994; Öngür et al., 2003). Their function has been implicated in theory of mind, the ability to infer the mental states of others (Gallagher and Frith, 2003). Macaques do not possess a strict homologue to the portion of area 32 that is activated in human theory of mind studies (i.e. anterior cingulate area 32) (Öngür et al., 2003). However, because we chose this area to investigate the evolution of this unique human behavioral capacity, for comparative purposes, we were limited to the most similar anatomical territory of the medial prefrontal cortex of macaques, defined as prelimbic cortex (i.e. prelimbic area 32) (Carmichael and Price, 1994; Öngür et al., 2003; Petrides and Pandya, 1999).

Area 24 occupies most of the anterior cingulate gyrus in an arc around the genu of the corpus callosum (Carmichael and Price, 1994; Öngür et al., 2003; Vogt et al., 1987, 1995). It is characterized by the Von Economo neurons that are widely connected to neurons in many other parts of the brain (Fajardo et al., 2008). Anterior cingulate cortex has an important role in emotional self-control as well as focused problem-solving, error recognition, and adaptive response to changing conditions, functions are central to intelligent behavior (Allman et al., 2006).

## 1.2 Is human brain different from primate brain?

The first step in the evolutionary ascent of the human cerebral cortex is its enlargement, especially of the prefrontal cortex, the cortical region related to some of remarkable cognitive abilities such as personality expression, planning, and decision making (Passingham and Smaers, 2014; Roth and Dicke, 2012). In absolute terms, the human frontal lobe is three times larger than that of our closest living relatives, the great apes, but the significance of this fact is unclear. Comparative studies showed that the gray matter of the human prefrontal cortex has the expected volume for a primate with the same brain size (Barton and Venditti, 2013; Herculano-Houzel, 2009; Herculano-houzel et al., 2007; Semendeferi et al., 2002; Smaers et al., 2011; Uylings and van Eden, 1990). The debate on the size of prefrontal cortex regarding the grey matter and the white matter is still ongoing. There are studies that agree on larger-than-expected prefrontal cortex in humans (Deacon, 1997; Passingham and Smaers, 2014; Schoenemann, 2006 Uylings and van Eden, 1990), whereas others claim that the human prefrontal cortex does not diverge from the allometric rule of great apes (Barton and Venditti, 2013; Donahue et al., 2018; Herculano-Houzel, 2012).

The general size studies cannot comprehend the possible primate – human differences (Gabi et al., 2016; Semendeferi et al., 2002) so the focus of research was moved onto the number of neurons – first in the whole cerebrum, then in the specific areas (Azevedo et al., 2009; Gabi et al., 2016). Greater cortical size in humans compared with other primates does not reflect an increased relative number of cortical neurons and the ratios between glial cells and neurons in the human brain structures are similar to those found in other primates, and their numbers of cells match those expected for a primate of human proportions (Azevedo et al., 2009). The prefrontal region of both human and nonhuman primates holds about 8% of cortical neurons, with no clear difference across humans and other primates in the distribution of cortical neurons or white matter cells along the anteroposterior axis (Gabi et al., 2016).

The cognitive abilities attributed to a frontal advantage may be due to differences in individual cortical areas and to a richer interconnectivity, none of which required an increase in the overall relative size of the frontal lobe during hominid evolution (Semendeferi et al., 2002; Teffer and Semendeferi, 2012).

## 1.3 Cortical microcircuits

An explanation of the cellular mechanism for the enormous cortical expansion in surface without a comparable increase in thickness has been offered by the radial unit hypothesis According to this model, an increase in the number of neural stem cells by symmetrical divisions before the onset of neurogenesis would result in an exponential increase in the number of founder cells that give rise to radial cortical columns (Rakic, 2009). Differences in the duration of neurogenesis, which increases more rapidly with brain size for the cerebral cortex than for subcortical areas, lead to a systematic increase in the ratio of the cortical to subcortical regions (Charvet and Finlay, 2012). It appears that the evolution of the human brain was accompanied by modifications in local circuitry and interconnectivity of selected parts of the brain (Schoenemann, 2006; Striedter, 2005).

A brain microcircuit has been defined as the organization of nerve cells into specific patterns that carry out the information processing characteristic of a given brain region (Shepherd, 2004).The cerebral cortex with each microcircuit is made of the main cellular elements: glutamatergic pyramidal cells and inhibitory GABAergic interneurons. Pyramidal cells represent about 80% of the neurons in the cortex and specialize in transmitting information between different cortical areas and to other regions of the brain. GABAergic interneurons, on the other hand, control and orchestrate the activity of pyramidal cells.

Pyramidal cells and interneurons in the cerebral cortex are organized along two main dimensions – laminar and columnar. The first axis divides the cortex into a variable number of layers depending on the cortical area. Neurons within the same cortical layer share important features, including general patterns of connectivity (Molyneaux et al., 2007). The second axis reflects the vertical organization of neuronal circuits within a column of cortical tissue. Neurons within a given column are stereotypically interconnected in the radial dimension, share extrinsic connectivity, and function as the basic units underlying cortical operations. The idea was that neurons, glia, and their connections form a vertical system which unites the cells of each minicolumn into a coordinated functional unit (Mountcastle, 1997). Evolutionary changes in connectivity of cortico-cortical network are speculated be connected to changes in the number and width of minicolumns (Buxhoeveden, 2012). In this context, the smallest unit of cortical anatomy is the minicolumn, defined as a narrow radial array of single neurons. Fundamentally uniform architecture of cortical minicolumn, with the number of neurons within (defined as the number of neurons within a strip of tissue 30-μm wide and 25-μm thick from pial surface to white matter) is nearly invariant at 110 neurons across cytoarchitectonic areas and species is indeed suggesting that functional differences are principally a result of wiring (Rockel et al., 1980). Analysis of the morphometric variability of minicolumns among macaque monkeys, humans, and chimpanzees confirmed that there

are differences in minicolumn width across species, but the core column space (i.e., the space that contains the majority of neurons and fibers and is distinguishable from the adjacent, cell-poor neuropil space) remains relatively invariant, suggesting that this subcomponent of the cortical minicolumn may be evolutionary conserved (Opris and Casanova, 2014; Raghanti et al., 2010).

### 1.4 Interneurons

It was already Ramon y Cajal who suggested that extraordinary human mental abilities are closely related to the increase in the number and diversity of cortical interneurons and not the pyramidal cells.

Comparative studies furthermore indicate that variability in subtle subcomponents of the columnar organization in human and non-human primates, such as the composition of the interneuron subtypes, are a primary source of interspecies differences in minicolumn (Raghanti et al., 2010; Sherwood et al., 2012). Humans deviate from other primates in having a greater width of minicolumns in specific cortical areas, especially in the prefrontal cortex, owing to constituents of the peripheral neuropil space (Casanova et al., 2003; Teffer and Semendeferi, 2012). These findings support the idea that human evolution, after the split from the common ancestor with chimpanzees, was accompanied by discrete modifications in local circuitry and interconnectivity of selected parts of the brain.

Interneurons come into place as intra- and inter-columnar processing supervisors of this highly complex cortical network comprised from minicolumns (Buzsaki and Draguhn, 2004; DeFelipe et al.; Hendry et al., 1987; Petilla Interneuron Nomenclature Group et al., 2008; Raghanti et al., 2010). These neurons are extremely heterogeneous and can be divided into subpopulations based on morphology, electrophysiology, synaptic connectivity and gene expression (DeFelipe et al., 2013; Markram et al., 2004; Petilla Interneuron Nomenclature Group et al., 2008). As majority of cortical GABAergic neurons only branches inside the cortex they are defined as local circuit neurons (interneurons) (Petilla Interneuron Nomenclature Group et al., 2008). In primates, the three calcium-binding proteins are expressed in largely non-overlapping subpopulations of cortical interneurons (DeFelipe et al., 2013; Gabbott et al., 1997 a,1997b; Gabbott and Bacon, 1996a, 1996b; Hendry et al., 1987; Zaitsev et al., 2005). More than 80% of all cortical GABAergic neurons express one of three calcium-binding proteins (parvalbumin, calbindin and calretinin) making these molecules a suitable marker for identification of different main cortical GABAergic neuron subpopulations (Barinka et al., 2015; Rudy et al., 2011; Sherwood et al., 2010; Toledo-Rodriguez et al., 2004).

Different classes of interneurons interact with pyramidal cells to modulate cortical circuit processing, with calbindin (CB) and calretinin (CR) neurons involved mostly in intra-columnar communication, and parvalbumin (PV) interneurons involved in trans-columnar signaling (Caputi et al., 2009; Kawaguchi and Kubota, 1997; Raghanti et al., 2008; Tremblay et al., 2016). Their targets are mainly principal neuron compartments but they can also target other cortical GABAergic neurons (Caputi et al., 2009).

Cortical parvalbumin expressing GABAergic neurons are predominantly multipolar and include large basket and chandelier cells (Conde et al., 1994; Gabbott and Bacon, 1997 a,1997b). The large basket cells have long-range axons that extend horizontally, targeting the perikaryon of pyramidal cells of different minicolumns (DeFelipe, 1997; Lund and Lewis, 1993; Somogyi et al., 1998). Chandelier cells, which are immunoreactive for parvalbumin, also provide lateral inhibition, making synaptic connections with the axon initial segments of pyramidal cells (Hu et al., 2014; Markram et al., 2004; Wang et al., 2018). These various morphological classes of parvalbumin cells regulate the rhythmic oscillations of pyramidal cell populations. Cortical calretinin interneurons have variable morphology and include bipolar, double bouquet, and Cajal-Retzius cells (DeFelipe, 1997; Rio and Defelipe, 1996). Bipolar and double bouquet calretinin expressing cells have axonal arbors that extend vertically, mostly targeting the dendrites of pyramidal cells in different layers of the cortex within a narrow column (DeFelipe, 1997; Gabbott et al., 1997 a,1997b; Rio and Defelipe, 1996). The characteristic phenotype of calbindin interneurons in primate cortex is the double bouquet cell (Gabbott and Bacon, 1997 a,1997b; Kawaguchi and Kubota, 1997). As with the calretinin double bouquet cells, calbindin double bouquet axons provide vertical inhibition to pyramidal cells within the minicolumn (Casanova et al., 2003; Favorov and Kelly; Opris and Casanova, 2014). In most non-primates except carnivores, calbindin interneurons are mainly multipolar and bitufted (Yáñez et al., 2005). Both calretinin and calbindin interneurons exhibit characteristics of non-fast-spiking cells in nonhuman primate cortex, with longer spike frequency and spike adaptation, but without distinctive differences between the two subpopulations (Zaitsev et al., 2005).

Since GABAergic network acts as intrinsic modulator of cortical output (DeFelipe et al., 2013) significant changes appear in organization and laminar distribution of GABAergic neurons. There are numerous studies analyzing laminar distribution and density of these neurons in mammals. However due to different methodology and lack of systematic approach these studies cannot comprehend interspecies differences (Gabbott et al., 1997 a,1997b; Gabbott and Bacon, 1996a, 1996b; Hof et al., 1999; Sherwood et al., 2010; Zaitsev et al., 2005).

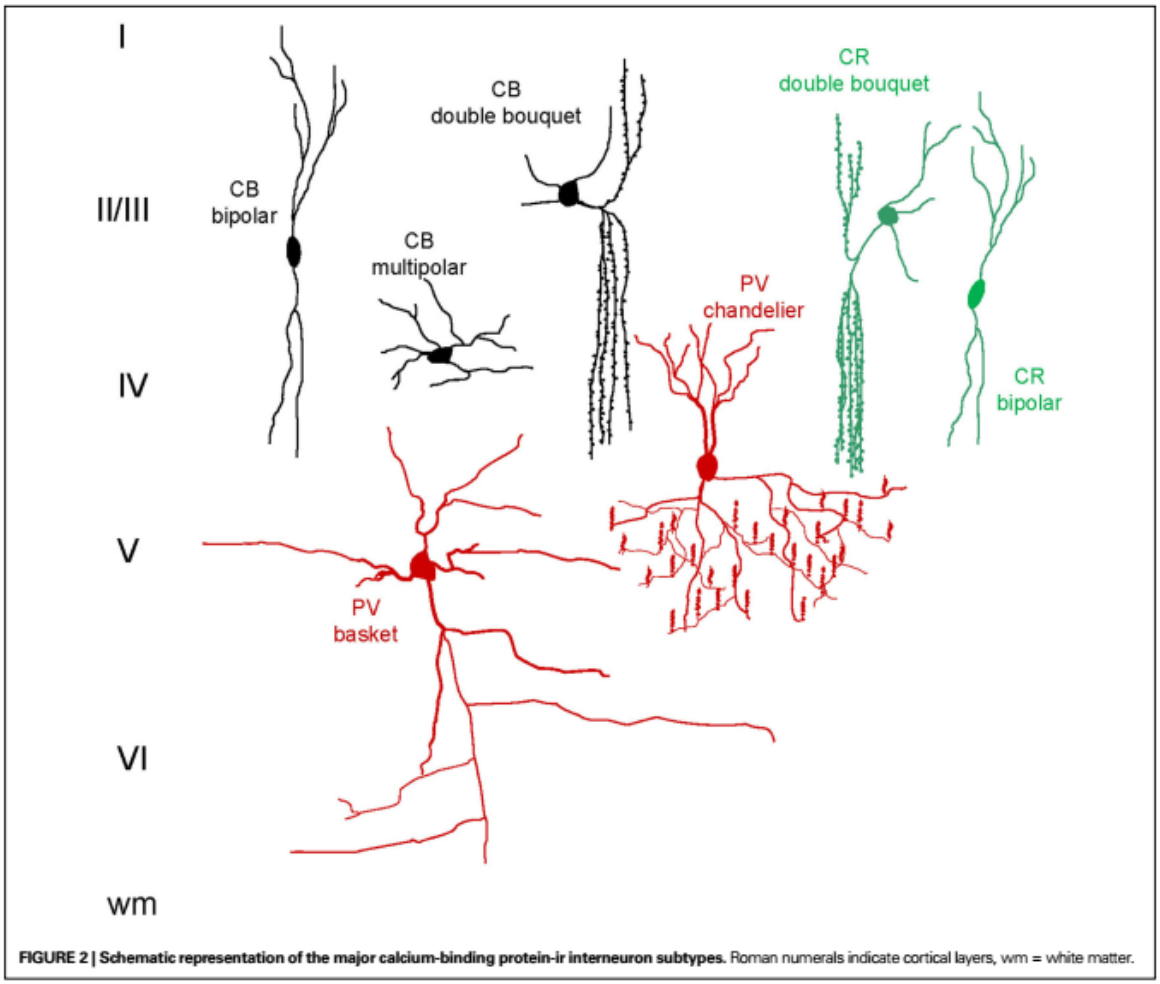


**Figure 1.1** Representative drawing of three major calcium binding interneuron subtypes of the cerebral cortex and their most common morphology. CB – calbindin, CR – calretinin, PV – parvalbumin.

*Copyright © 2010 Raghanti, Spocter, Butti,Hof and Sherwood.* (Raghanti et al., 2010)

Through mammalian evolution the number of GABAergic interneurons increases more than principal neurons. In the primate neocortex they exceed 20% of all cortical neurons whereas in rodents cortical interneurons represent around 15% of total neuron number (Gabbott et al., 1997 a,1997b; Gabbott and Bacon, 1996a, 1996b; Hendry et al., 1987; Kawaguchi and Kubota, 1997; Rio and Defelipe, 1996; Tremblay et al., 2016).

This large increase in proportion of GABAergic neurons is not affecting all subpopulations synchronously and is due principally to an increase in number of calretinin neurons (Džaja et al., 2014; Hladnik et al., 2014; Rio and Defelipe, 1996). Other two main subpopulations, (i.e. parvalbumin and calbindin/somatostatin), do not show such a robust increase in proportion.

## 1.5 Calretinin

Del Rio and DeFelipe (1996) have estimated that GABAergic neurons in layers II and III of the human associative temporal cortex represent around 1/3 of the total neuron number, and almost half of them express calretinin. Calretinin positive neurons were present in greatest density in deep layer I and layer II, calbindin immunoreactive cells were most dense in layer II and superficial part of layer III, and parvalbumin containing neurons were present in greatest density in the middle cortical layers (Rio and Defelipe, 1996). In addition, the relative density of calretinin labeled neurons was approximately twice that of the calbindin and parvalbumin positive neurons. However, within each group of labeled neurons, their laminar distribution and relative density did not differ substantially across regions of the prefrontal cortex (Conde et al., 1994).

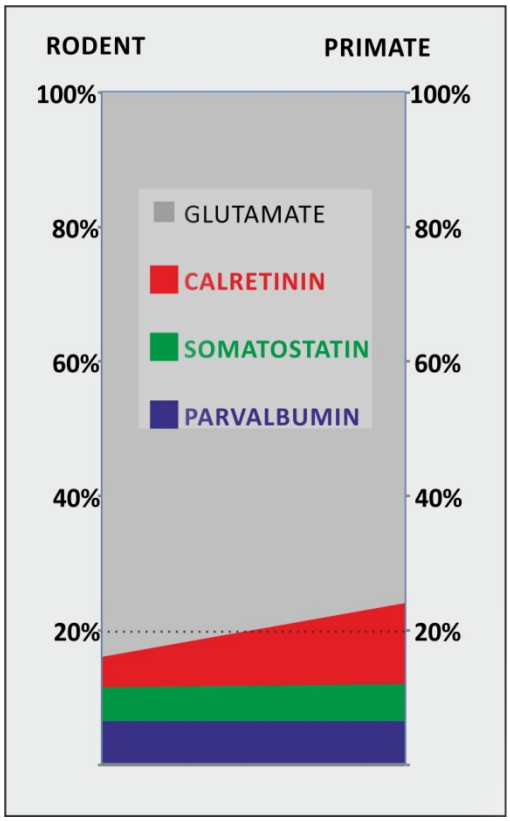


**Figure 1.2** There is 50% increase in cortical GABAergic neurons from rodents (≈16%) to primates (≈24%), which can be attributed to threefold increase in number of calretinin neurons (shown in red; from ≈4% in rodents to ≈12% of the total neuron number in primates).

(Hladnik et al., 2014)

Most of the studies suggest that in the human, where higher order associative areas comprise at least 50% of the neocortical surface, calretinin becomes the dominant population representing almost 50% of cortical GABAergic neurons (Barinka et al., 2010a; Conde et al.,

1994; Gabbott et al., 1997 a,1997b; Tremblay et al., 2016; Zaitsev et al., 2005). The substantial difference in methodological approach makes these studies almost incomparable. There is also empirical evidence that there is much greater phylogenetic variation in the number of neurons underneath 1mm$^2$ of cortex than was previously thought (Herculano-Houzel et al., 2008).

A study by Ma et al. (2013) suggested, that in the human and monkey calretinin neurons are two times more numerous in the frontal and parietal cortical areas compared to the rest of the neocortex (Ma et al., 2013). Our previous study, comparing orbital frontal cortex in the rat with complementary area 14 in the rhesus monkey, showed a four to five fold increase in the proportion of calretinin neurons, mostly in upper cortical layers. In layers II/III of the human orbito-frontal cortex calretinin neurons cover more than 20% of the total number of neurons (Džaja, 2015), that is a 8 times more than in rat.

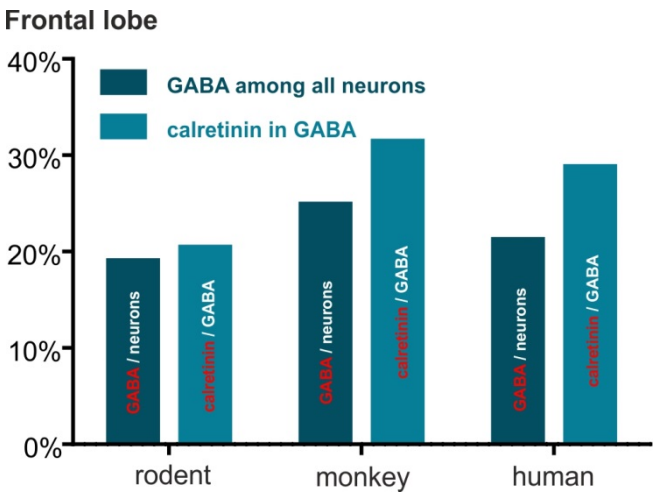


**Figure 1.3** The overview of literature data on GABAergic cells and calretinin neurons percentage. Data extrapolated from following articles: Džaja et al., 2014; Gabbott and Bacon, 1996a, 1996b, 1997; Kawaguchi and Kubota, 1997; Melchitzky et al., 2005; Uematsu et al., 2008; Zaitsev et al., 2005.

All these data indicate that during evolution there is an increase in calretinin proportion in the upper cortical layers of higher associative regions. Nevertheless the relation between exponentially increased number of calretinin neurons within human associative areas and tremendous increase in cognitive capability in humans is still hypothetical (Forbes and Grafman, 2010). We presume that disproportional increase in the number of calretinin neurons is the basis for significant changes in neuronal network organization and substantially different processing modes (Burkhalter, 2008).

### 1.5.1 Molecular profile of calretinin neurons in the primate brain

With raising numbers of calretinin neurons and increased efficiency in cortical networks the calretinin neuron neurotransmitter profile could be changed. In rodents, almost 100 % of calretinin neurons in the neocortex seem to use GABA as a neurotransmitter (Gonchar et al., 2007; Gonchar and Burkhalter, 1997; Uematsu et al., 2008). On the other hand, in monkey and human neocortex, about 25 % of calretinin neurons were found not to express GABA (Melchitzky et al., 2005; Rio and Defelipe, 1996). So the GABAergic profile of calretinin neurons although often presumed by the literature was not directly confirmed in the primate neocortex. This question was addressed in this study where we confirmed the GABAergic profile showing that all these neurons in the primate brain express mRNAs for the vesicular GABA transporter (VGAT) and one of the synthesizing enzyme for GABA, the glutamic acid decarboxylase 67 (GAD67) as well as in study by Rocco et al. where they showed that calretinin neuron *boutons* express GAD67 (Rocco et al., 2016).

### 1.5.2 Laminar distribution and interspecies studies

Calretinin neurons in neocortex are mostly located in cortical layers II and III, both in rodents and primates. The density of calretinin neurons decreases with depth in neocortex and they are rare in infragranular layers, when compared to the supragranular ones. The calretinin neurons most commonly have bipolar or bitufted vertically oriented somatodendritic morphology, with fusiform or oval perikaryon (Barinka et al., 2010a; Conde et al., 1994; Gabbott et al., 1997 a,1997b; Gabbott and Bacon, 1996a, 1996b; Gonchar et al., 2007; Gonchar and Burkhalter, 1997; Rogers et al., 1990; Zaitsev et al., 2005). Their dendrites often extend to layer I superficially and to infragranular layers deeply. On the contrary, the dendritic tree is quite narrow in horizontal direction. Besides these bipolar neurons, other morphological types of calretinin neurons, typically multipolar and horizontally oriented neurons, were consistently found in the neocortex in the majority of the above cited studies. The distribution of calretinin neurons is similar but not absolutely homogenous among various neocortical areas.

The idea that there is more calretinin cells in primates is not new but it was studied with different methodologies so the results are not directly comparable. In human general pattern of calretinin immunoreactivity was found to be similar, but the density of calretinin neurons was significantly lower in the frontal than in the temporal, occipital and parietal association cortices (Barinka et al., 2010b; Hof et al., 1993a). Gabbot and Bacon in 1996 and 1997 did a comparative study on medial prefrontal cortex in rat, monkey and human areas 24, 25 and 32. They confirmed the resemblance in neocortical calretinin neuron morphology between

species, but they found a significant difference in proportion of neurons expressing calretinin between rat and primates. In medial prefrontal cortex, the calretinin neurons constituted 4% of the total neuronal population in the rat, but 11% in the monkey and 8% in the human, what is similar to other studies performed (Conde et al., 1994; Gabbott et al., 1997 a,1997b; Gabbott and Bacon, 1996a, 1996b; Gonchar et al., 2010; Rio and Defelipe, 1996). Altogether, the calretinin neurons are significantly more numerous in primate frontal cortex when compared to rodents, both absolutely and relatively to the other GABA interneurons.

Since the prefrontal cortex is the location of human specific cognitive functions such as decision making, planning and emotional response (Barbas, 2000; Gallagher and Frith, 2003; Goel and Grafman, 1995; Goldman-Rakic, 1991; Hoshi, 2006) the idea is that if calretinin neurons do have a role in more efficient neuronal networks they should be more numerous in areas of high demand. The study comparing rodents to primates tested this hypothesis in orbitofrontal area 14 since it is the only part of prefrontal cortex with clear correlate in rodent brain. The results showed a major increase in calretinin population in primate brains. This was the main reason to keep trying to identify their role in primate brain (Džaja, 2015; Džaja et al., 2014).

### 1.6 Calretinin neuron lifespan changes and pathology

Executive abilities emerge from cortico-cortical interactions between laminar prefrontal cortical microcircuits and their disruption was linked to a broad spectrum of neurologic and psychiatric disorders such as depression, autism, schizophrenia, Alzheimer's disease and drug addiction (Barinka et al., 2010b; Beasley et al., 2002; Brisch et al., 2015; Hof et al., 1993b; Luscher et al., 2010; Rajkowska et al., 2007; Takano, 2015).

The development of interneuron markers is protracted in the human dorsolateral prefrontal cortex, extending well into the toddlerhood and beyond the teenage years. Calretinin mRNA is down-regulated in the first few years of postnatal life, with a significant decrease in expression between the neonatal period and infancy, and also between infancy and all later developmental periods (Fung et al., 2010).The immunohistochemical analysis revealed a similar trend toward a decrease number of calretinin positive neurons in old brains when compared with the young (Bu et al., 2003).

Majority of neurological and psychiatric disorders with cortical pathology involve some level of disorganization in GABAergic network (Ansen-Wilson and Lipinski, 2017; Friocourt and Parnavelas, 2011; Marín, 2012). Some disorders can only be found in humans, such as depression ,schizophrenia (Benes and Berretta, 2001; Brisch et al., 2015; Cotter et al., 2002; Eyles et al., 2002; Luscher et al., 2010; Rajkowska et al., 2007) and autism (Chahrour and

Zoghbi, 2007; Takano, 2015), and in others, such as epilepsy, symptomatology is more complex in humans (Barinka et al., 2010b; Kuchukhidze et al., 2015).

There were many studies trying to link the number of certain GABAergic neuron population to psychiatric disorders. While they showed the change in calbindin and parvalbumin neuron numbers, the number of calretinin cells remained unaffected (Brisch et al., 2015; Cotter et al., 2002; Hof et al., 1993a; Lewis et al., 2005; Luscher et al., 2010; Rajkowska et al., 2007). Their number were shown to increase in focal cortical dysplasia or other drug resistant forms of epilepsy (Barinka et al., 2010b).

In the prefrontal cortex of patients with schizophrenia studies consistently showed decreased numbers of calbindin interneurons while calretinin interneuron density remains preserved (Beasley et al., 2002; Cotter et al., 2002; Eyles et al., 2002; Woo et al., 1998).

Alzheimer's disease is also associated with a selective decrease of cortical calbindin neurons in humans (Beasley et al., 2002; Ferrer et al., 1993). It has also been reported in the canine expression of dementia of the Alzheimer's type (Pugliese et al., 2004) while both, parvalbumin and calretinin neuronal subpopulations are spared (Ferrer et al., 1993; Hof et al., 1993b; Pugliese et al., 2004).

There are studies indicating that increased or unchanged number of calretinin or calbindin neurons in specific disorders may have a protective role (Hattori et al., 2017; Hof et al., 1993a; Kuchukhidze et al., 2015). Therefore, it is important to understand human-specific features in organization and development of cortical GABAergic network, especially for calretinin neuron population. Whether they are resistant to general disorders or have a protective role or their role is crucial for cortical microcircuits work has still not been answered.

The hypothesis of this research is that different higher order prefrontal cortical areas will differ in proportion of calretinin neurons inside and between primates. Therefore, the aim is to determine the proportion, density and laminar distribution in areas 9, 32 and 24 in monkey and human brain and to identify the molecular profile of calretinin neurons in the primate brain. For quantitative analysis, stereological approach was used and qualitative findings were based on immunohistochemistry or immunohistofluorescence and *RNAscope* methods.

## 2. Hypothesis

There are differences in proportion and laminar distribution of calretinin neurons between higher associative areas of prefrontal cortex in monkey and humans that are principally related with molecularly specific subpopulation of GABAergic neurons.

## 3. General and specific aims

### 3.1 General aim

The aim of this study is to determine the proportion, laminar distribution and neurotransmitter phenotype of calretinin expressing neurons in mesocortical (area 24) and neocortical (area 9, area 32) associative frontal regions in *Maccaca mulatta* and *Homo sapiens*.

### 3.2 Specific aims

Specific aims for this study are:

I. To determine the density and proportion of calretinin neurons in all cortical layers in areas 9, 24 and 32 in the prefrontal cortex of three human and three monkey brains.

II. To determine if cortical calretinin neurons have GABAergic neurotransmitter phenotype using co-labeling with in-situ hybridization.

III. To determine the proportion of each main GABAergic neuron subpopulation and level of overlap between them (calretinin, calbindin/somatostatin and parvalbumin) in areas 9, 24 and 32, using double labeling.

# 4. Materials and methods

## 4.1 Histological samples

Three postmortem adult human and three adult macaque monkey brain sections were used in this study.

### 4.1.1 Human tissue samples

Postmortem human brain tissue used in this study is a part of Zagreb Neuroembryological collection and includes 3 adult subjects (30-45 years old) with 6 hours postmortem delay (PMD, i.e. interval between death and fixation of the tissue). The tissue was collected from University of Zagreb Department of Forensic Medicine during routine autopsies. Medical records revealed no previous neurological and psychiatric history and neuropathological findings were unremarkable. All subjects died without preagonal state so the PMD represents the interval for neuron death. The tissue was obtained with the approval of the Ethics Committee of Zagreb University School of Medicine, and is currently regulated by Ethics Committee approval number 380-59-10106-14-55/152 from July 1, 2014.

The information on the subject's identity and history is stored in hidden records and the brain tissue is given a code name indicating only the age of the specimen. Specimens used in this study are:

ČO 384 (male, 46 years, cause of death: sudden cardiac arrest, PMD 6 hours)

ČO 386 (male, 37 years, cause of death: sudden cardiac arrest, PMD 6 hours)

ČO 387 (male, 44 years, cause of death: methadone/benzodiazepine overdose, PMD 6 hours)

Whole brains were immersion-fixed using 4% paraformaldehyde in 0.1M phosphate buffer (pH 7.4). Subsequently, tissue blocks were cut following Talairach coordinates (Talairach and Szikla, 1980). Following a standard procedure the tissue blocs were then dehydrated in a graded series of sucrose (10%, 20%, and 30%) and afterwards cryoprotected, frozen and stored at -80°C until further processing. Serial sections of blocks containing frontal mesocortical Brodmann areas 24 and 32, and neocortical area 9, were cut at 60μm on cryostat and stored in cryoprotective solution at –20°C until histological processing.

### 4.1.2 Monkey tissue samples

Postmortem monkey brain tissue used in this study is a part of Dr. Esclapez Brain Collection, INS, INSERM, Marseille, France. This study includes brain tissue from 3 adult *Macaca mulatta* monkeys aged 10-12 years that were purpose bred and maintained for experimental and other scientific purposes under controlled and standardized conditions with regard to their genealogy, health and care at *Station de Primatology Centre National de la Recherche Scientific* (SdP CNRS). Well documented breeding histories, sanitary backgrounds and individual records containing detailed information is stored for all the animals of the colony. All experimental procedures were in compliance with the National Institutes of Health's Guide for the Care and Use of Laboratory Animals, guidelines of European Communities Council (86/609/EEC) and approved by Zagreb's School of medicine Committee for animal welfare and the *Comité d'éthique en Neurosciences INT-Marseille* (Protocol A2-10-12).

The monkeys were primarily used in electrophysiological studies. Following the end of the original experiments monkeys were deeply anesthetized and perfused transcardially with a fixative solution of 4% paraformaldehyde in 0.12M sodium phosphate buffer (PB), pH 7.4. After perfusion, the brains were removed from the skull, blocks of brains containing the frontal lobes were post-fixed in the same fixative for 2 hours at room temperature, rinsed in PB, cryoprotected in 20% sucrose overnight, frozen on dry ice and sectioned in frontal plane at 40μm with a cryostat (Microm). Serial sections containing the frontal mesocortical Brodmann area's 24 and 32, and neocortical area 9 were rinsed in 0.01M phosphate-buffered saline (PBS), pH 7.4, collected sequentially in tubes containing an ethylene glycol-based cryoprotective solution and stored at −20°C until histological processing.

## 4.2 Histological staining

For both species, a cresyl violet histological staining was performed on every tenth section in order to delineate (determine) the different regions of interests (areas 24, 32 and 9) throughout the rostral-caudal extent of the brain.

### 4.2.1 Single labeling immunohistochemistry

After determining the rostrocaudal and lateral borders of every tenth section (5 in total) and its adjacent sections (5 in total) were processed for immunohistochemical detection of the neuron-specific nuclear protein (NeuN) and of the calcium binding protein calretinin (CR) according to previously described protocol (Esclapez et al., 1994; Hsu and Raine, 1981). Free floating sections were rinsed in PB and pretreated for 30 minutes in 1% $H_20_2$ in order to quench endogenous peroxidases. After being rinsed in PB and in 0.02M potassium phosphate-buffered saline (KPBS, pH 7.2-7.4) they were preincubated in 3% normal goat or horse serum (NGS, NHS, Vector Laboratories) diluted in KPBS containing 0.3% Triton X-100 for 1 hour at room temperature and then incubated overnight at 4°C in the primary antibody (Table 2.1) diluted in KPBS containing 1% NGS or NHS and 0.3 % Triton X-100.

**Table 2.1.** Primary antibodies and dilution used for single labeling immunohistochemistry.

| **Antibody** | Human | Monkey |
|---|---|---|
| Rabbit anti-Calretinin - Polyclonal (Swant, 7699/3H) | | 1:5000 |
| Mouse anti-Calretinin - Monoclonal (Swant, 6B3) | 1:2000 | |
| Mouse anti-NeuN – Monoclonal – clone a60 (Merck, MAB377) | 1:4000 | 1:8000 |

After several rinses in KPBS, sections were incubated for 1 hour at room temperature in biotinylated goat or horse anti-rabbit or anti mouse immunoglobulin G (IgG; Vector Laboratories) diluted 1:200 in KPBS containing 3% NGS or NHS and then for 1 hours at room temperature in an avidin-biotin-peroxidase complex solution prepared in KPBS according to the manufacturer's recommendations (Vectastain ABC kit, Vector Laboratories). The peroxidase activity was visualized using Ni-3.3'-diaminobenzidine tetrahydrochloride (NiDAB, Sigma fast tablets; Sigma) for 15 minutes. Sections were rinsed in KPBS, mounted onto *Superfrost Plus* slides, dehydrated in graded series of alcohol, cleared in xylene and coverslipped with *Permount* or *Histomount* (National Diagnostics). Controls were included in all of experiments. In all cases, no cross-reactivity was detected when the primary antibodies were omitted.

### 4.2.2 Simultaneous immunohistofluorescent detection of calretinin, calbindin, parvalbumin and somatostatin

Double labeling was used to determine the level of overlap between the different GABAergic neuron subpopulations containing calbindin, somatostatin, parvalbumin, and calretinin.

Sections were processed for the simultaneous detection of calretinin with calbindin or parvalbumin or somatostatin, according to previously described protocol (Soussi, 2010). They were rinsed for 30 minutes in PB and 1 hour in KPBS. Sections were then incubated for 1 hour at room temperature in 3% normal donkey serum (NDS, Vector Laboratories) and overnight at 4°C in the following solution of primary antibodies (calretinin-calbindin, calretinin-parvalbumin, calretinin-somatostatin) diluted in KPBS containing 0.3% Triton X-100 and 1% NDS.

**Table 2.2** Primary antibodies and dilution used for double labeling immunohistochemistry.

| **Antibody** | Monkey |
|---|---|
| Mouse anti-Calbindin D-28k - Monoclonal (Swant, 300) | 1:3000 |
| Mouse anti-Parvalbumin – Monoclonal (Swant, 235) | 1:4000 |
| Rabbit anti-Somatostatin - Polyclonal (Penninsula, T-4103) | 1:4000 |
| Rabbit anti-Calretinin – Polyclonal (Swant, 7699/3H) | 1:3000 |
| Mouse anti-Calretinin – Monoclonal (Swant, 6B3) | 1:3000 |

Following several rinses in KPBS, sections were incubated for 1 hour at room temperature in Alexa 488 conjugated donkey anti-rabbit (1:100; Molecular Probes) and Cy3-conjugated donkey anti-mouse antibody (1/100; Jackson ImmunoResearch laboratories) diluted in KPBS. Sections were then mounted on *Superfrost* slides and dried overnight. After this they were rapidly hydrated in double distilled $H_2O$ (2-3 seconds) and cover slipped in *Fluoromount G*.

Overall, the distribution, density and morphology of neurons labeled with monoclonal calretinin antibody did not differ from sections labeled with polyclonal calretinin antibody (see Figure 5.22).

### 4.2.3 Simultaneous detection of VGAT or GAD65/GAD67 mRNAs and calretinin combining fluorescent in situ hybridization (*RNAscope* technology) and immunohistofluorescent methods

Sections were processed for simultaneous detection of vesicular GABA transporter (VGAT) or one of the synthesizing enzyme for GABA, the glutamic acid decarboxylase GAD65 and GAD67 mRNAs in combination with calretinin immunohistofluorescence as previously described (Billwiller et al., 2019). Free floating section were first treated with 3% $H_2O_2$ for 10 minutes, rinsed in PB mounted on *SuperFrost Plus* slides (Fisher Scientific) and air dried at room temperature overnight. They were then processed for fluorescent *RNAscope* in situ hybridization according to manufacter's protocol. Briefly, sections were treated with 100% ethanol incubated in antigen retrieval buffer maintained at a boiling temperature (100°C to 103°C) for 10 minutes, rinsed in PB, and immediately treated with protease III for 30 minutes at 40°C. They were incubated in a solution containing both *RNAscope*® Probe - Hs-SLC32a1-C3 for detection of VGAT mRNA or Mmu-GAD2-C2 for detection of GAD65 mRNA and in a different experiment the *RNAscope*® Probe Hs-GAD1-C2 probe for the detection of GAD67 mRNA. After hybridization, sections were then processed for visualization using the RNA-scope Multiplex Fluorescent reagent Kit v2 (Advanced Cell Diagnostics) and the Tyramide Signal Amplification (TSA™) Plus Cyanine 3 (Perkin Elmer, (Wang et al., 2012).).

After the *RNAscope* assay, sections were rinsed in 0.02M potassium phosphate-buffered saline (KPBS, pH 7.2-7.4) and processed for immunohistofluorescent detection of calretinin. Sections were incubated for 1h at room temperature in 3% normal donkey serum (NDS, Vector Laboratories) and overnight at 4°C in the rabbit polyclonal antiserum directed against calretinin (1:3000) diluted in KPBS containing 0.3% Triton X-100 and 1% NDS. After several rinses in KPBS, the sections were incubated for 2 hours in Alexa 488-conjugated donkey anti-rabbit (1:200; Invitrogen).

Two experiments were performed to simultaneously assess VGAT mRNA and calretinin in monkey and human prefrontal cortex.

## 4.3 Quantitative and qualitative analysis of histological sections

### 4.3.1 Position of areas 9, 32 and 24 and their characterization

In monkey analysis was performed on coronal sections of macaque monkey frontal lobe, where the most rostral sections were positioned 1 cm anterior to corpus callosum and the most caudal ones included the anterior part of genu (Figure 2.1A). Cortical regions of interest were identified based on topological location and distinctive regional cytoarchitecture recognizable on Nissl-stained sections. Cytoarchitectural features were relied upon for identification of cortical regions since there is great individual variation in their gross anatomical location. These sections encompass prefrontal Brodmann areas 9-14, 24, 25, 32 and 46. The area 9 occupies a significant portion of the lateral frontal cortex continuing from area 46 around the *sulcus principalis* and on the medial prefrontal cortex that is composed of Brodmann areas 24 (anterior cingulate cortex or anterior limbic cortex) and area 32 (prelimbic cortex) (Carmichael and Price, 1994; Öngür et al., 2003; Petrides et al., 2011; Petrides and Pandya, 1999; Vogt et al., 1987, 2013).

In human analysis was done on coronal sections of the prefrontal cortex in a block encompassing dorsal part of frontal lobe (Figure 2.1B) above rostrum of corpus callosum according to Von Economo and Talairach (Mai et al., 2008; Talairach and Szikla, 1980; Triarhou, 2007). Here, Brodmann area 9 is located on the dorsal part, on both, lateral and medial surfaces at the top of the frontal lobe extending along the middle third of the superior frontal gyrus and adjacent portions of the middle frontal gyrus. Area 24 was positioned in the cingulate gyrus above anterior part of the genu of the corpus callosum, and area 32 was dorsal to area 24. The surface of the anterior cingulate gyrus is composed of areas 25 and 24. In the depths of the rostral callosal sulcus is area 33. Surrounding the rostral and dorsal borders of areas 25 and 24 is the cingulofrontal transitional area 32 (Öngür et al., 2003; Petrides et al., 2011; Petrides and Pandya, 1999; Rajkowska and Goldman-Rakic, 1995a; Vogt et al., 1995, 2013).

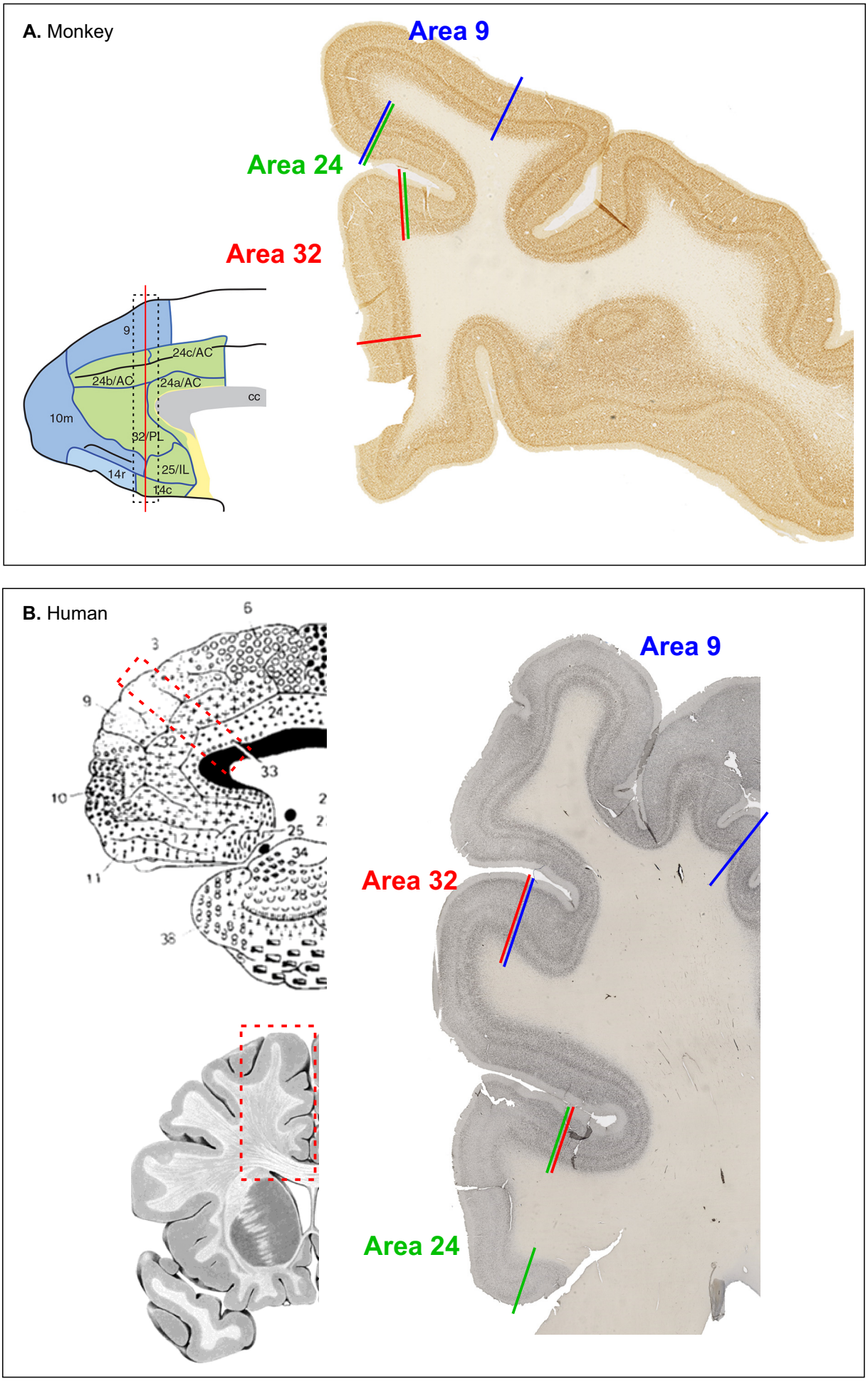


**Figure 5.2** The position of Brodmann areas **9**, **24**, **32** on a **monkey** (A) and **human** (B) brain sections stained with **NeuN**. Presented sections are at midlevel in blocks used for quantitative analysis (square shown on schema).

#### 4.3.1.1 Stereology on single labeled sections

Quantitative analysis was performed on serial sections' reconstructions in rostrocaudal extent of each area of interest with defined lateral borders. After randomly choosing the first section every tenth was used for the analysis encompassing in total five sections stained with NeuN and its adjacent sections stained with calretinin (5 sections) in each area. This way the number of NeuN and calretinin neurons was estimated using the optical fractionator method (West et al., 1991).

These analyses were performed with two computer-assisted systems using Stereo Investigator software (MicroBrightfield, Baltimore, MD). The first computer-assisted system included a PC connected to a digital video camera (DEI-479, Optronics, Santa Barbara, CA) and to a Nikon microscope (90i, Nikon, Melville, NY). The microscope was equipped with a motorized stage (MAC 2000, Ludl Electronics Products, Hawthorne, NY). The second system is equipped with MBF-DV-46 digital camera, attached to z-axis motorized Olympus BX61 microscope and an x-y axis motorized stage, controlled by MAC 5000 controller (Ludl Eletronic Products Ltd.). Analysis was always done with a 60x air objective.

The borders between cortical areas tend not to be sharp or distinct, thus, sampling was limited to a representative region within the cortical areas of interest. That is, once the cortical area was identified in each series of Nissl-stained sections, five sections from anterior to posterior (every $10^{th}$) were included in stereological analyses. The sections used in this study were chosen via systematic randomized approach. First section was randomly chosen and following ones were every $10^{th}$ in a line along the area of interest. Calretinin labeled sections were in between Nissl and NeuN labeled ones. Cortical lamination was defined on NeuN stained sections because this staining reveals distinct features in each area that are not recognizable on Nissl stained sections. Thus, we analyzed the cortical layers separately as layers Ia, Ib II, III, IV, Va, Vb, VIa, VIb and WM (undelaying white matter) (Figure 5.10).

Neurons were counted within a probe volume defined by the counting frame and the dissector height. The dissector height (20µm) used in this study is the real thickness of sections minus 2µm on each side of the section to exclude irregularities due to cutting processes. The real thickness of sections (14-24µm) resulted from shrinkage of the sections (40-60µm thick) following histological treatment. The size of the counting frame was 100 x 100 µm. Only neurons within the counting frame or overlapping the right or superior border of the counting frame, and which came into focus while focusing down through the dissector height, were counted. To estimate the number of labeled neurons each region was entirely sampled randomly and systematically.

Quantitative analysis included following data per each layer: total volume, total number and density of neuron (NeuN) and total number and density of calretinin neurons. Total number of NeuN positive cells accounts for total number of neurons (Sarnat et al., 1998). Based on these data following parameters were determined: neuron proportion in each layer (i.e. relation of number of neurons in particular layer to total neuron number), calretinin neuron proportion (i.e. relation of number of calretinin neurons to total neuron number in particular layer), and calretinin neuron distribution (i.e. number of calretinin neurons in particular layer to total number of calretinin neurons). Different areas and species were compared for all of the latter parameters in each layer.

#### 4.3.1.2 Neurolucida quantification on double labeled sections

Quantitative analysis of double labeled neurons was performed as follows: single confocal images obtained from confocal microscope (Zeiss LSM 510) were imported in Neurolucida software. Three sections from each double labeling were used for quantification of each labeling and co-labeling in a column within each of the areas of interest. The lateral boundary of the virtual area was the line perpendicular between pia and white matter that followed positioning and orientation of cortical neurons (Bok, 1929). In the defined area all single and double labeled neurons were marked with different markers and the numbers automatically provided by the software. Density of particular neuron class was calculated as number of neurons per surface ($mm^2$) of counted area in each section. Based on number of counted cells calretinin/parvalbumin and calretinin/calbindin and calretinin/somatostatin ratio was calculated for each section.

### 4.3.2 Image acquisitions

Image from immunohistochemical labeled sections were acquired with an automatized Olympus-PROVIS system equipped with a high quality digital Nikon video camera (Eclipse DXM 1200) and Hamamatsu Nanozoomer 2.0 scanner using a single optical plane at 40x magnification, corresponding to 0.226µm/pixel resolution (Hamamatsu, Japan). Images from immunohistofluorescent labeled sections were acquired with laser confocal microscope (Zeiss, LSM 510 META). Sequential acquisitions of the different fluorophore were performed with Argon 458/477/488/514nm lasers using the tile scan function in order to image the entire region of interest.

## 4.4. Statistical analysis

In this study different statistical analyses were performed using the STATISTICA software version 10 (Statsoft, Tulsa, OK, USA, licensed to University of Zagreb School of Medicine). The one way ANOVA for parametric analysis and nonparametric rank transformation procedure according to Conover and Iman (Conover and Iman, 1981) was performed. The a posteriori (post-hoc) Student-Newman–Keuls (SNK) test for multiple comparisons was applied to determine statistical differences between areas and layers.

For comparison between species student t-test was used to determine the differences between each layer and a total number of neurons and number of calretinin neurons.

# 5. Results

## 5.1 Cytoarchitectonic organization of monkey areas 9, 32 and 24 assessed through Nissl and NeuN labeled sections

Cytoarchitectonic organization was studied on NeuN (Figure 5.1) and Nissl (Figure 5.2) stained sections. The NeuN staining is labeling cell bodies of neurons while Nissl staining labels both neurons and glial cells. Therefore, the identification of cortical layers crucial for demarcation of neighboring areas is more reliable on NeuN sections. This was particularly useful for the characterization of layer I and identification of layer IV.

Sublamination of layer I in an upper neuron sparse zone, and a lower more populated zone is clear on NeuN labeling in all three areas (Figure 5.3), whereas such sublamination is difficult to identify on Nissl staining (Figure 5.4). NeuN labeling was particularly useful to visualize such sublamination in area 9 (Figure 5.3A) where layer I is thinner than in other two areas. NeuN labeling showed that in area 32 (Figure 5.3B), neurons are clustered forming islands in both the deep-part of layer I and the upper-part of layer II making the border between the two layers difficult to identify. In contrast, in areas 9 and 24 (Figure 5.3C), the border between layer I and II is clear due to the difference in neuron density and intensity of labeling.

Layer III is thicker in area 32 than in other two areas (Figure 5.1B), but neurons are less densely packed and not as intensively labeled as in area 9 (Figure 5.1A) and 24 (Figure 5.1C). There is a superficial to deep increase in neuronal cell body size in areas 9 and 24 whereas area 32 doesn't show this feature. Area 9 is characterized by the presence of large and strongly labeled pyramids in layer IIIC that can be observed in both Nissl and NeuN labeling (more detailed description is given in following chapter).

Layer IV (Figure 5.5) was clearly visible in area 9 and 32 on NeuN labeled sections. On Nissl sections of area 9, layer IV is continuous but thinner and is at points hard to identify (Figure 5.6A). Nissl staining of area 32 (Figure 5.6B) reveals recognizable but discontinuous layer IV, showing large differences in thickness. When stained with NeuN, layer IV of area 32 (Figure 5.5B) shows constant thickness though whole area, although it was thinner than in area 9 (Figure 5.5A). In area 24, NeuN labeling (Figure 5.5C) revealed a cell sparse strip delineating layers III and V which was not visible on Nissl stained sections (Figure 5.6C). In addition to better recognition of layer IV, sublamination of layers V and VI was more prominent on NeuN slides. More detailed descriptions of laminar organization of NeuN labeled, including the cell morphology, is given hereafter.

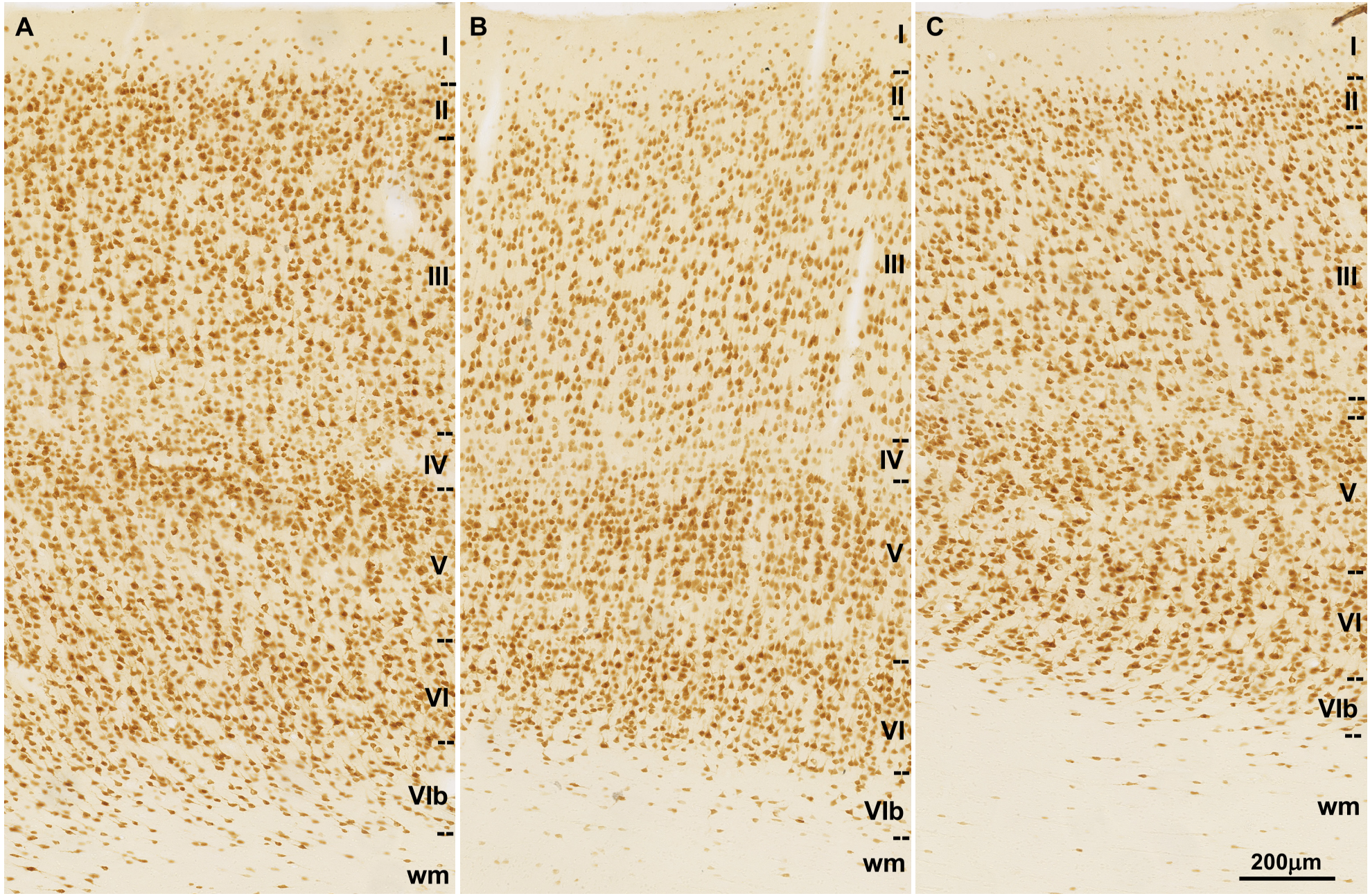


**Figure 5.1** Areas **9** (A), **32** (B) and **24** (C) in monkey. Immunohistochemical anti-**NeuN** staining.

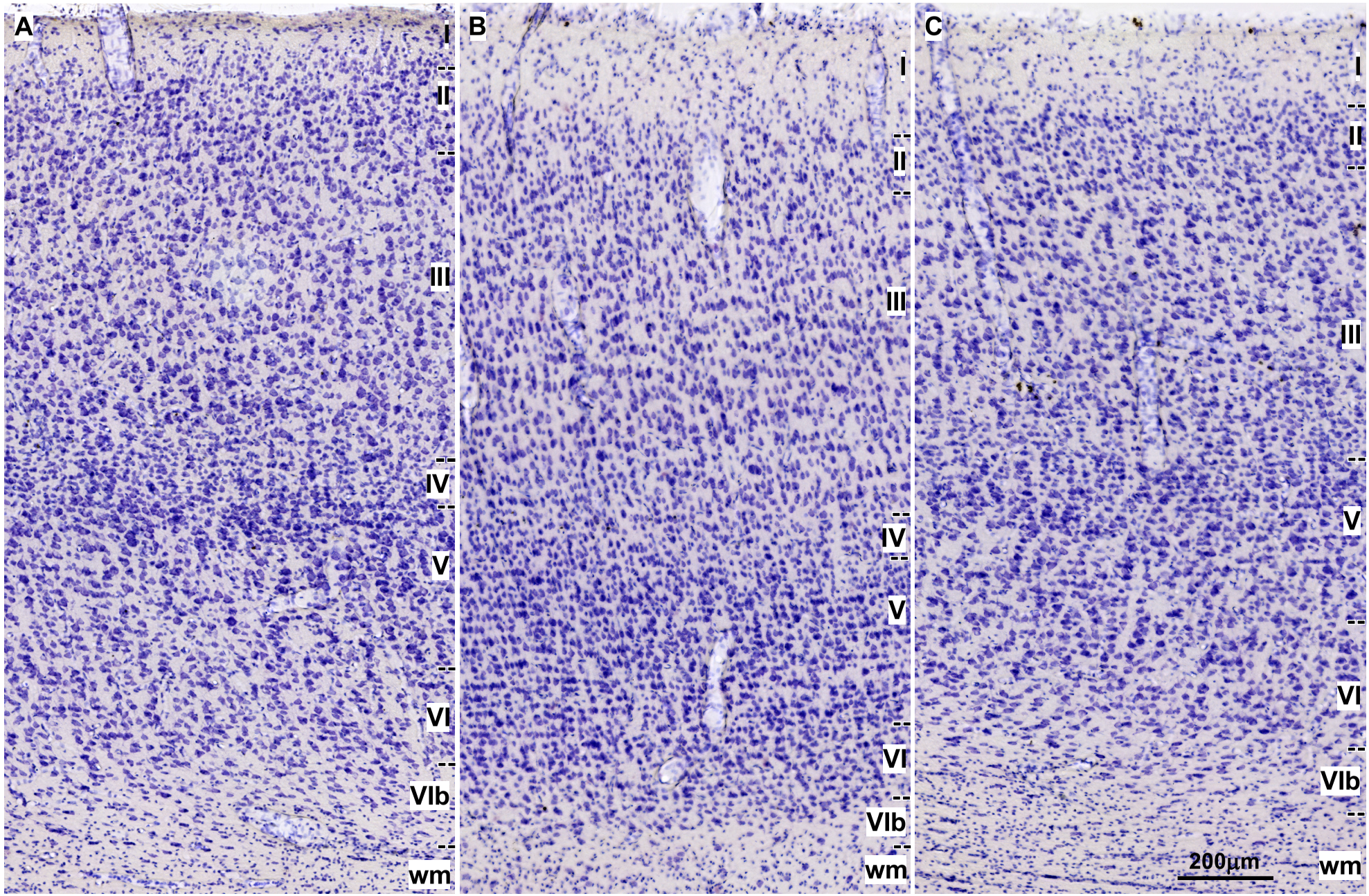


**Figure 5.2** Areas **9** (A), **32** (B) and **24** (C) in monkey. **Nissl** staining.

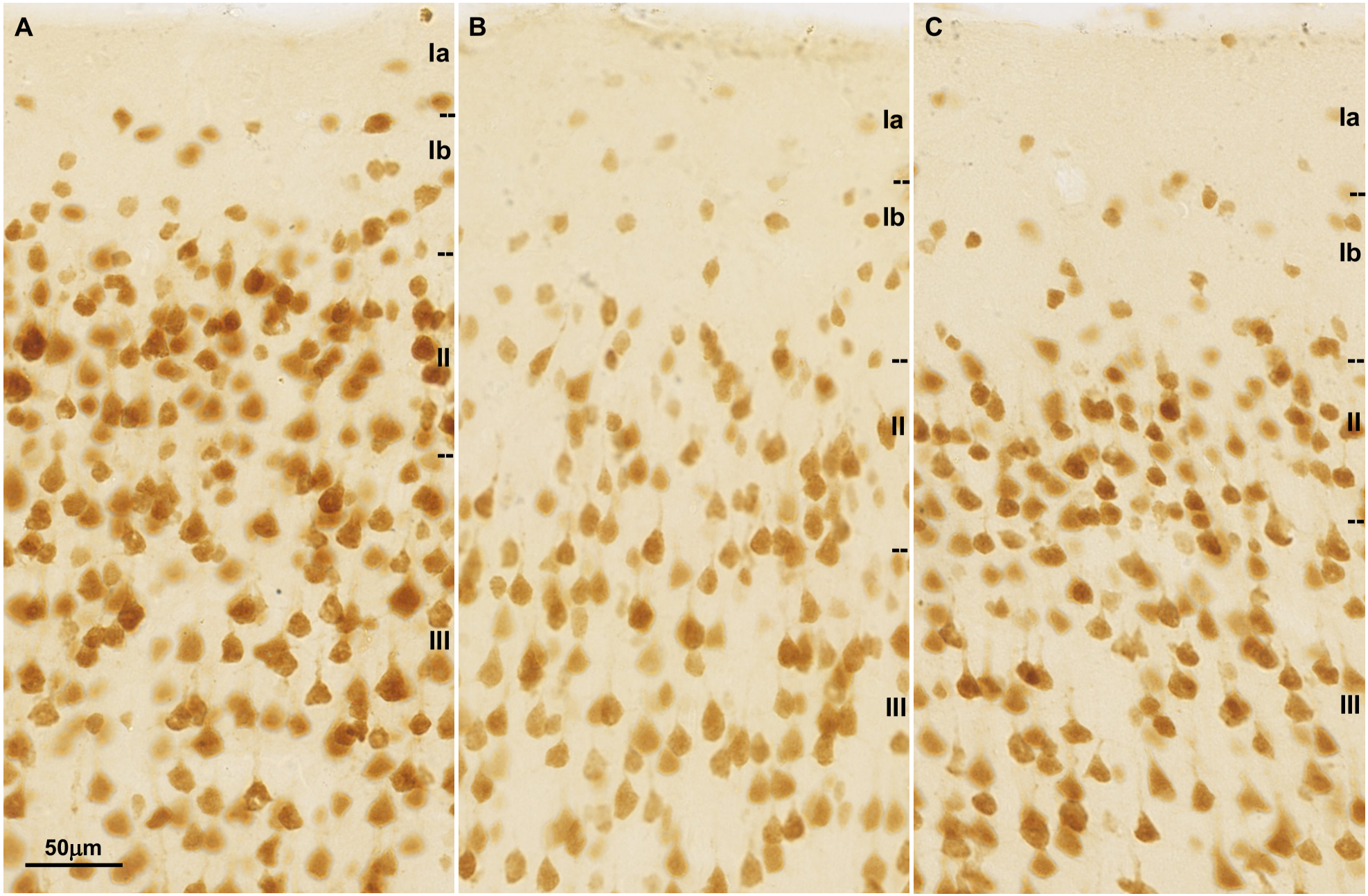


**Figure 5.3** Areas **9** (A), **32** (B) and **24** (C) in monkey. Immunohistochemical anti-**NeuN** staining of upper cortical layers (I-IIIa).

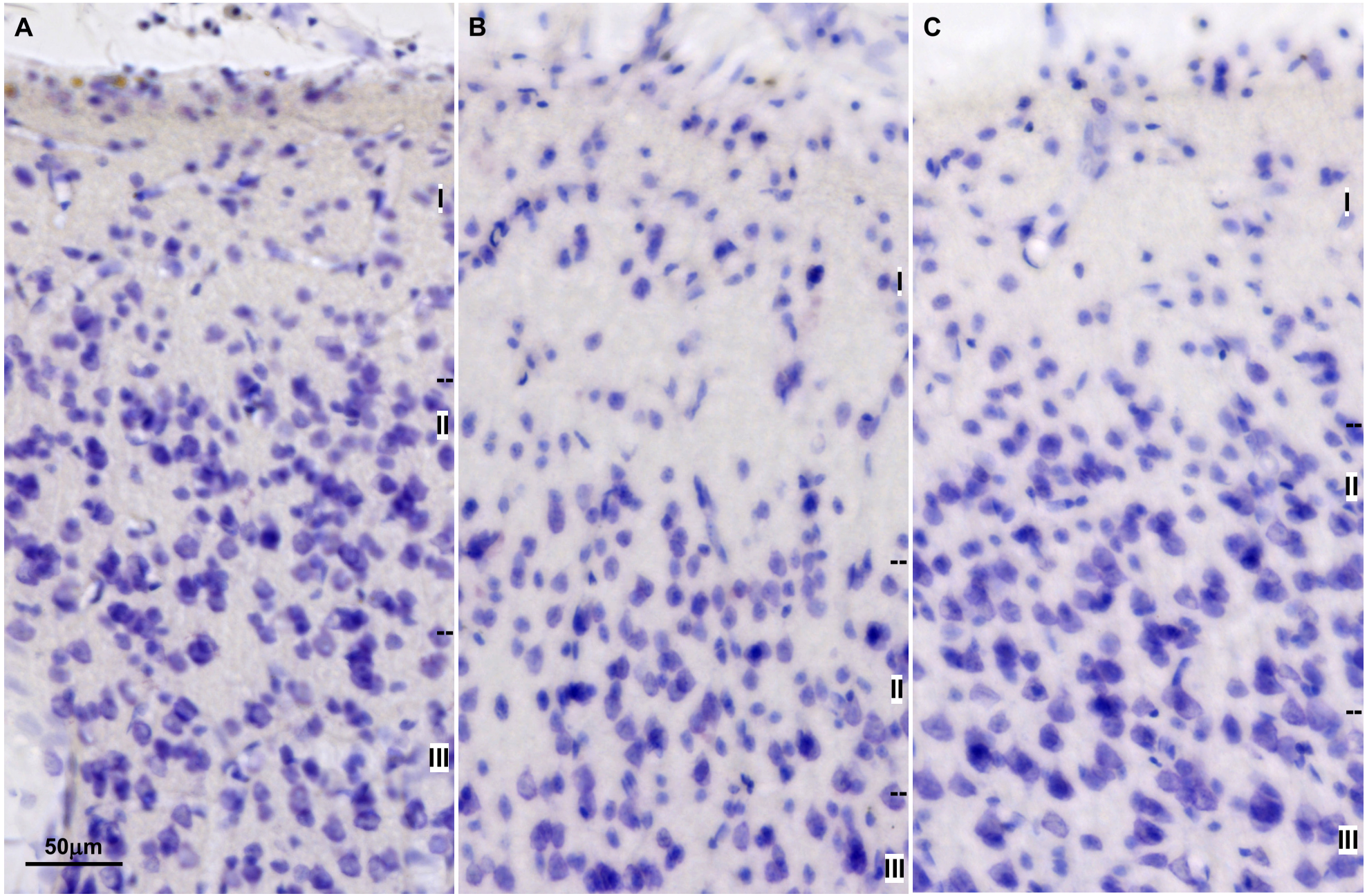


**Figure 5.4** Areas **9** (A), **32** (B) and **24** (C) in monkey. **Nissl** staining of upper cortical layers (I-IIIa).

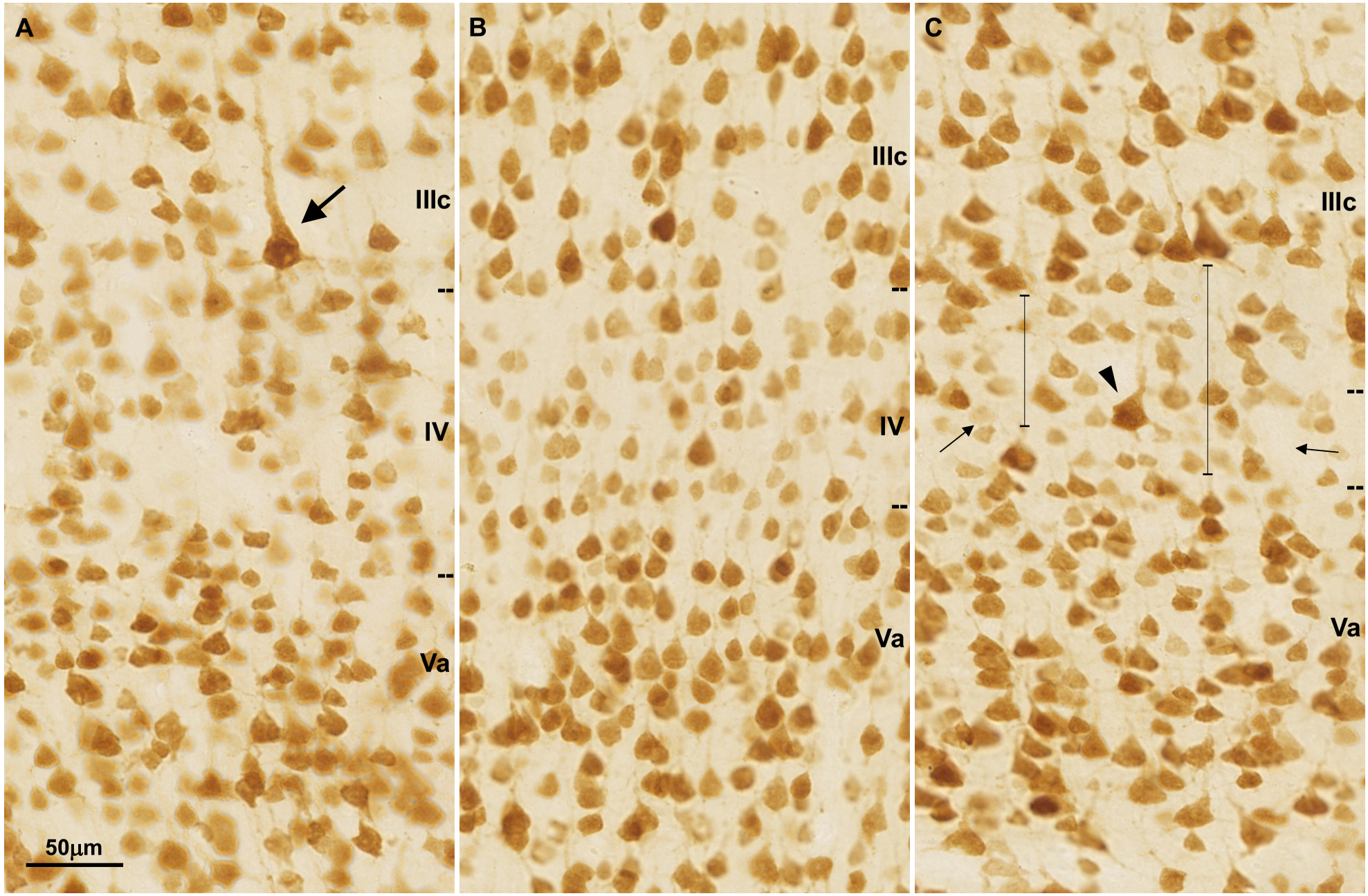


**Figure 5.5** Areas **9** (A), **32** (B) and **24** (C) in monkey. Immunohistochemical anti-**NeuN** staining of middle cortical layers (IIIc-V). Arrow in area 9 (A) indicates typical large pyramids in layer IIIc. In area 24 (C) neurons typical for layer IIIc and V are in most of places divided with cell sparse band (arrows) 50-100μm thick (bar). Arrowhead points on large pyramidal neurons, typical for layer IIIc, positioned in the middle the band dividing layer III and V.

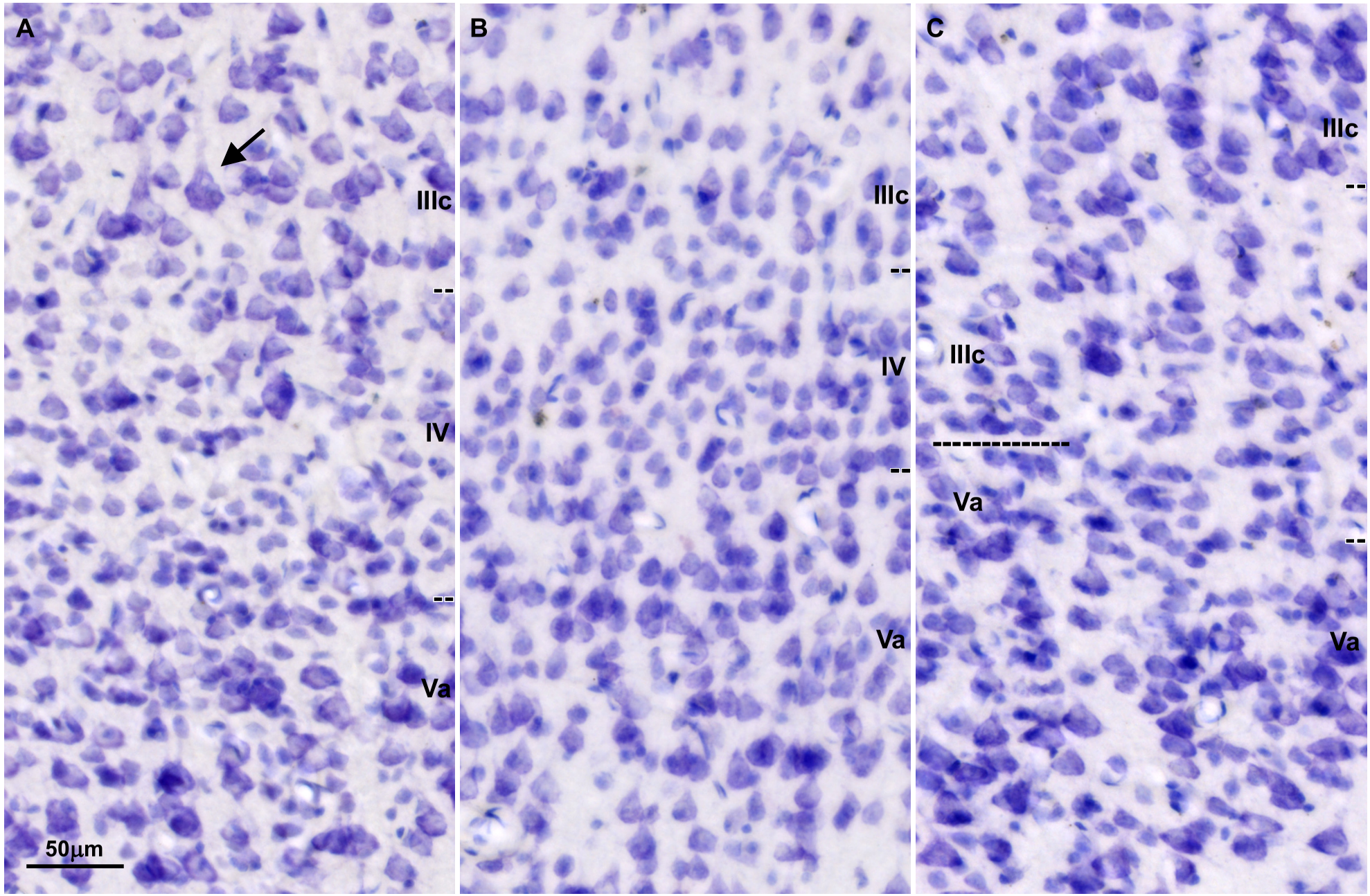


**Figure 5.6** Areas **9** (A), **32** (B) and **24** (C) in monkey. **Nissl** staining of middle cortical layers (IIIc-V). Arrow in area 9 (A) shows typical large pyramids in layer IIIC. In area 24 (C), neurons typical for layer IIIC and V are occasionally separated for 50-100μm with pale pyramids (right part of panel), while in other parts they are placed next to each other (left part of panel).

## 5.2 Laminar organization and cell morphology of monkey areas 9, 32 and 24 on NeuN labeled sections

**Area 9**

Area 9 is granular cortex with a straightforward demarcation of six layers (Figure 5.7). There is a prominent sublamination of layer V and relatively thick transitional layer to white mater, layer VIb.

Layer I can be clearly divided in two parts (Figure 5.3A). An upper part sparse in neurons and a lower one with neurons scattered near the border with layer II. The density of these neurons gradually decreases from the border with layer II to mid part of layer I.

The upper border of layer II has a wavy appearance due to aggregates of very small cells intermixed with medium sized non-radially oriented (parallel with pial surface) pyriform-bipolar neurons. Layer II is composed of heavily labeled small round, oval and triangular neurons. The upper part of layer III is also densely packed with neurons making the border between layer II and III indistinct. In contrast to the upper part of layer III which is compact, the lower part (IIIc) is not as dense and contains large pyramidal neurons with strongly labeled cell body and proximal apical and basal dendrites (Figure 5.5A). These pyramidal neurons are the most prominent neurons found in area 9, and the largest neurons across all three areas analyzed. In layer IIIc, very small, faintly labeled medium sized pyramidal-shaped neurons are intermixed with large heavy labeled cells. Such faintly labeled small pyramidal cells as well as round shaped neurons are forming narrow but clear layer IV, along with small heavily labeled pyramidal cells that seem as displaced from layer Va. Layers II and V are compact layers giving the area 9 its typical horizontally stratified cytoarchitectonic appearance.

Layer V is divided into the upper sublayer Va formed by densely packed small to medium sized pyramidal neurons. The lower sublayer Vb, lighter in appearance than layer Va, contains numerous small round to oval shaped faintly labeled neurons and scattered, strongly labeled medium sized pyramids.

Layer VI can be divided in two sublayers based on the cell density. In upper part, sublayer VIa is densely packed with a multipolar and spindle (fusiform) shaped cells. Layer VIb is composed of medium sized oval, triangularly shaped and multipolar neurons. The density of cells in layer VIb is lower than in layer VIa, showing a gradual dispersion of cells from layer VIa towards white matter. Therefore, borders of layer VIb, both with layer VIa and with white mater, are not sharp.

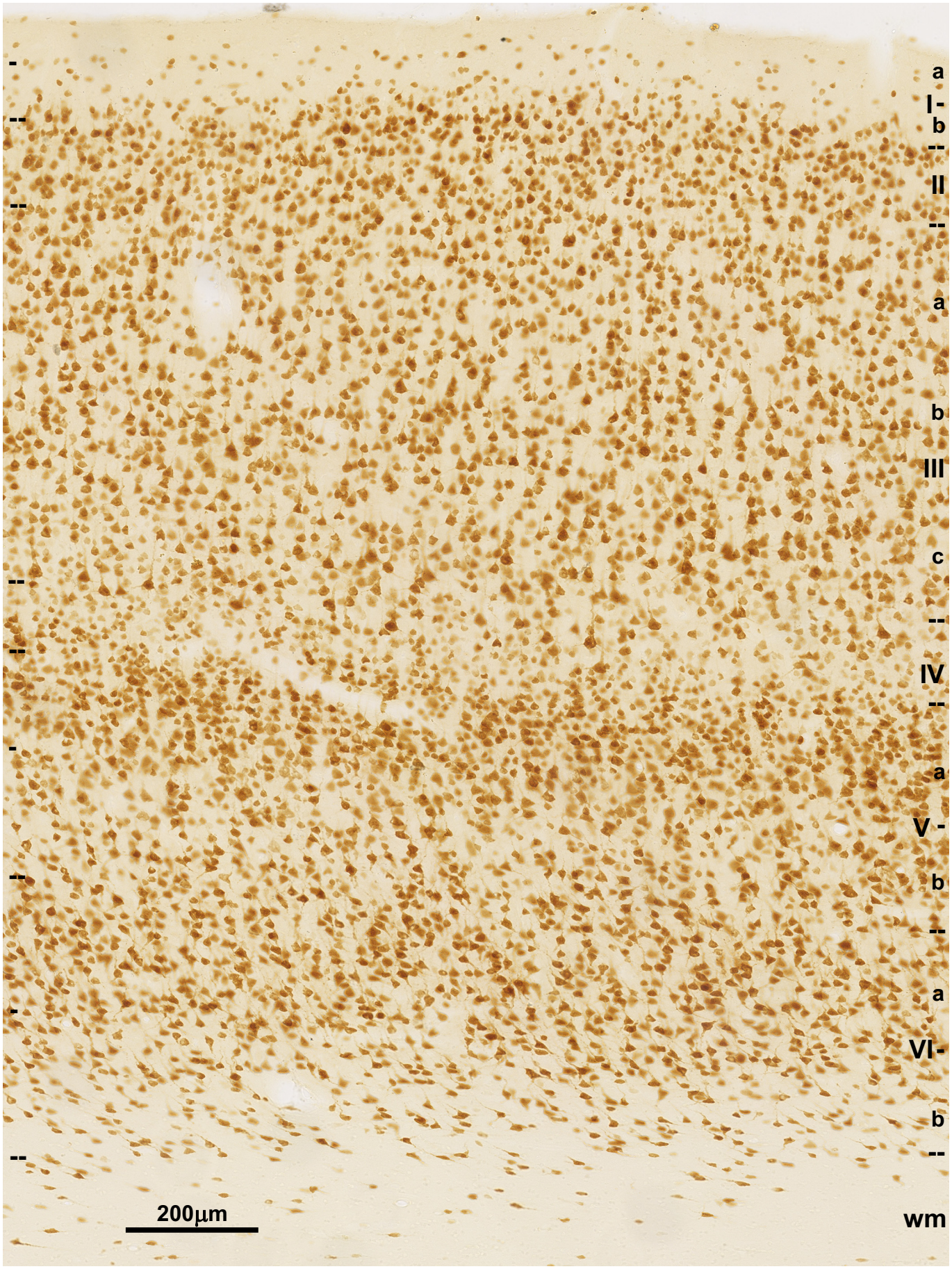


**Figure 5.7** Area **9** in monkey, immunohistochemical anti-**NeuN** staining.

**Area 32**

Area 32 (Figure 5.8) clearly displays six cortical layers, including a thin layer IV (Figure 5.5B).

Layer I contains scattered small round and oval shaped neurons in its upper half (Figure 5.3B). In its lower half, these neurons are more densely packed and grouped in small islands. The layer II is of irregular thickness, having also “island like” organization. In layer II cells are forming larger aggregates than in layer I, and at higher magnification, small pyramidal neurons of layer II seems to be intermixed with layer I neurons. Layer II contains also medium sized non-radially oriented moderately labeled pyriform-bipolar neurons.

Due to irregularity in thickness of layer II and a discrete layer IV, area 32 in monkey can be described as dysgranular cortex.

Pyramidal neurons of layer III do not have apparent superficial to deep increased gradient in cell body size. Indeed, neurons in the lower part of layer III (IIIc) have only slightly larger cell body size (Figure 5.5B) than the neurons in the upper part and in the layer II (Figure 5.3B). Consequently, the layer II and III are in continuity and their border is hard to delineate.

Layer IV contains a distinct population of small sized neurons distributed in a thin band above layer V (Figure 5.5B). Layer V contains pyramidal-shaped neurons. This layer is subdivided into two sublayers based on the density and the labeling intensity of the neurons. The upper part has a denser, more compact appearance with strongly labeled neurons. Both sublayers, Va and Vb, are composed of small and medium size pyramids. These medium size neurons have roughly the same cell body size than the largest pyramids of layer IIIC. Therefore, layer V although clearly divided into sublayers, has common composition regarding size and shape of cells.

Layer VI, is composed of medium sized pyramidal-shaped neurons, perpendicularly oriented bipolar cells and a few multipolar neurons. The sublayers of layer VI can be distinguished based on cell density. The sublayer VIa has scattered strongly labeled medium size pyramidal neurons similar to that found in layer V. The density of these neurons decreases in layer VIb, and this sublayer is actually a transitional zone towards the white mater.

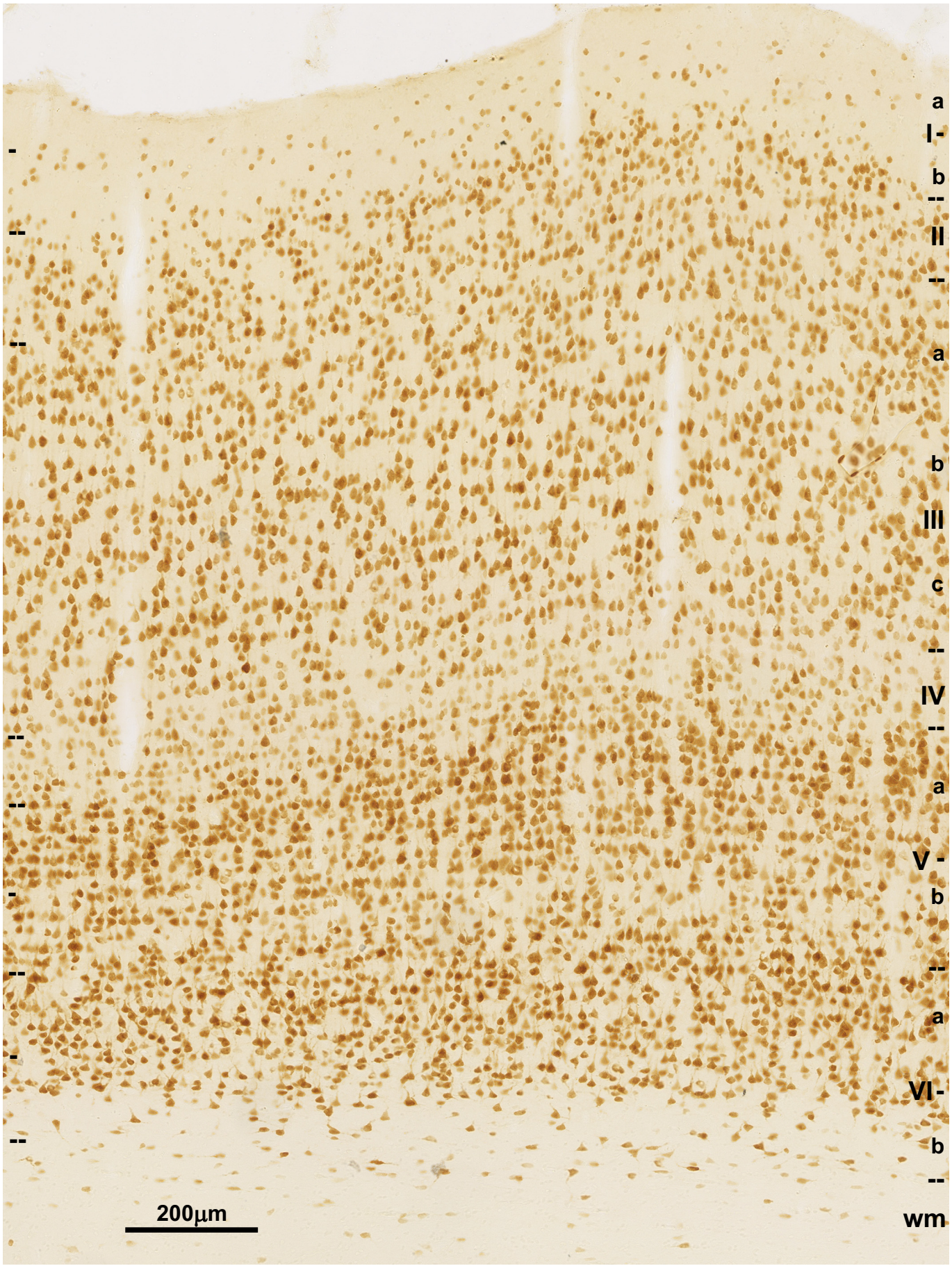


**Figure 5.8** Area **32** in monkey, immunohistochemical anti-**NeuN** staining.

**Area 24**

Area 24 is considered to be agranular cortex (Figure 5.9). Indeed layer IV is not apparent on Nissl stained sections. However, NeuN labeling reveals a thin band of small, faintly labeled cells between layers III and V (Figure 5.5C).

As in the others two analyzed areas, layer I can be divided into a neuron sparse upper half, and a lower half with a relatively higher neuron density (Figure 5.3C). The distinction between layer I and II is clear due to striking increase in labeling intensity of neurons. The thin upper part of layer II contains small oval to round shaped neurons, whereas the rest of layer II is composed of intermixed small to medium size pyramidal neurons. Occasionally, medium to large sized pyriform shaped neurons can be also seen in layer II.

Layer IIIa contains neurons of the same size as those of layer II. The neuronal density abruptly decreases from layer II to layer IIIa delineating clearly these the two layers. Layer III pyramidal neurons show superficial to deep increase in cell body size. In the thin deep part, large neurons are intermixed with small faintly labeled, oval or triangularly shaped cells.

Layer IV is not present in this area but there is a sparse strip of cells dividing medium sized pyramidal neurons of layer IIIc from small pyramids of layer Va (Figure 5.5C).

Layer Va is dense, packed mostly with small pyramidal neurons that increase in size with depth. The layer Vb is thin and less densely populated with neurons than layer Va. Neurons in these layers are strongly labeled and have an irregular triangular shape.

Layer VIa is almost as dense as layer Va and contains medium sized fusiform, bipolar, multipolar or triangularly shaped neurons. Layer VIb neurons are not uniform in size and there are clumps of medium to large neurons. There is an abrupt decrease in neuronal density of layer VIb when compared to the upper part, the layer VIa.

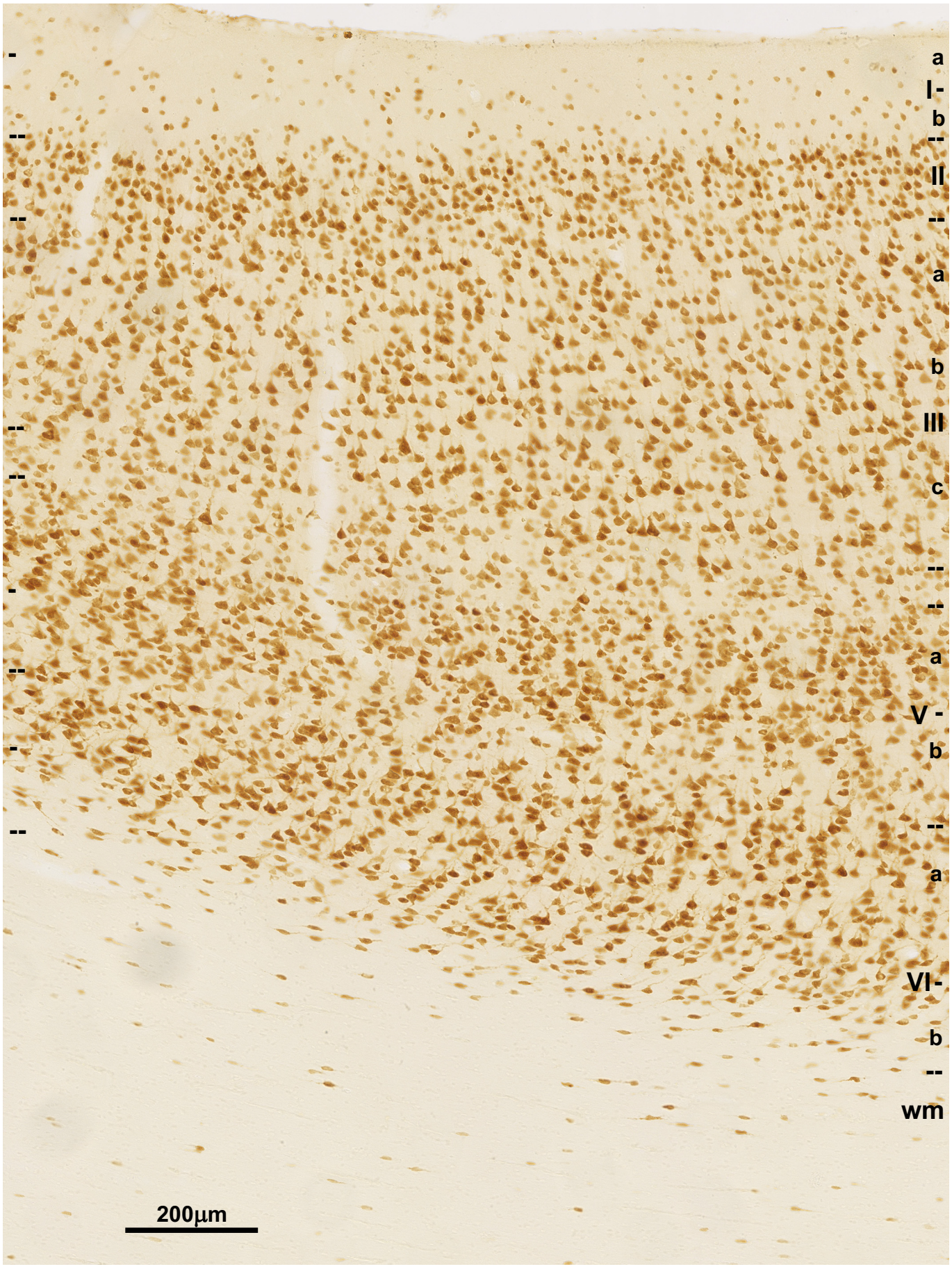


**Figure 5.9** Area **24** in monkey, immunohistochemical anti-**NeuN** staining.

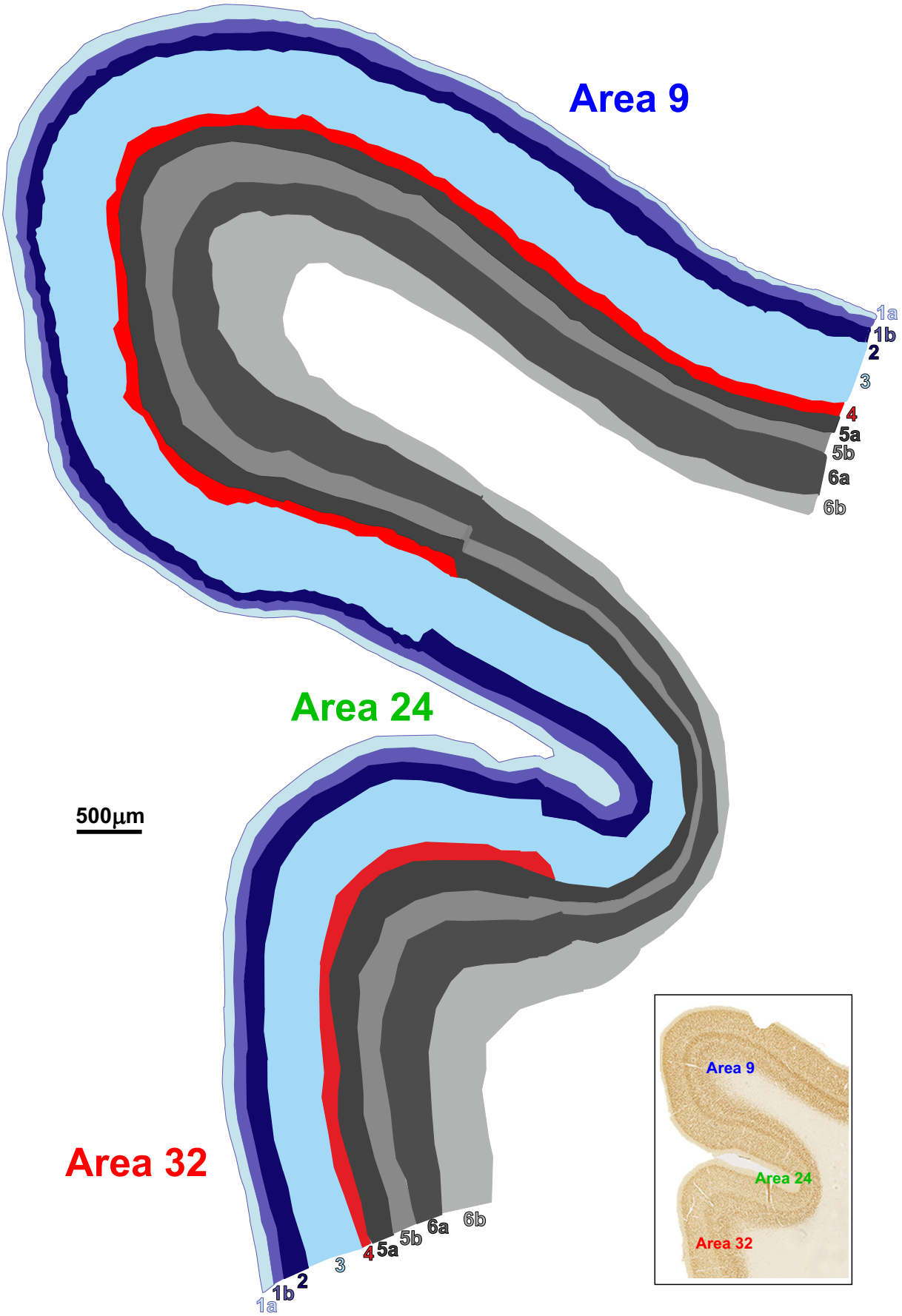


**Figure 5.10** Computer reconstruction of **NeuN** stained section in monkey used in stereological analysis showing areal and laminar organization. Small panel is part of microphotography from figure 4.1A.

### 5.2.1 Quantitative analysis of NeuN labeled sections

The total number of NeuN labeled neurons and total volume were estimated for each sublayer in each analyzed area (Figure 5.10) for each animal (n= 3). The proportion of neurons positioned to particular layer and neuron density were calculated. The mean values with standard deviation (SD) are provided in tables 5.1, 5.2 and 5.3.

**Table 5.1 Proportion (%) of NeuN labeled cells** from total neuronal pool located in particular layer of monkey areas 9, 24 and 32 (NeuN cell number per layer / total number of NeuN cells in particular area).

| | **Area 9** | SD | **Area 32** | SD | **Area 24** | SD |
|---|---|---|---|---|---|---|
| Ia | **0.7%** | 0.1% | **1.0%** | 0.4% | **0.9%** | 0.4% |
| Ib | **2.6%** | 0.3% | **3.3%** | 1.0% | **3.7%** | 0.4% |
| II | **18.0%** | 5.4% | **14.7%** | 1.9% | **15.6%** | 2.4% |
| III | **31.6%** | 2.4% | **25.7%** | 3.9% | **30.4%** | 0.3% |
| IV | **7.1%** | 1.9% | **8.3%** | 0.7% | **Ø** | **ø** |
| Va | **14.6%** | 1.1% | **16.1%** | 2.0% | **15.7%** | 4.9% |
| Vb | **9.1%** | 0.4% | **10.2%** | 2.3% | **11.8%** | 2.5% |
| VIa | **9.6%** | 2.4% | **11.5%** | 0.7% | **13.0%** | 2.8% |
| VIb | **4.9%** | 1.6% | **7.6%** | 1.4% | **7.1%** | 1.6% |
| WM | **1.9%** | 0.8% | **1.6%** | 0.1% | **1.7%** | 0.3% |

The laminar proportions of neurons did not reveal robust inter-areal differences (Figure 5.11A, B). Around 4% of neurons are positioned in layer I, 7-8% in layer IV for areas 9 and 32, and the rest is distributed almost equally between layers II/III and V/VI.

However, some differences can be observed. In area 9 proportion of neurons located in layer I (3.3%) showed tendency (p=0.06) to be 30-40% lower than in areas 32 (4.3%) and 24 (4.6%). Statistical analysis performed on ranked values (ANOVA, SNK-post hoc) showed (Figure 5.12A) that area 32 contains lower amount of neurons (45%) in layers I–III than areas 24 (51%, p=0,014) and 9 (53%, p=0.012). It also reveals that in area 9 layers V–VI contain lower amount of neurons (38%) than in areas 32 (45%, p=0.014) and 24 (48%, p=0.03). Therefore, ratio of neurons (Figure 5.12B) located in supragranular versus infragranular layers (I-III : V-VI) was significantly higher in area 9 (1.4) when compared to areas 24 (1.1, p=0.014) and 32 (1, p=0.012).

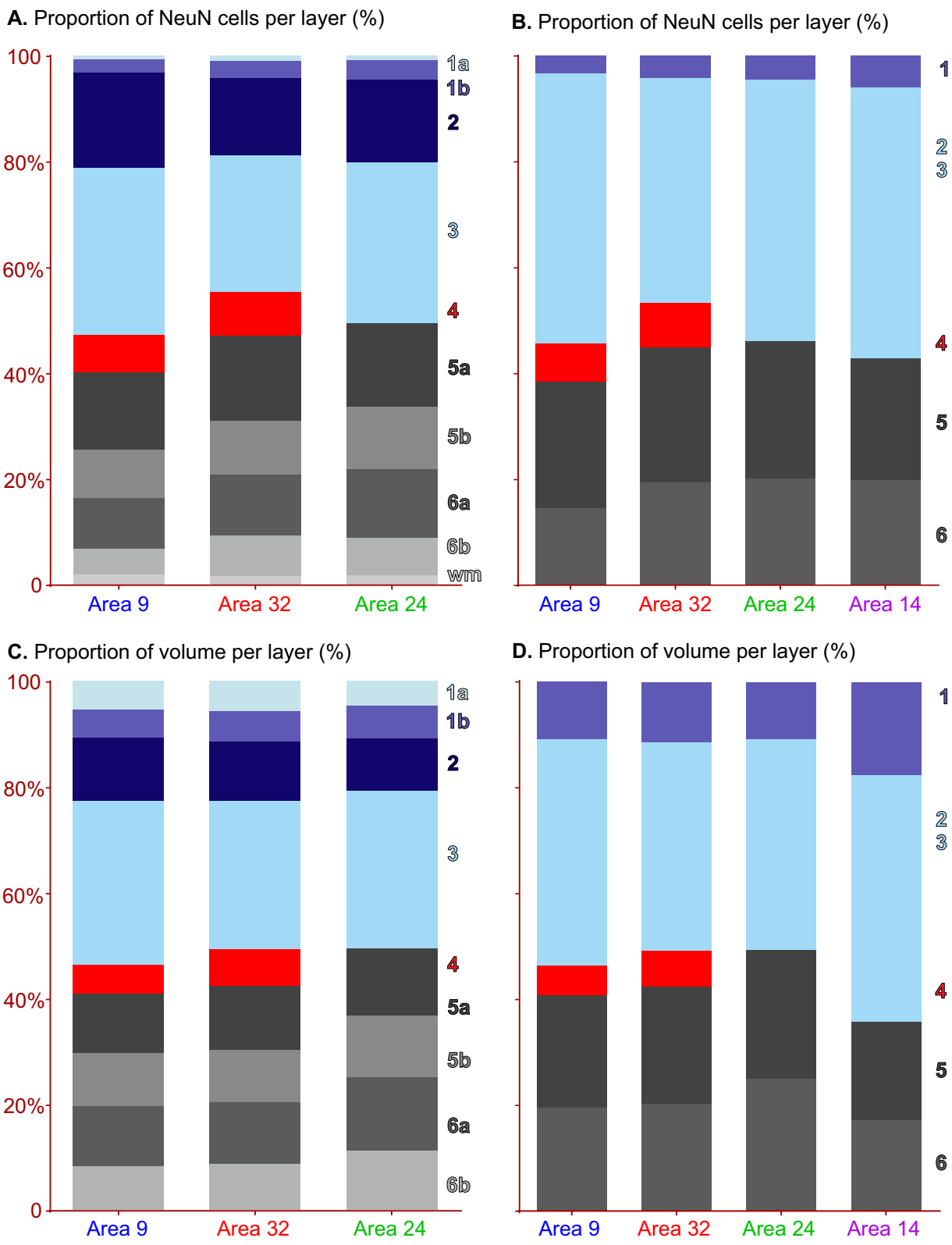


**Figure 5.11** Graphs are showing **laminar proportion of neurons** (A, B) and **layer volumes** (C, D) assessed on **NeuN** stained sections in monkey. Proportion is calculated as follows: volume and number of NeuN positive cells in particular layer was divided by total volume and total number of NeuN positive cells in whole area. Proportion is shown as percentage and on graphs B and D values obtained in this study are presented in the way to be comparable with data from area 14 obtained in previous study (Džaja 2015, PhD Thesis).

Note that these differences are statistically significant only when analysis is done on ranked values, because the ratio between supragranular and infragranular layers varies between animals from 1.15-1.64 in area 9, 0.97-1.24 in area 24 and 0.76-1.14 in area 32 (Figure 5.12). However, in all analyzed animals (n=3), area 9, when compared to areas 24 and 32, contains the highest proportion of neurons in layers II-III and lowest in layers V-VI.

Quantitative analysis revealed that 3/4 of the neurons within layer I are located in its lower part (Table 5.1). This confirms the qualitative data (Figure 5.3) showing a clear sublamination of layer I in monkey with an upper neuron sparse sublayer Ia, and a more densely populated lower part, layer Ib.

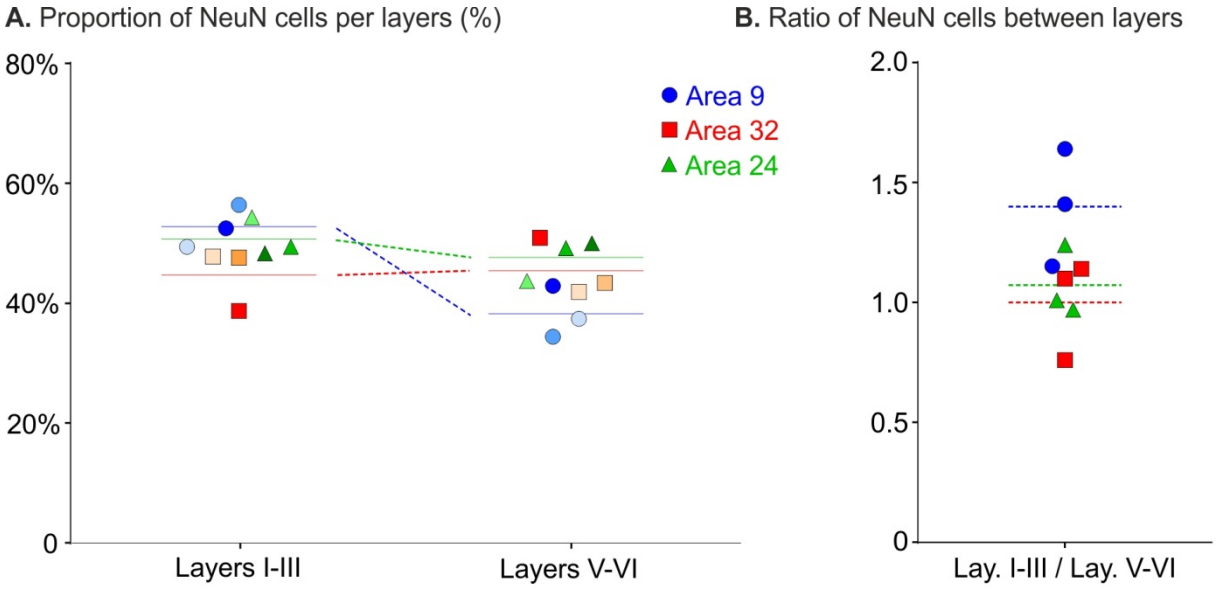


**Figure 5.12** Graphs show **proportion** from total pool of **NeuN** labeled cells located in monkey **layers I-III** and **V-VI** (A) and neuron **ratio** of **layers I-III versus layers V-VI** (B).

The proportion of volume (Table 5.2, Figure 5.11C, D) taken by each layer is relatively consistent in all three areas (variation between animals is up to 3%) (Figure 5.13). There are two half's in general, layers I-III take up half of total volume, and layers IV-VI the other half. The volume of layer I accounts for 10-12%, layer IV for 5-7% and layers II-III for 39-43% of total volume in all areas. The layers V-VI account for 40-43% of the total volume in areas 9 and 32 and 50% in area 24. The volume ratio between layers II-III versus layers V-VI is above 1 (ratio = 1.05) in area 9, whereas the ratio in areas 32 (0.9) and 24 (0.8) shows that in this two areas the volume of layers V-VI is higher than that in layers II-III.

**Table 5.2 Proportion (%) of layer volume** in relation to total volume of monkey areas 9, 24 and 32 (layer volume / total area volume). SD - standard deviation.

| | **Area 9** | SD | **Area 32** | SD | **Area 24** | SD |
|---|---|---|---|---|---|---|
| Ia | **5.5%** | 0.7% | **5.8%** | 1.2% | **4.7%** | 0.8% |
| Ib | **5.3%** | 1.0% | **5.7%** | 0.7% | **6.1%** | 0.5% |
| II | **12.0%** | 2.9% | **11.3%** | 1.9% | **9.9%** | 1.0% |
| III | **30.9%** | 2.4% | **28.1%** | 2.6% | **29.9%** | 4.3% |
| IV | **5.5%** | 0.8% | **6.8%** | 0.7% | **Ø** | **ø** |
| Va | **11.2%** | 1.7% | **12.2%** | 0.3% | **12.6%** | 2.5% |
| Vb | **10.1%** | 0.7% | **9.9%** | 1.5% | **11.8%** | 3.4% |
| VIa | **11.3%** | 1.9% | **11.6%** | 1.2% | **13.9%** | 1.4% |
| VIb | **8.2%** | 1.7% | **8.7%** | 0.9% | **11.1%** | 1.2% |

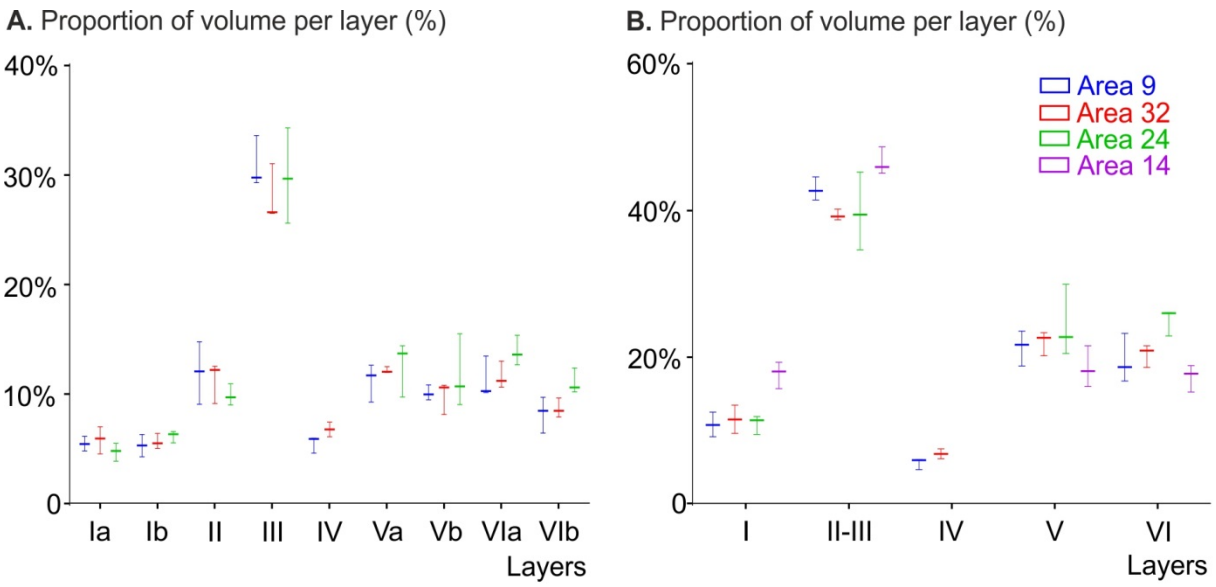


**Figure 5.13** Graphs show **proportion of volume** per particular layer in monkey (A). Proportion is shown in percentage and on graph B values obtained in this study are presented in the way to be comparable with data from area 14 obtained in previous study (Džaja 2015, PhD Thesis).

Neuronal densities are comparable between areas (Table 5.3; Figure 5.14). The highest density is in area 9 with 62 000 neurons per $mm^3$ (range 52 000-77 000), while in area 24 density is around 10% lower (55 000 neurons per $mm^3$; range: 44 000–66 000), and 20% lower in area 32 (51 000 neurons per $mm^3$, 42 000–54 000) (Table 5.3). Due to variations between animals, overall differences in neuron density between areas are statistically significant only when analysis is done on ranked values. This way the neuron density in layers II and III was in area 9 significantly higher than in area 32 (ANOVA, SNK post-hoc, performed on ranked values, $p = 0.012$) and 24 (ANOVA, SNK post-hoc, performed on ranked values, $p = 0.014$).

**Table 5.3. - NeuN density** per layer in monkey areas 9, 24, 32 presents the mean value (1000 cells / $mm^3$) of each layer with standard deviation (SD) in each area. Overall neuronal densities from layers I-VI and II-VI are presented in the last two rows.

| | **Area 9** | SD | **Area 32** | SD | **Area 24** | SD |
|---|---|---|---|---|---|---|
| Ia | **7.6** | 0.9 | **8.8** | 0.7 | **10.7** | 2.6 |
| Ib | **31.6** | 5.3 | **29.3** | 4.1 | **33.7** | 3.7 |
| II | **92.3** | 5.9 | **69.3** | 14.0 | **87.1** | 4.7 |
| III | **64.5** | 8.2 | **47.0** | 6.0 | **57.1** | 5.8 |
| IV | **79.8** | 6.2 | **63.1** | 7.8 | **Ø** | **ø** |
| Va | **85.9** | 19.9 | **66.8** | 2.1 | **68.9** | 11.1 |
| Vb | **57.5** | 9.5 | **52.3** | 2.3 | **58.1** | 9.6 |
| VIa | **53.7** | 9.7 | **50.6** | 3.2 | **52.7** | 9.9 |
| VIb | **38.3** | 8.5 | **44.8** | 3.4 | **37.0** | 7.7 |
| WM | **7.8** | 1.6 | **3.8** | 1.3 | **2.5** | 0.7 |
| I-VI | **61.9** | 13.4 | **51.0** | 6.7 | **54.7** | 6.7 |
| II-VI | **67.0** | 14.2 | **55.2** | 7.4 | **58.4** | 7.4 |

Layer II has the highest density across all areas (Figure 5.14). Layer Ib (in all areas) has similar neuronal density than that of layer VIb (32 000 versus 44 000 neurons per $mm^3$). Upper part of the layer Ia has densities that are either comparable to density in underlying white matter (8000 neurons per $mm^3$ in area 9) or twice the value of white matter neuronal density in other areas.

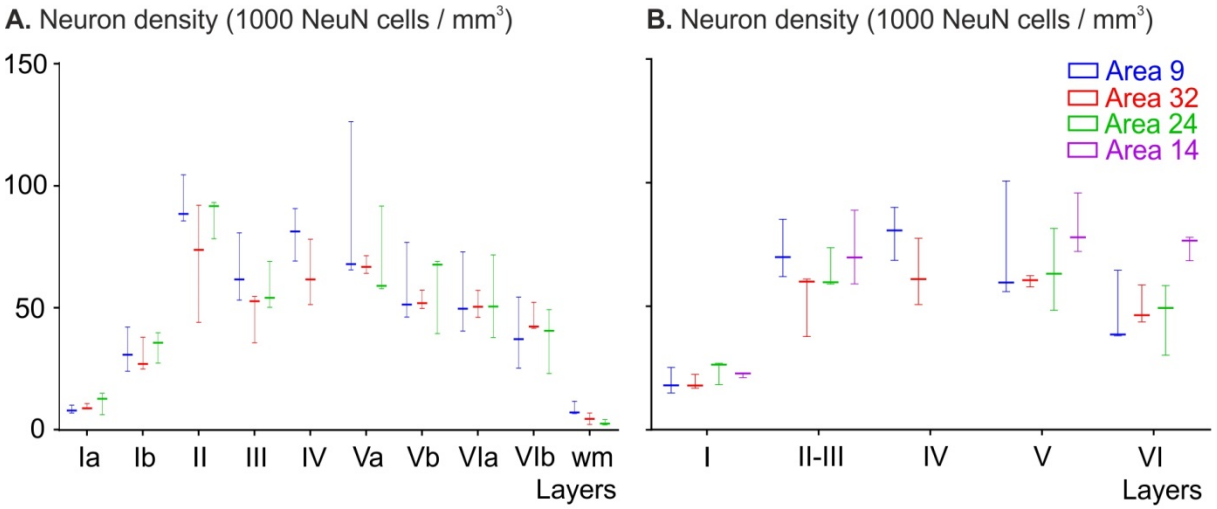


**Figure 5.14** Graphs show **neuronal density** in particular layer in monkey (A). Values shown on graph B are values obtained in this study and presented in the way to be comparable with data from area 14 obtained in previous study (Džaja 2015, PhD Thesis).

## 5.3. Laminar distribution and morphological features of calretinin labeled neurons of monkey areas 9, 32 and 24

All investigated areas display numerous calretinin containing neurons distributed across all layers and in the underlying white matter (Figure 5.15). In all examined areas (Figures 5.16, 5.17, 5.18) the vast majority of calretinin neurons are located in layer II and adjacent part of layers I and III, whereas calretinin neurons are sparse in layer IV, V and VI.

In layer I, calretinin containing neurons were located in its lower part. These neurons display multipolar or pyriform cell body shape, the type of calretinin neurons occasionally found in other cortical layers. Few calretinin neurons located below the pial surface have large cell body and well-labeled horizontally oriented dendrites resembling to Cajal Retzius cells. These neurons were also observed along the border with layer II.

Most of the calretinin containing neurons display small to medium size cell body (10-15 µm in diameter) with an oval or pyriform shape (Figure 5.19, see chapter 5.4). Most of them have intensely labeled soma and many display well-labeled processes. The dendritic tree of most of these calretinin neurons shows a radial orientation (perpendicular to pia). Axon like process was observed for almost all calretinin-labeled neurons. These axons of calretinin neurons located in the middle layers display mainly a vertical orientation for and their morphology corresponds to double bouquet cells with bitufted dendritic morphology. Bitufted cells usually have ovoid somata and an axon arbor that often cross the cortical column.

In the layer VI neurons are often horizontally oriented particularly along the border with white matter (see chapter 5.4).

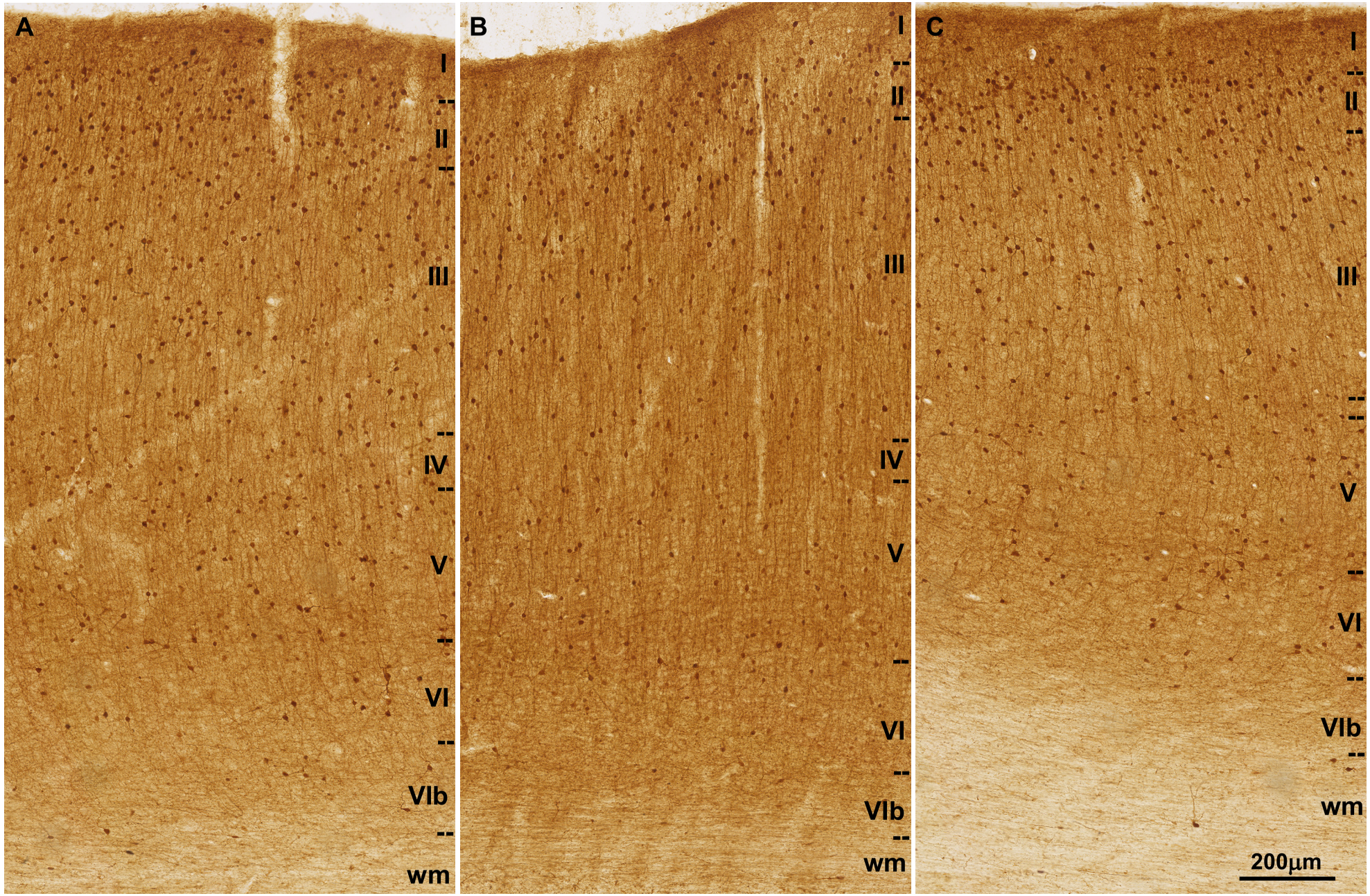


**Figure 5.15** Areas **9** (A), **32** (B) and **24** (C) in monkey. Immunohistochemical anti-**calretinin** (rabbit polyclonal) staining.

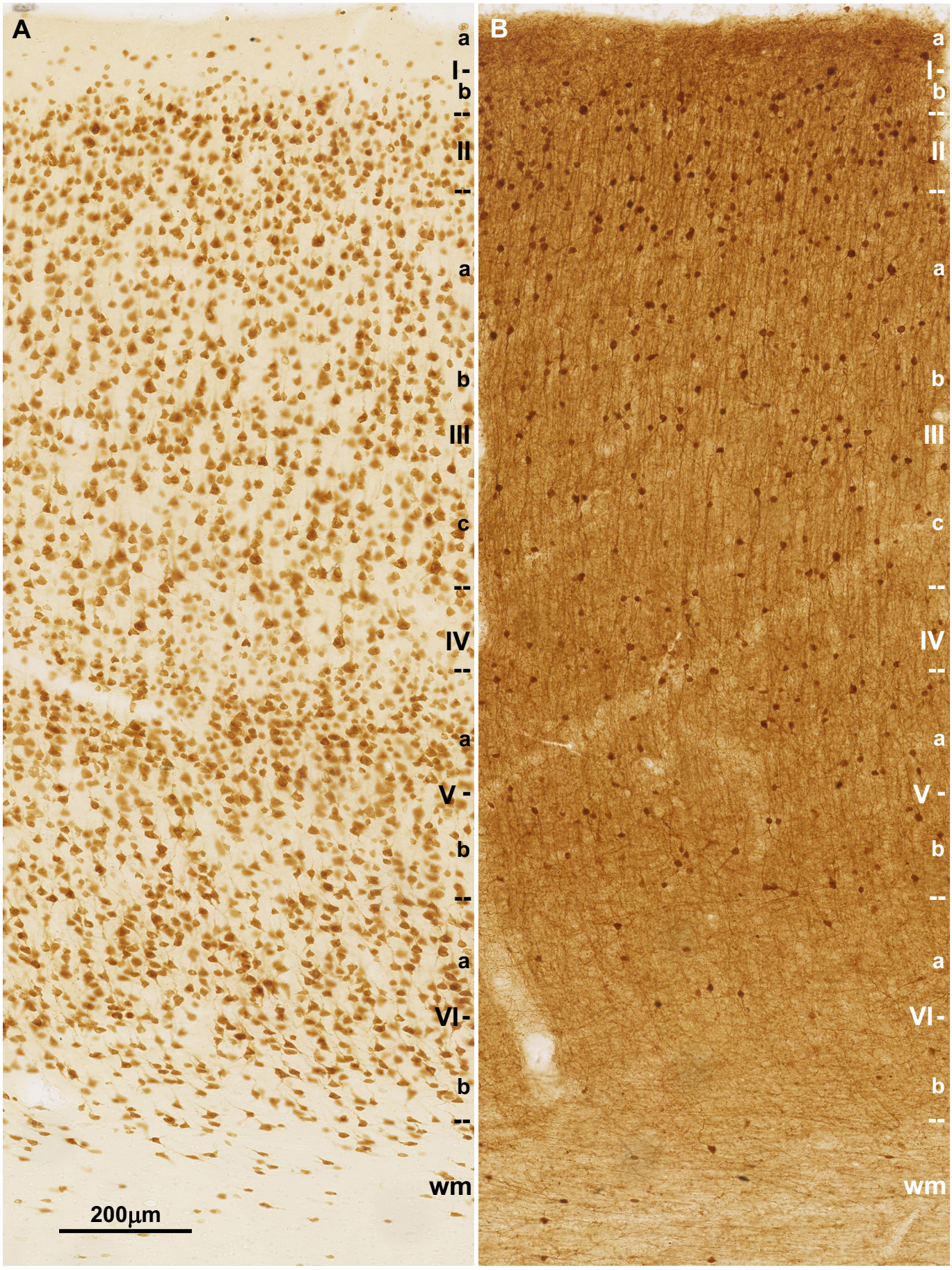


**Figure 5.16** Area **9** in monkey. Immunohistochemical anti-**NeuN** (A) and anti-**calretinin** (B) staining of neighboring sections.

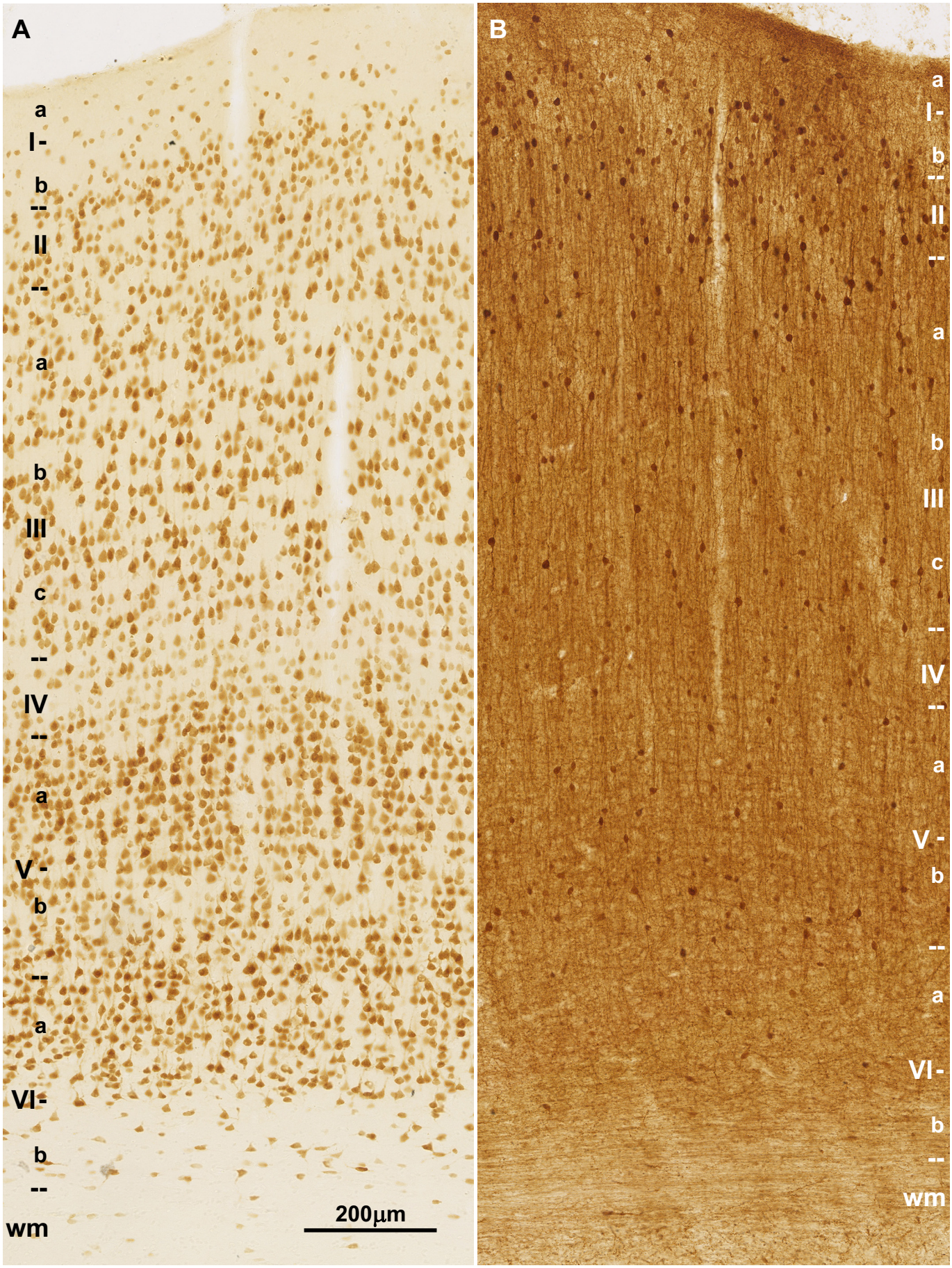


**Figure 5.17** Area **32** in monkey. Immunohistochemical anti-**NeuN** (A) and anti-**calretinin** (B) staining of neighboring sections.

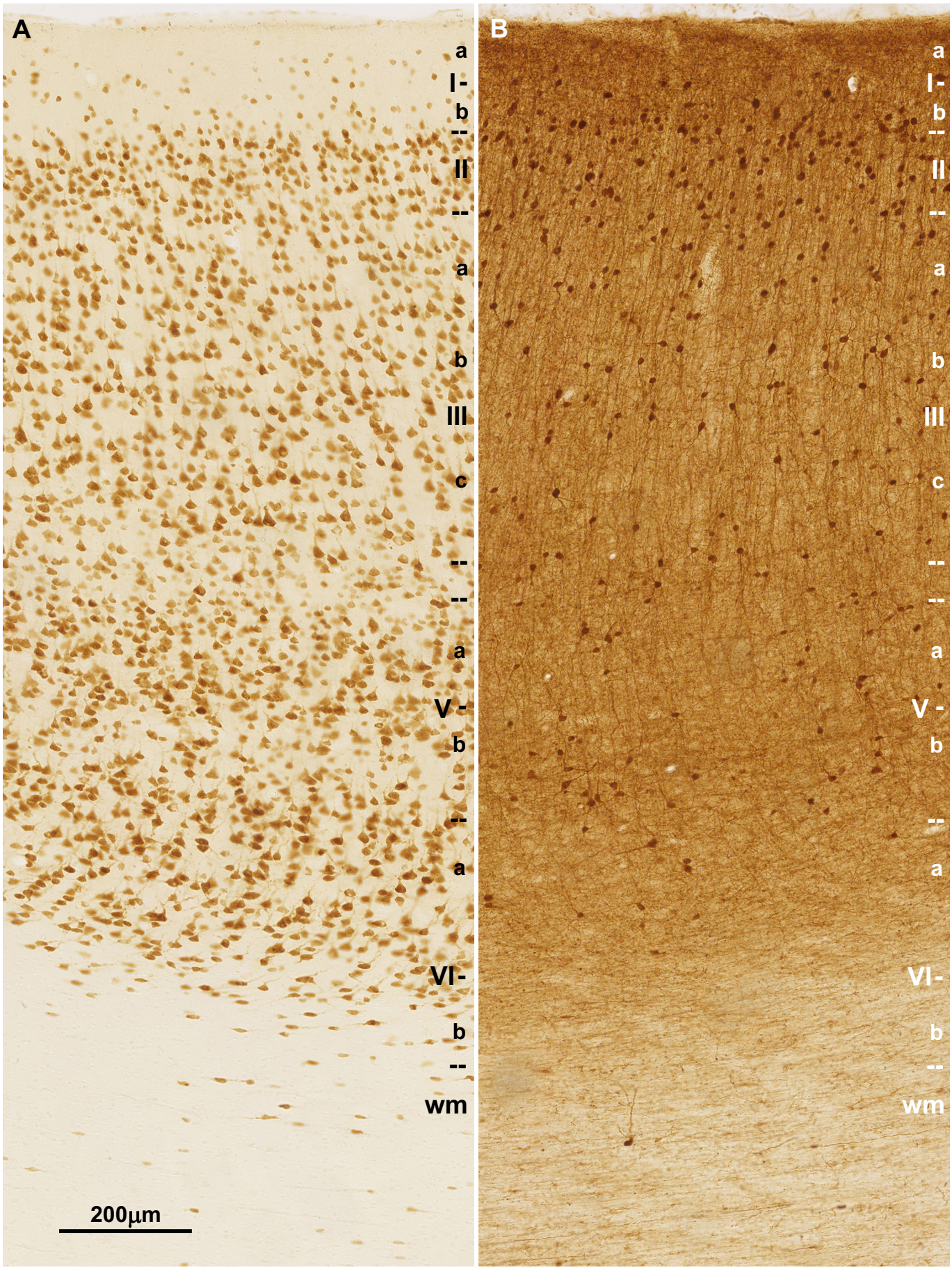


**Figure 5.18** Area **24** in monkey. Immunohistochemical anti-**NeuN** and anti-**calretinin** staining of neighboring sections.

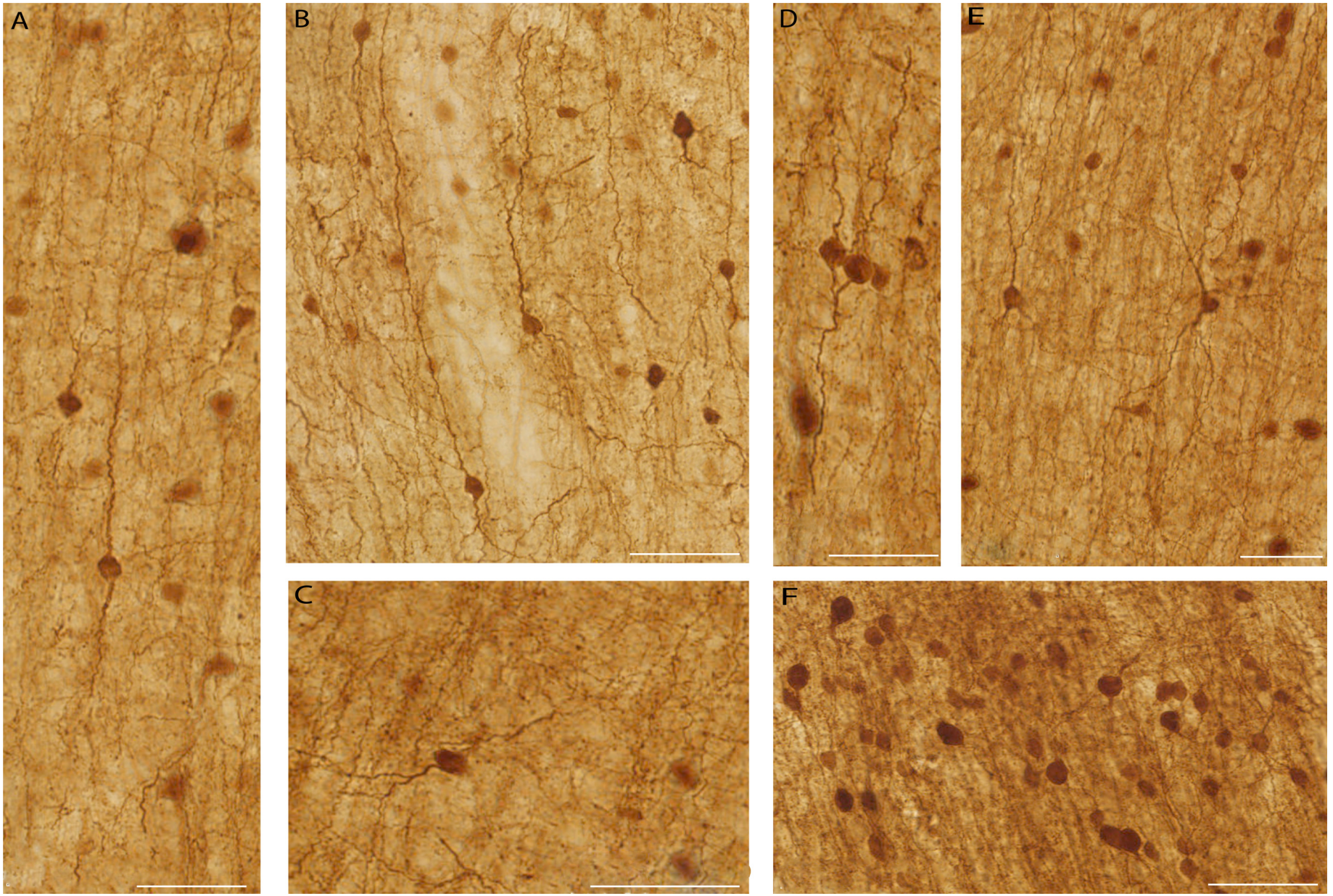


**Figure 5.19** Morphology of **calretinin neurons** in the monkey area 9 (A, B, E), 32 (F) and 24 (C, D) show different morphology: neurons with prominent ascending dendrite (A, B), deep located neurons with horizontally directed processes (C), neurons with bipolar/bitufted morphology (D), a multipolar neuron (E) and oval neurons of layer II. Scale bar - 50µm.

### 5.3.1 Quantitative analysis of calretinin neurons throughout cortical layers

Quantitative analysis did not reveal differences in laminar distribution, density and proportion between the analyzed areas. In all areas (9, 34, 24) around 3/4 of calretinin neurons were located in upper (I-III) cortical layers with 40-45% located in layers I and II (Table 5.4; Figure 5.20 A, B).

**Table 5.4 Laminar distribution of calretinin labeled neurons** in monkey (relative distribution (%) per layer).

| | **Area 9** | SD | **Area 32** | SD | **Area 24** | SD |
|---|---|---|---|---|---|---|
| Ia | **1.9%** | 1.2% | **2.1%** | 1.6% | **1.9%** | 0.4% |
| Ib | **8.8%** | 3.3% | **8.9%** | 4.3% | **10.8%** | 2.5% |
| II | **35.0%** | 13.0% | **31.5%** | 6.1% | **27.4%** | 4.2% |
| III | **31.1%** | 7.2% | **30.6%** | 3.8% | **33.9%** | 2.8% |
| IV | **4.4%** | 1.6% | **4.4%** | 0.8% | **Ø** | **ø** |
| Va | **7.2%** | 2.7% | **6.3%** | 1.0% | **7.4%** | 0.6% |
| Vb | **4.5%** | 1.5% | **5.5%** | 1.6% | **6.7%** | 2.0% |
| VIa | **3.5%** | 1.8% | **6.3%** | 1.4% | **5.4%** | 0.8% |
| VIb | **1.6%** | 0.8% | **2.5%** | 0.9% | **3.0%** | 0.9% |
| WM | **2.0%** | 1.0% | **2.0%** | 1.1% | **3.7%** | 0.9% |

**Table 5.5 Density of calretinin labeled neurons** per layer in monkey areas 9, 32 and 24 (1000 cells/mm$^3$)

| | **Area 9** | SD | **Area 32** | SD | **Area 24** | SD |
|---|---|---|---|---|---|---|
| Ia | **2.4** | 0.9 | **2.7** | 1.9 | **3.2** | 0.7 |
| Ib | **16.7** | 5.4 | **10.0** | 3.6 | **13.9** | 3.1 |
| II | **25.5** | 13.7 | **17.8** | 5.7 | **26.4** | 13.5 |
| III | **9.3** | 6.6 | **6.4** | 1.6 | **9.9** | 4.3 |
| IV | **7.1** | 4.8 | **3.8** | 1.4 | **Ø** | **ø** |
| Va | **5.2** | 4.7 | **3.1** | 1.0 | **5.2** | 2.4 |
| Vb | **4.2** | 3.4 | **3.3** | 1.2 | **4.7** | 1.7 |
| VIa | **2.9** | 2.5 | **3.1** | 0.6 | **3.3** | 1.3 |
| VIb | **1.8** | 1.6 | **1.8** | 0.8 | **2.1** | 0.7 |
| WM | **1.2** | 1.0 | **0.9** | 0.9 | **0.8** | 0.4 |
| **I-VI** | **8.6** | 4.5 | **7.7** | 1.7 | **7.8** | 3.1 |
| **II-VI** | **8.0** | 4.8 | **7.8** | 2.4 | **7.7** | 3.4 |

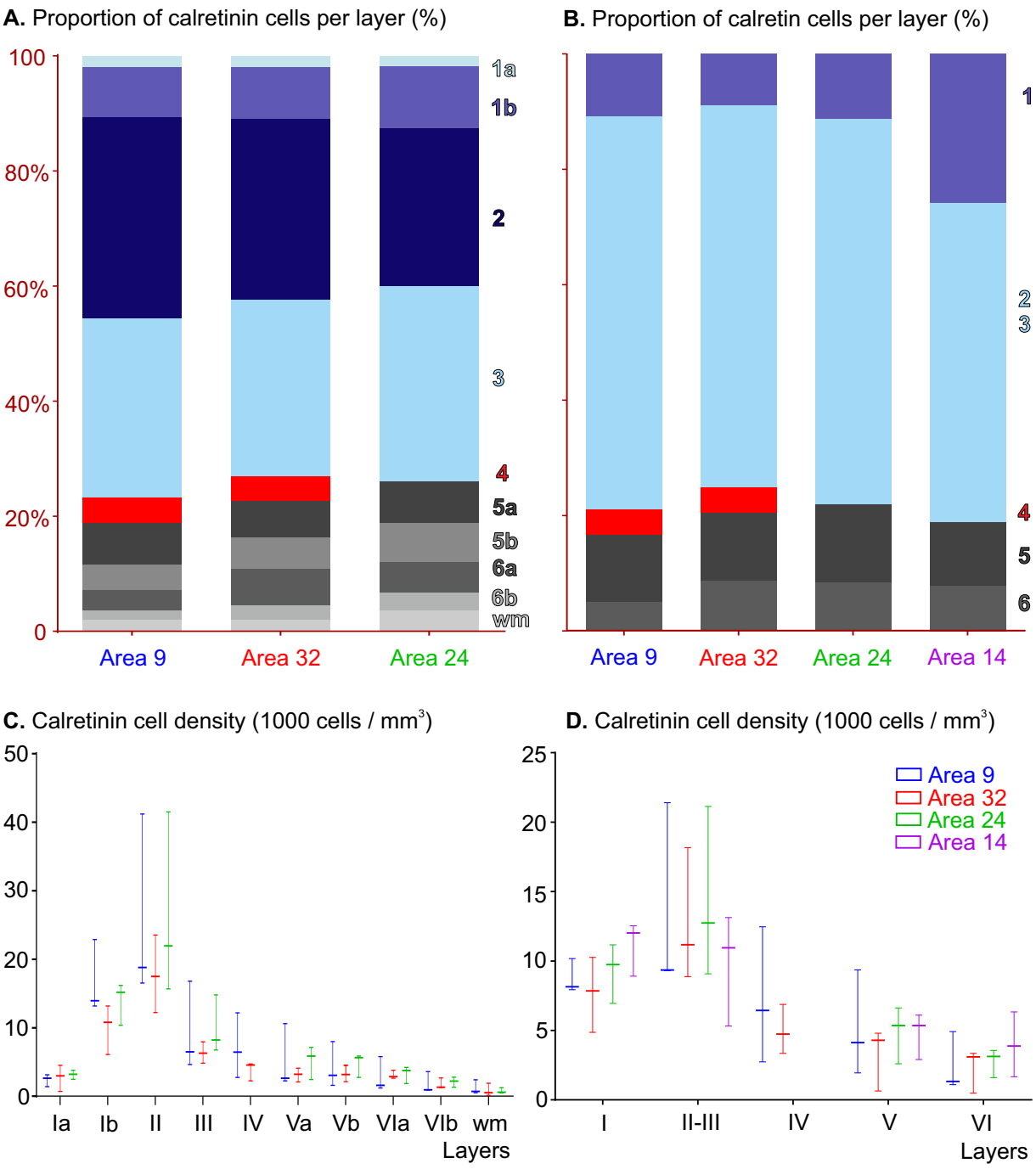


**Figure 5.20** Graphs show **laminar distribution** (A, B) and **density of calretinin** immunolabeled neurons in particular layer (C, D). Density is shown as 1000 of calretinin positive cells per 1mm$^3$. Values shown on graph B and D are values obtained in this study and presented in the way to be comparable with data from area 14 obtained in previous study (Džaja 2015, PhD Thesis).

In all areas examined, layer II and Ib have higher density of calretinin neurons than other cortical layers (Table 5.5; Figure 5.20 C,D). The layer Ib has significantly higher proportion (43%) of calretinin containing neurons than other layers (ANOVA, SNK-post hoc, p=0.0002). Taken together, in all cortical layers around 10 000 neurons per $mm^3$ contain calretinin. Thus, calretinin neurons represent at least 15% of cortical neurons. These calretinin neurons are most densely packed in layer II of area 9 and 24, with an average of 26 000 neurons per $mm^3$. The lower layers (IV-VI) have lower densities, with an average of 5000 neurons per $mm^3$ confirming qualitative observations.

**Table 5.6 Proportion of calretinin labeled neurons** in areas 9, 32 and 24 in monkey (number of calretinin neurons / total number (NeuN) of neurons – shown as %).

| | **Area 9** | SD | **Area 32** | SD | **Area 24** | SD |
|---|---|---|---|---|---|---|
| Ia | **33.5%** | 16.6% | **29.1%** | 17.4% | **32.9%** | 15.4% |
| Ib | **43.4%** | 12.9% | **44.3%** | 25.5% | **40.3%** | 4.1% |
| II | **26.1%** | 10.9% | **34.1%** | 12.7% | **26.3%** | 12.3% |
| III | **13.5%** | 6.4% | **18.7%** | 6.0% | **15.9%** | 4.1% |
| IV | **8.7%** | 4.9% | **8.2%** | 3.1% | **Ø** | Ø |
| Va | **6.5%** | 2.8% | **5.9%** | 1.0% | **7.3%** | 3.0% |
| Vb | **6.9%** | 3.8% | **8.2%** | 1.7% | **7.9%** | 0.8% |
| VIa | **4.9%** | 2.9% | **8.1%** | 0.7% | **6.1%** | 1.8% |
| VIb | **4.3%** | 2.2% | **4.9%** | 1.5% | **5.8%** | 0.5% |
| WM | **14.2%** | 6.6% | **29.6%** | 3.3% | **20.7%** | 9.4% |
| **I-VI** | **13.2%** | 4.1% | **15.3%** | 3.2% | **14.0%** | 3.0% |
| **II-VI** | **12.2%** | 4.2% | **14.2%** | 3.6% | **12.8%** | 3.2% |

The proportion of calretinin neurons in layer Ia (32%) and layer II (29%) is also significantly higher (ANOVA, SNK-post hoc, p=0.0002) when compared to all other layers (Table 5.6). In layer III the proportion of calretinin neurons (16%) is 2-3 times higher but not statistically significant than in layers IV-VI (5%-8.5%) due to high inter-individual differences. Calretinin proportion in layer III varies between subjects up to 3 fold (8% to 24%) (Table 5.7; Figure 5.21 A, B).

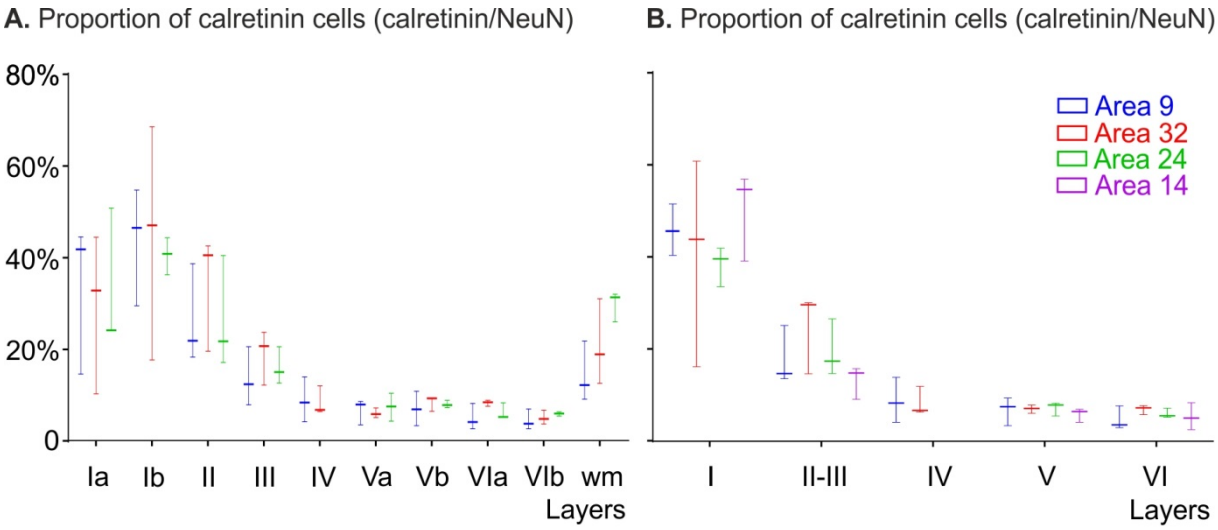


**Figure 5.21** Graphs show **proportion of calretinin labeled neurons** (number of calretinin labeled per number of NeuN labeled cells) in particular layer. Values shown on graph B are values obtained in this study and presented in the way to be comparable with data from area 14 obtained in previous study (Džaja 2015, PhD Thesis).

In layer I, the lower part contains more than 80% of layer I neurons expressing calretinin and they are relatively densely packed, with an average of 13 000 per $mm^3$, that is more than in any other layer. Despite the gradual decrease in neuronal (NeuN) density through layer VI and underlying white matter, the calretinin proportion is around 4–5 times higher in underlying white mater (14%-30%) than in layer VIb. This proportion is comparable to that of calretinin neuron in layer III and is significantly higher than proportion found in lower layers (IV-VI) (Table 5.5, 5.6; Figure 5.20, 5.21). This shows that the layer VIb is clearly different in density and proportion of calretinin neurons from cortical lamina, but also from deep part of white mater.

**Table 5.7.** Proportion of calretinin **labeled neurons** in areas 9, 32 and 24 shown for each monkey (number of calretinin neurons / total number (NeuN) of neurons – shown as %).

| layers | **area 9** | | | **area 32** | | | **area 24** | | |
|---|---|---|---|---|---|---|---|---|---|
| | MV | MVII | MVIII | MV | MVII | MVIII | MV | MVII | MVIII |
| Ia | 14.4% | 44.3% | 41.6% | 10.1% | 44.3% | 32.7% | 23.9% | 50.6% | 24.0% |
| Ib | 46.3% | 29.3% | 54.6% | 17.5% | 68.4% | 46.9% | 36.1% | 40.7% | 44.2% |
| II | 38.5% | 21.7% | 18.2% | 40.4% | 42.4% | 19.4% | 40.3% | 17.0% | 21.6% |
| III | 20.4% | 7.7% | 12.2% | 23.6% | 20.5% | 12.0% | 20.4% | 12.5% | 14.8% |
| IV | 13.8% | 4.1% | 8.2% | 11.8% | 6.6% | 6.2% | Ø | Ø | Ø |
| Va | 8.5% | 3.4% | 7.8% | 7.0% | 5.0% | 5.7% | 7.4% | 4.2% | 10.2% |
| Vb | 10.7% | 3.2% | 6.7% | 9.1% | 6.3% | 9.2% | 8.7% | 7.1% | 7.7% |
| VIa | 8.1% | 2.5% | 4.0% | 7.4% | 8.7% | 8.3% | 5.1% | 5.1% | 8.2% |
| VIb | 6.8% | 3.6% | 2.5% | 3.6% | 4.6% | 6.6% | 5.3% | 6.2% | 5.8% |
| WM | 21.6% | 9.0% | 12.0% | 18.8% | 12.4% | 30.9% | 25.8% | 31.2% | 31.9% |
| **I-VI** | **17.8%** | **9.7%** | **12.1%** | **16.7%** | **10.8%** | **14.4%** | **17.6%** | **16.5%** | **11.6%** |
| **II-VI** | **16.9%** | **9.1%** | **10.7%** | **15.9%** | **9.5%** | **12.9%** | **17.7%** | **14.4%** | **10.6%** |

## 5.4. Double labeling of GABAergic subpopulations in areas 9, 32, 24 and 14

The distribution pattern and morphology of calretinin neurons observed using immunohistofluorescent detection (both polyclonal and monoclonal antibodies) were similar to that observed when using DAB immunohistochemistry (see Figure 5.22).

Simultaneous immunohistofluorescent detection of calretinin with parvalbumin or calbindin, showed that the population of calretinin neurons does not overlap with the other two major subpopulations of GABAergic neurons expressing calcium binding proteins, neither with neurons expressing somatostatin (Table 5.8).

**Table 5.8.** Densities of calretinin, calbindin and parvalbumin labeled neurons (number of neurons / $mm^2$) and density of double labeled cells in monkey areas 9, 32, 24 and 14.

| **calretinin (polyclonal)** / **calbindin** double labeled sections | | | | | | |
|---|---|---|---|---|---|---|
| | **calretinin** | **SD** | **calbindin** | SD | co-localized | SD |
| **area 9** | **5.21** | 2.70 | **1.95** | 1.21 | **0.04** | 0.09 |
| **area 32** | **5.46** | 3.09 | **2.54** | 1.17 | **0.02** | 0.03 |
| **area 24** | **5.84** | 2.57 | **2.59** | 1.29 | **0.00** | 0.01 |
| **area 14** | **5.31** | 2.45 | **3.30** | 1.47 | **0.03** | 0.03 |
| | | | | | | |
| **calretinin (polyclonal)** / **parvalbumin** double labeled sections | | | | | | |
| | **calretinin** | SD | **parvalbumin** | SD | co-localized | SD |
| **area 9** | **5.35** | 2.01 | **2.70** | 0.84 | **0** | 0 |
| **area 32** | **5.54** | 2.43 | **1.72** | 0.75 | **0** | 0 |
| **area 24** | **6.37** | 3.13 | **2.80** | 1.67 | **0** | 0 |
| **area 14** | **4.13** | 0.95 | **1.91** | 1.18 | **0** | 0 |
| | | | | | | |
| **calretinin (monoclonal)** / **somatostatin** double labeled sections | | | | | | |
| | **calretinin** | SD | **somatostatin** | SD | co-localized | SD |
| **area 9** | **3.48** | 0.67 | **0.27** | 0.16 | **0.05** | 0.06 |
| **area 32** | **4.18** | 0.90 | **0.43** | 0.29 | **0.03** | 0.03 |
| **area 24** | **4.92** | 1.26 | **0.39** | 0.15 | **0.03** | 0.04 |
| **area 14** | **3.84** | 0.91 | **0.38** | 0.18 | **0.02** | 0.02 |

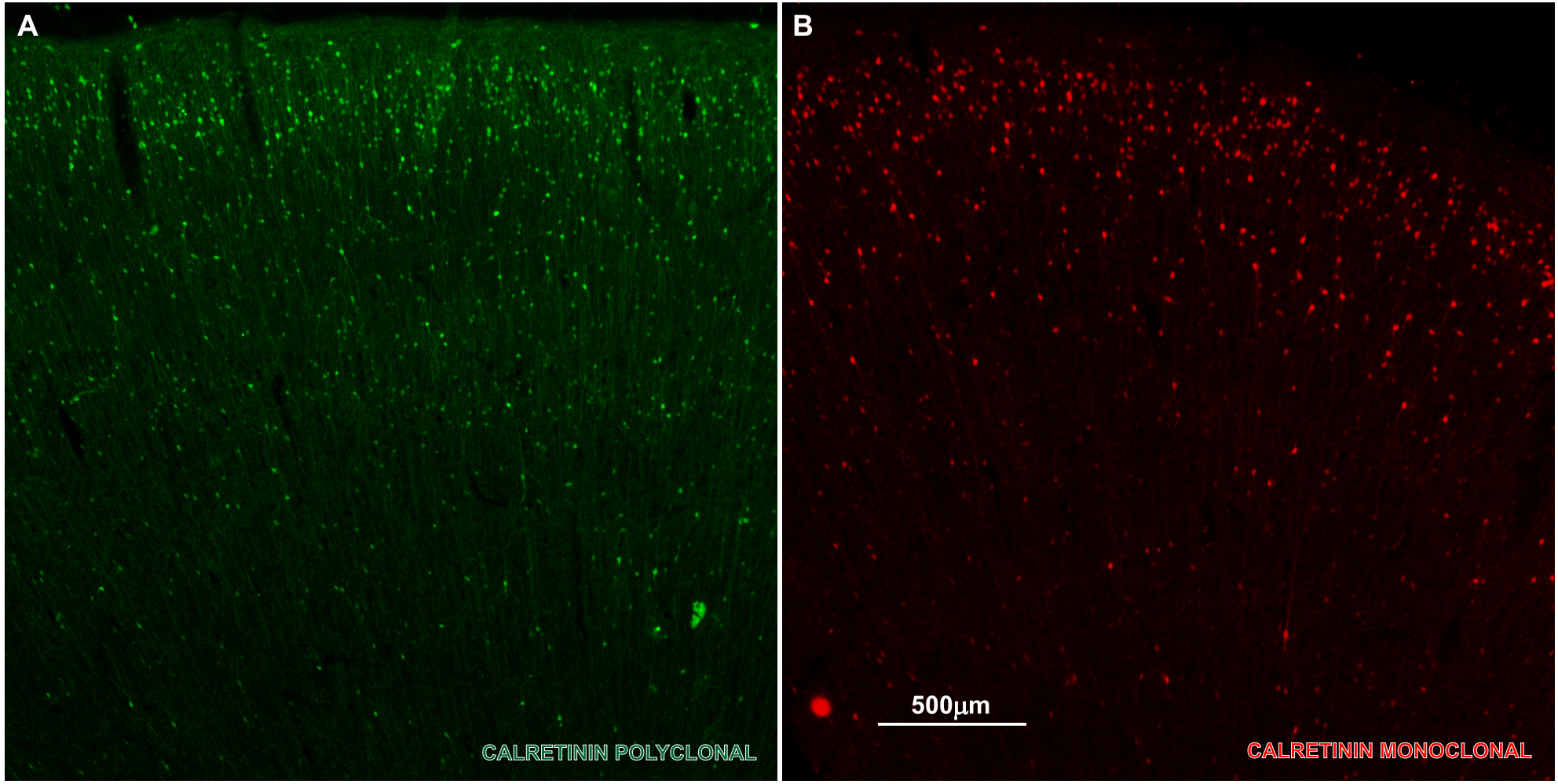


**Figure 5.22** Immunohistofluorescent labeling showing similarities in laminar distribution and density of **calretinin** neurons labeled with polyclonal (A) and monoclonal (B) antibody in monkey area **9**.

### 5.4.1. Quantitative analysis of double labeled sections in monkey

Quantitative analysis was performed by counting number of neurons on double-labeled sections stained with calretinin and parvalbumin, calbindin or somatostatin, in areas 9, 32, 24 and 14 (Figure 5.23). No regional differences were observed, regarding density (per surface) of the different populations of labeled neurons (Figure 5.24A, Table 5.8) or regarding the proportions of calretinin neurons among the entire population of calcium binding protein containing neurons (Figure 5.24B, Table 5.9).

We observed a high variability in this proportion of calretinin-labeled neurons from one section to another one (10 fold between lowest and highest value; Figure 5.24B). This was not related to particular region neither to a particular animal.

Not a single cell co-localizing calretinin and parvalbumin was found in analyzed sections. Co-localization with somatostatin and calbindin was found in less than 1% of the calretinin immunoreactive neurons (Table 5.8).

**Table 5.9.** The ratio between distinct GABAergic subpopulations on double labeled sections in areas 9, 32, 24 and 14.

| | **calretinin / calbindin** | | **calretinin / parvalbumin** | | **calretinin / somatostatin** | |
|---|---|---|---|---|---|---|
| | ratio | SD | ratio | SD | ratio | SD |
| **area 9** | **3.19** | 1.58 | **2.07** | 0.72 | **20.46** | 15.41 |
| **area 32** | **2.17** | 0.92 | **3.55** | 1.57 | **15.98** | 12.75 |
| **area 24** | **2.56** | 0.91 | **2.81** | 2.14 | **13.87** | 4.91 |
| **area 14** | **1.79** | 0.85 | **2.99** | 1.97 | **12.79** | 7.15 |

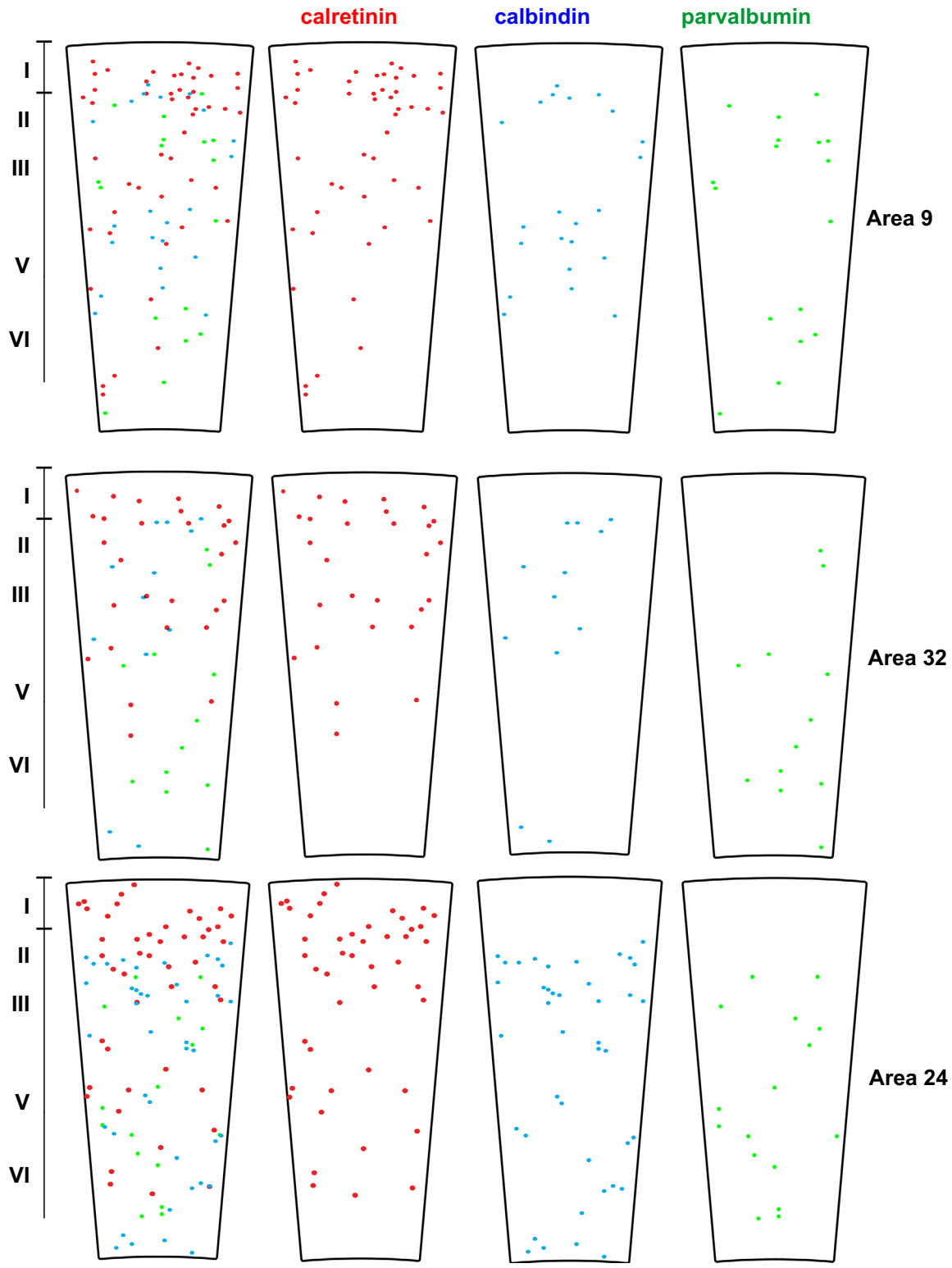


**Figure 5.23** Laminar distribution of immunofluorescent **calretinin**, **calbindin** and **parvalbumin** labeled neurons in monkey areas **9**, **32** and **24**. Neurons from neighboring immunohistofluorescent double labeled sections are plotted to show their spatial relations and laminar distribution.

**A.** Neuron density (number of neurons / $mm^2$) on double labeled sections

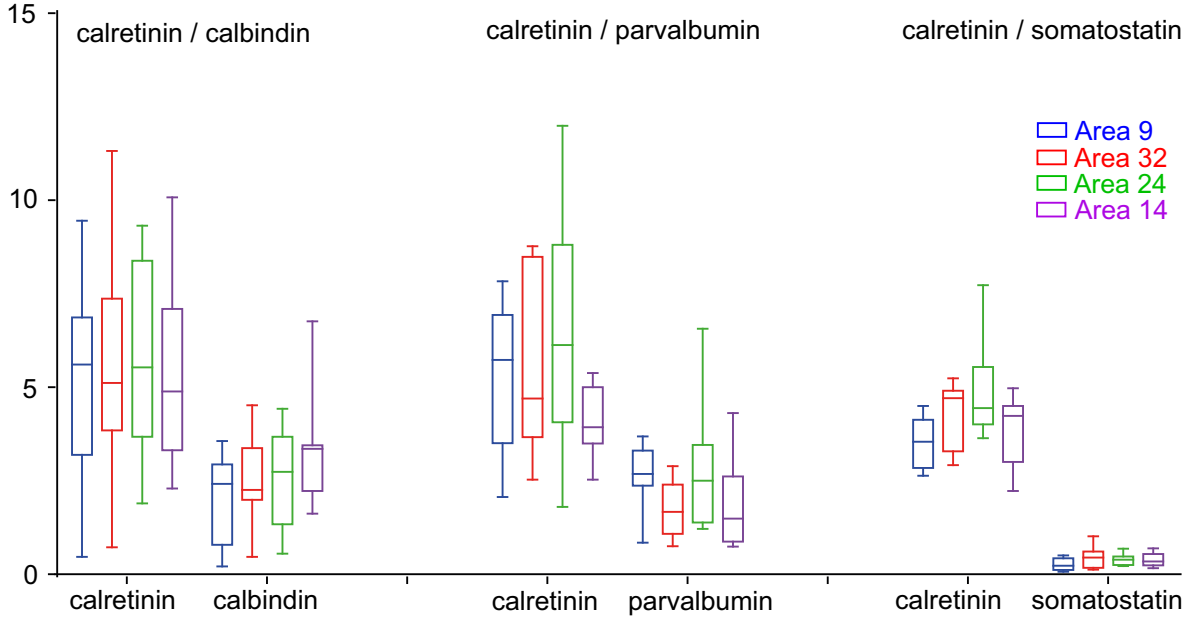


**B.** Ratio in number of neurons between different markers on double labeled sections

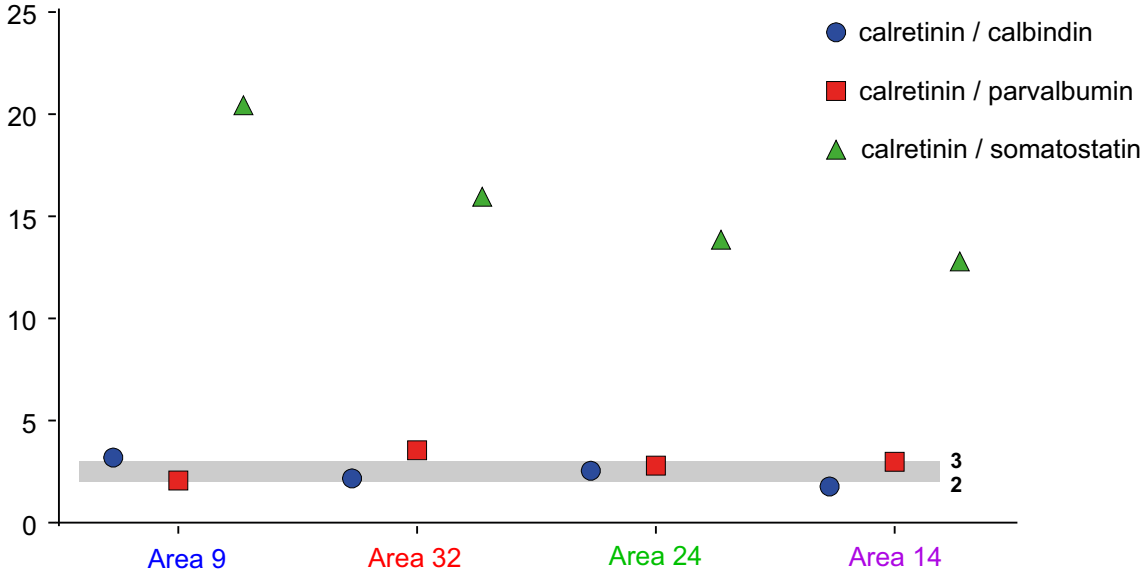


**Figure 5.24** Graphs are showing the density (A) and ratio (B) of **calretinin**, **calbindin**, **parvalbumin** and **somatostatin** immunohistochemically labeled neurons in monkey areas 9, 32, 24 and 14. Neurons are counted on Neurolucida software for **double labeled** analysis on calretinin/calbindin, calretinin/parvalbumin and calretinin/somatostatin sections.

### 5.4.2. Qualitative analysis of double labeled sections

Calbindin neurons, showed similar distribution as calretinin neurons (Figures 5.23 and 5.25), but calbindin neurons were not found in layer I, neither parvalbumin nor somatostatin stained neurons. Thus, from analyzed subpopulations, only calretinin neurons were found in layer I (Figure 5.26A).

Calbindin neurons were mainly found in layer II forming continuous belt of densely packed cells through layer II and relatively uniform distribution through all other cortical layers with slightly higher density in upper part of layer III (Figure 5.26B). No differences in the distribution and size of calbindin neurons were observed between area 9, area 32 and area 24 (Figures 5.23 and 5.25). Calbindin neurons are slightly bigger (diameter between 15-25μm) than calretinin ones and have a stellate shaped cell body and multidirectional dendrites. Calbindin was expressed in less than 1% of calretinin immunoreactive neurons.

Parvalbumin neurons were uniformly distributed through layers III – VI, having different laminar distribution then calretinin neurons. Also, in the middle layers there is a clear belt of parvalbumin reactive fibers (Figure 5.27). Most of parvalbumin labeled neurons have large oval-pyriform or triangular-multipolar somato-dendritic morphology (Figure 5.28). In layer V/VI the cell bodies of parvalbumin neurons are surrounded by calretinin labeled axon like processes with buttons, forming a calretinin reactive basket like structures around parvalbumin stained cell bodies (Figure 5.29). Small to medium sized, mainly oval-pyriform shaped parvalbumin reactive cells were the only parvalbumin cell class found in layer II, and were in area 9 more densely packed on this laminar position than in other two areas analyzed (Figure 5.23, 5.27, 5.28A).

Somatostatin neurons were sparsely located in the deep cortical layers (Figures 5.30 and 5.31) and in underlying white matter between the axon bundles without noticeable areal difference (Figure 5.31B). Most of them were medium to large multipolar and pyriform shaped cells with intensively stained cell bodies and long extending dendrites (Figure 5.31A). Few small round somatostatin labeled neurons are observed in layers II and III (Figure 5.32A) along with axon like somatostatin labeled processes displaying *en passant boutons*. These processes display horizontal orientation in superficial layers, being particularly dense in layer I (Figure 5.32B).

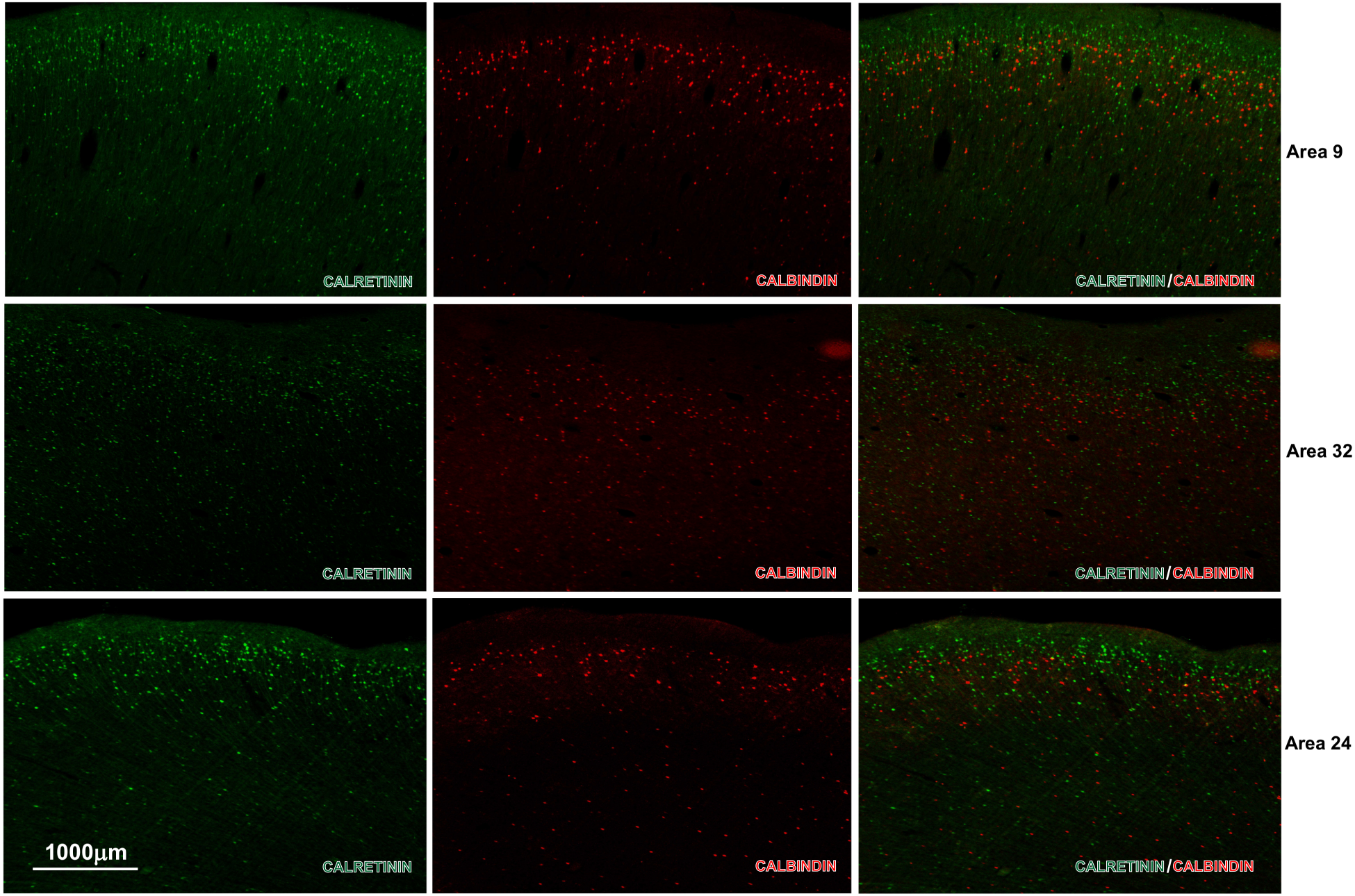


**Figure 5.25** Confocal acquisition of double labeled section using polyclonal antibody against **calretinin** (**green**) and monoclonal antibody against **calbindin** (**red**) in area **9** (upper row), **32** (middle row) and **24** (lower row) in monkey.

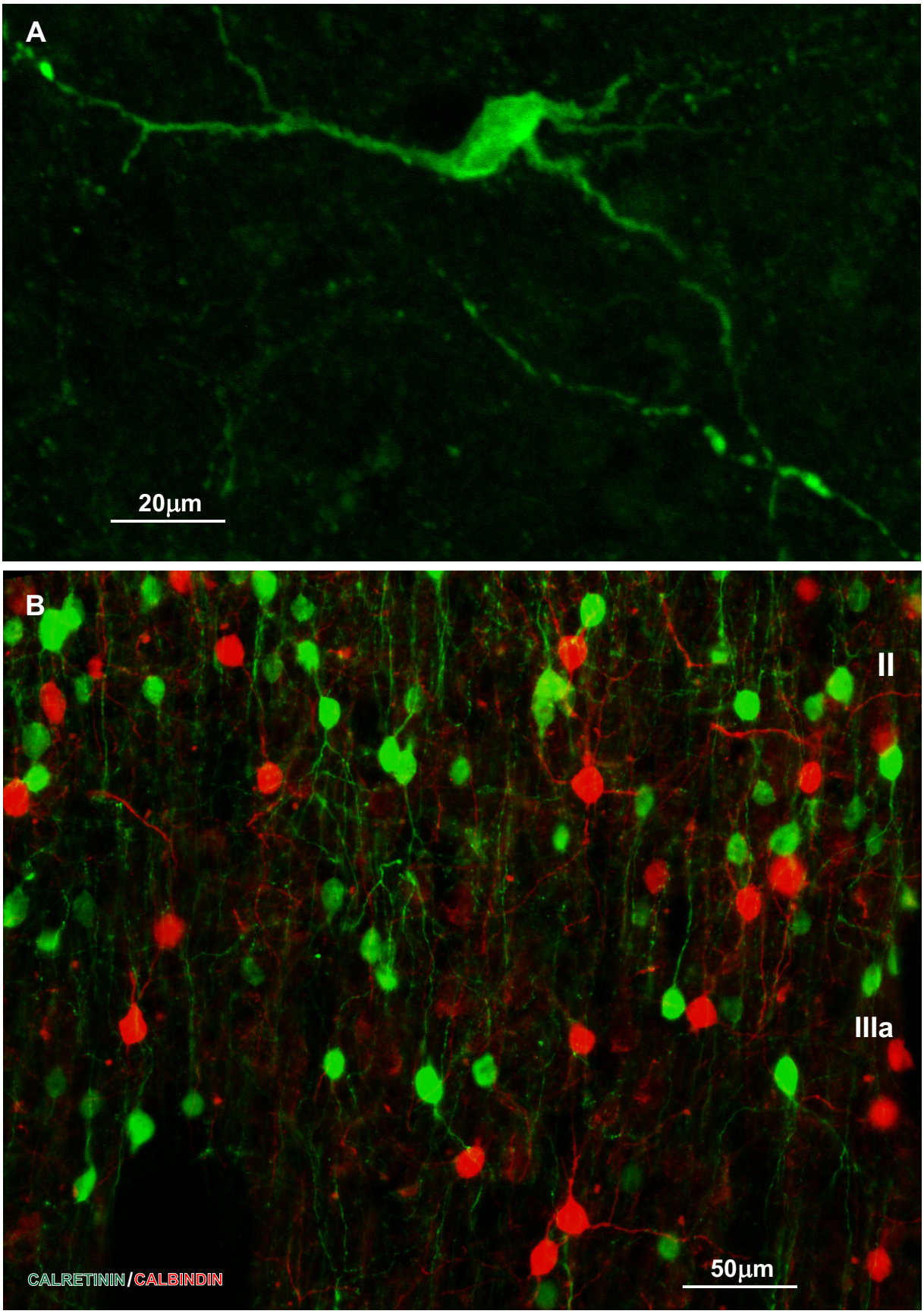


**Figure 5.26** Immunohistofluorescent labeling of Cajal-Retzius like **calretinin** labeled neuron of layer I in adult human area **9** (A) with long processes. A confocal acquisition of layer II and upper part of layer III double labeled (B) with polyclonal antibody against **calretinin** (**green**) and monoclonal antibody against **calbindin** (**red**) in monkey area **9**. In those layers calretinin and calbindin neurons are densely packed, but no co-localization is observed.

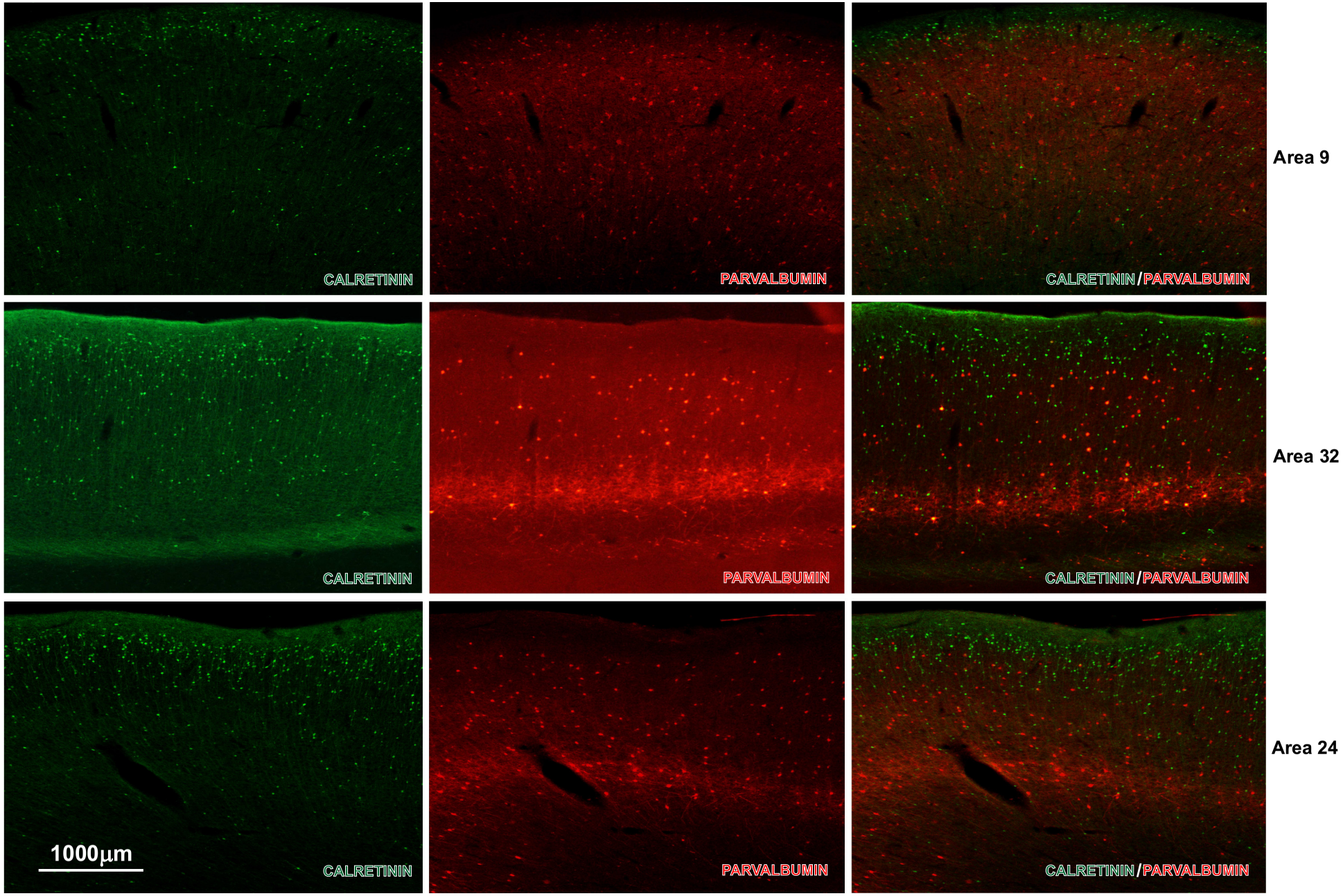


**Figure 5.27** Confocal acquisition of double labeled section using polyclonal antibody against **calretinin** (**green**) and monoclonal antibody against **parvalbumin** (**red**) in area **9** (upper row), **32** (middle row) and **24** (lower row) in monkey.

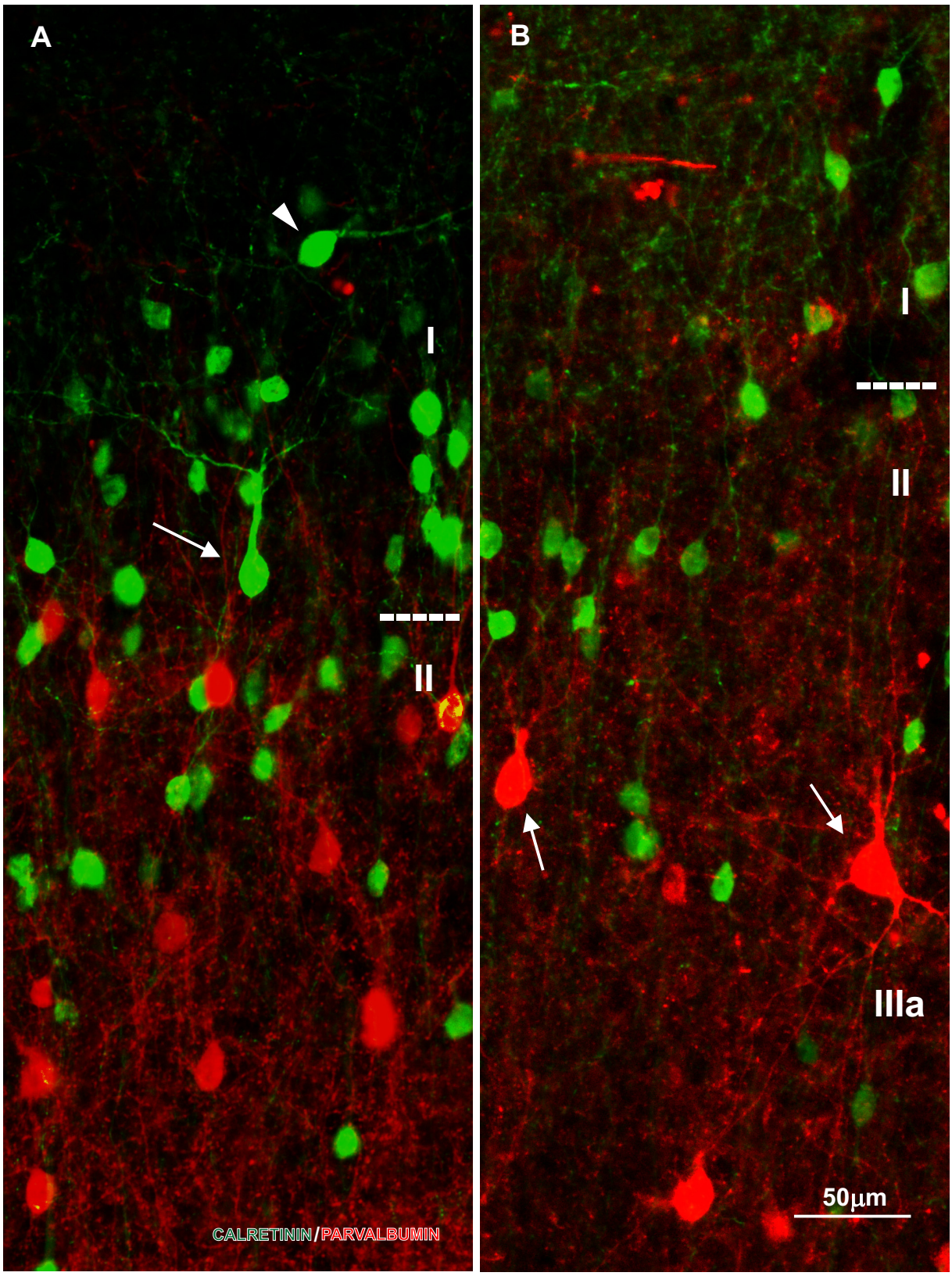


**Figure 5.28** Confocal acquisition of double labeled section using polyclonal antibody against **calretinin** (**green**) and monoclonal antibody against **parvalbumin** (**red**) of layers I and II in area **9** (A) and **32** (B) of monkey. In area 9 there is a higher density of small parvalbumin labeled neurons in layer II when compared to area 32. Arrows on panel B show a typical parvalbumin labeled neurons distributed uniformly through layers III-VI, that are larger than typical calretinin and calbindin labeled neurons. On panel A arrow indicates a pyriform shaped well bifurcated calretinin labeled neuron located around layer I/II border, and arrowhead indicates horizontal calretinin labeled neuron located in the upper part of layer I.

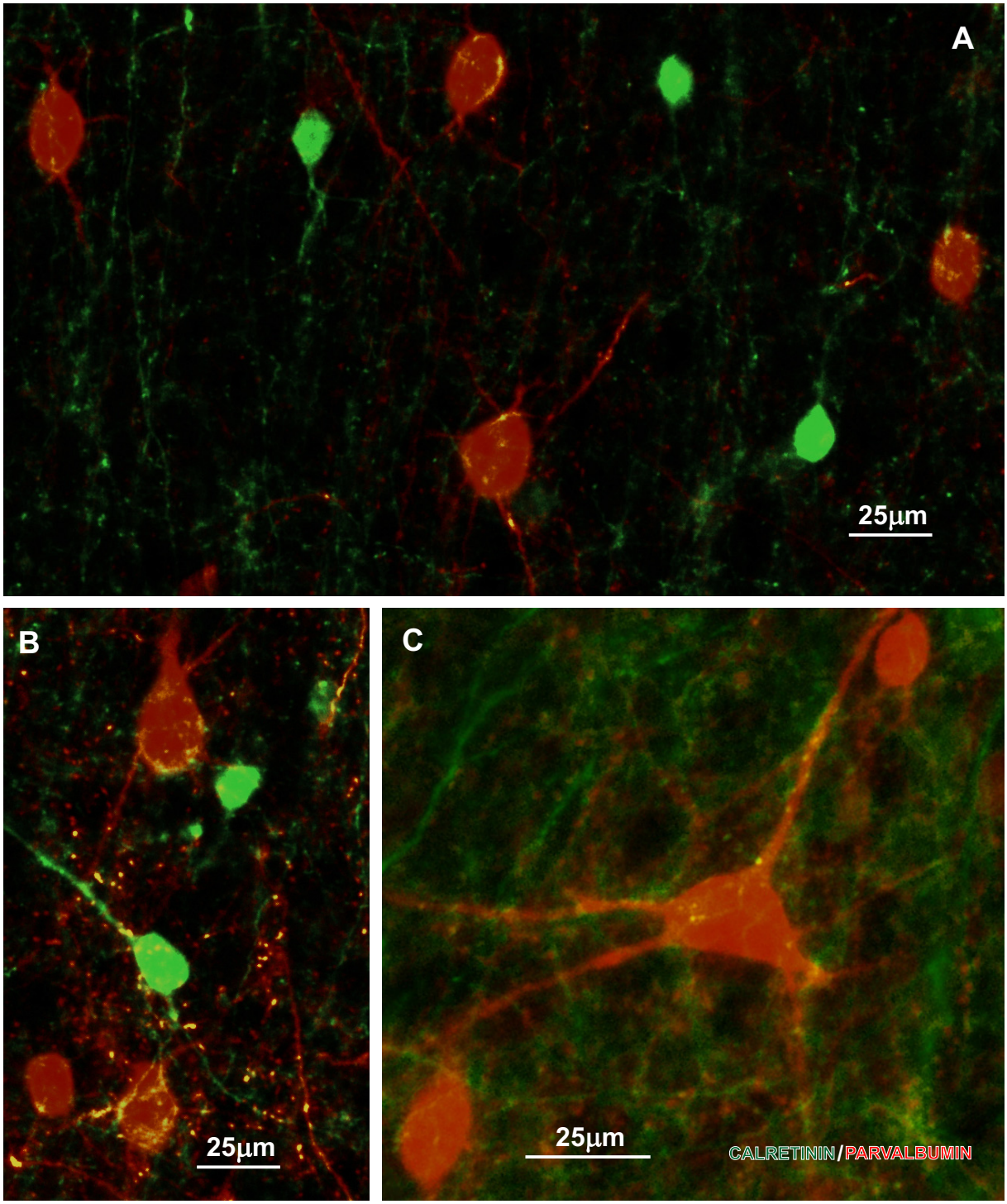


**Figure 5.29** Confocal acquisition of double labeled section using polyclonal antibody against **calretinin** (**green**) and monoclonal antibody against **parvalbumin** (**red**) in layers V/VI of area **32** (A, B) and **24** (C) of monkey. Calretinin neuron processes are forming a plexus around the soma and dendrites of parvalbumin neurons (yellow).

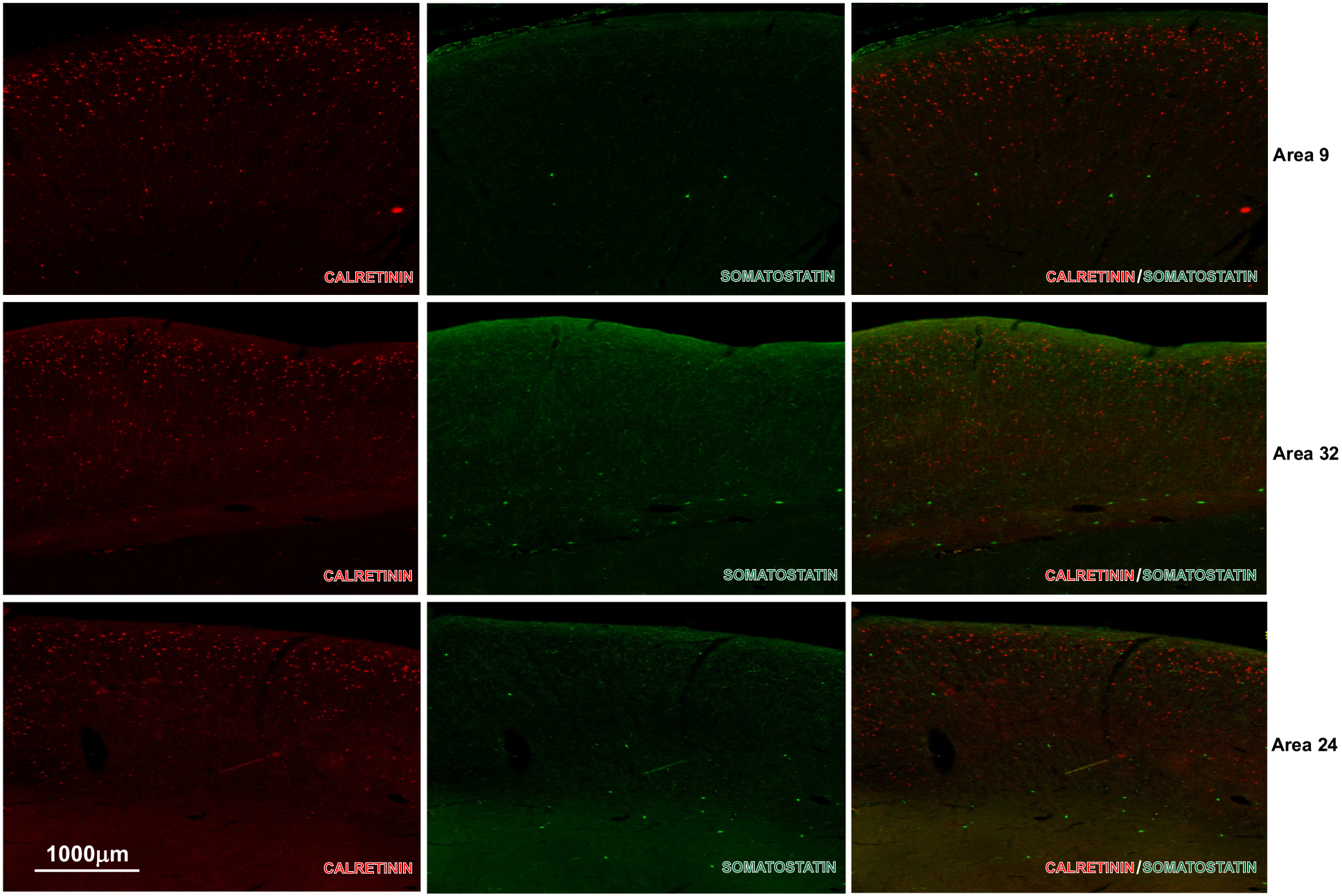


**Figure 5.30** Confocal acquisition of double labeled section using monoclonal antibody against **calretinin** (**red**) and polyclonal antibody against **somatostatin** (**green**) in area **9** (upper row), **32** (middle row) and **24** (lower row) in monkey.

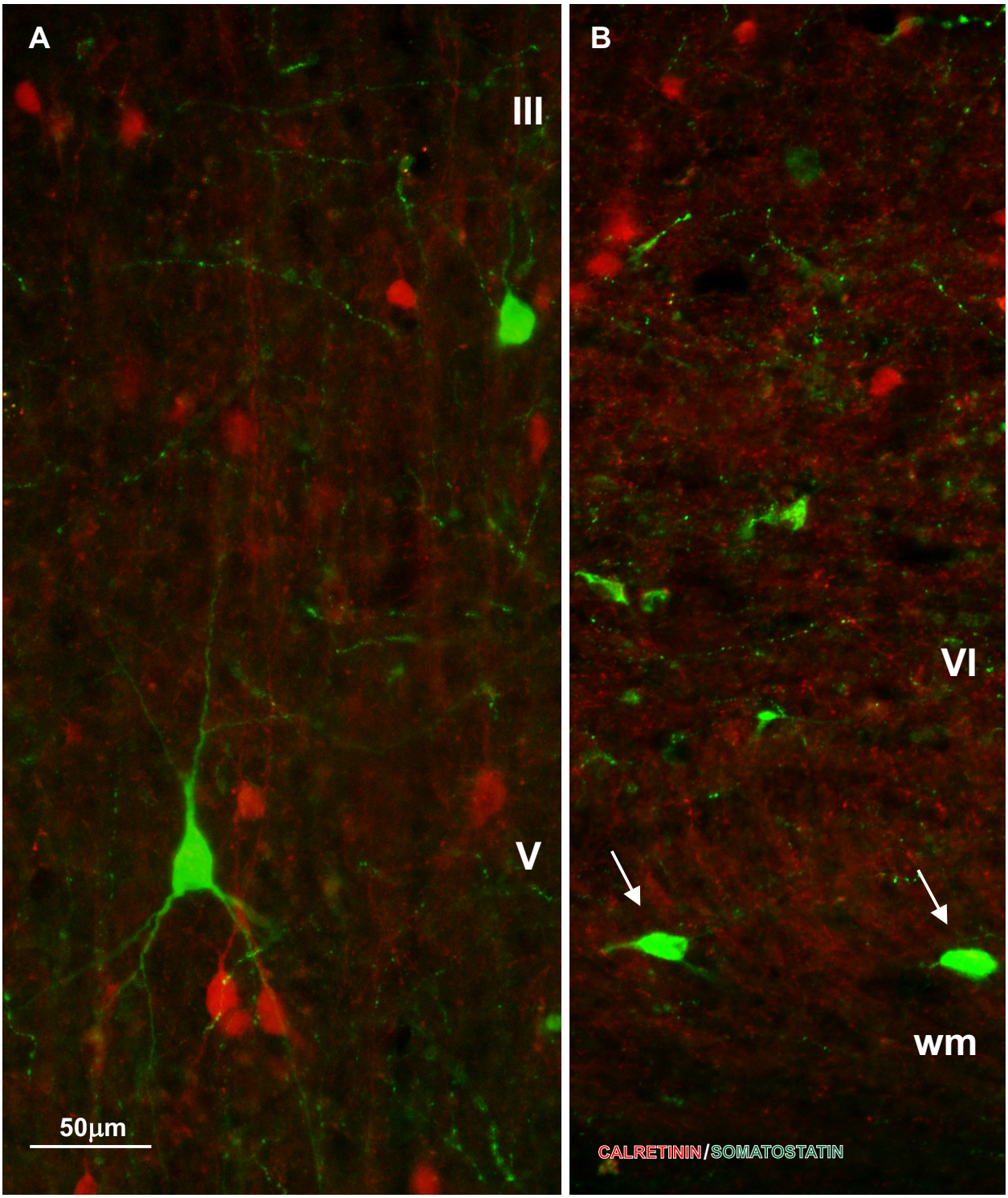


**Figure 5.31** Confocal acquisition of double labeled section using monoclonal antibody against **calretinin** (**red**) and polyclonal antibody against **somatostatin** (**green**) in layers III-VI of monkey areas **9** (A) and **32** (B). In layers II-VI, a typical large and well bifurcated somatostatin neurons are found. Arrows in the panel B point to horizontally oriented somatostatin neuron located at the border between cortex and white matter.

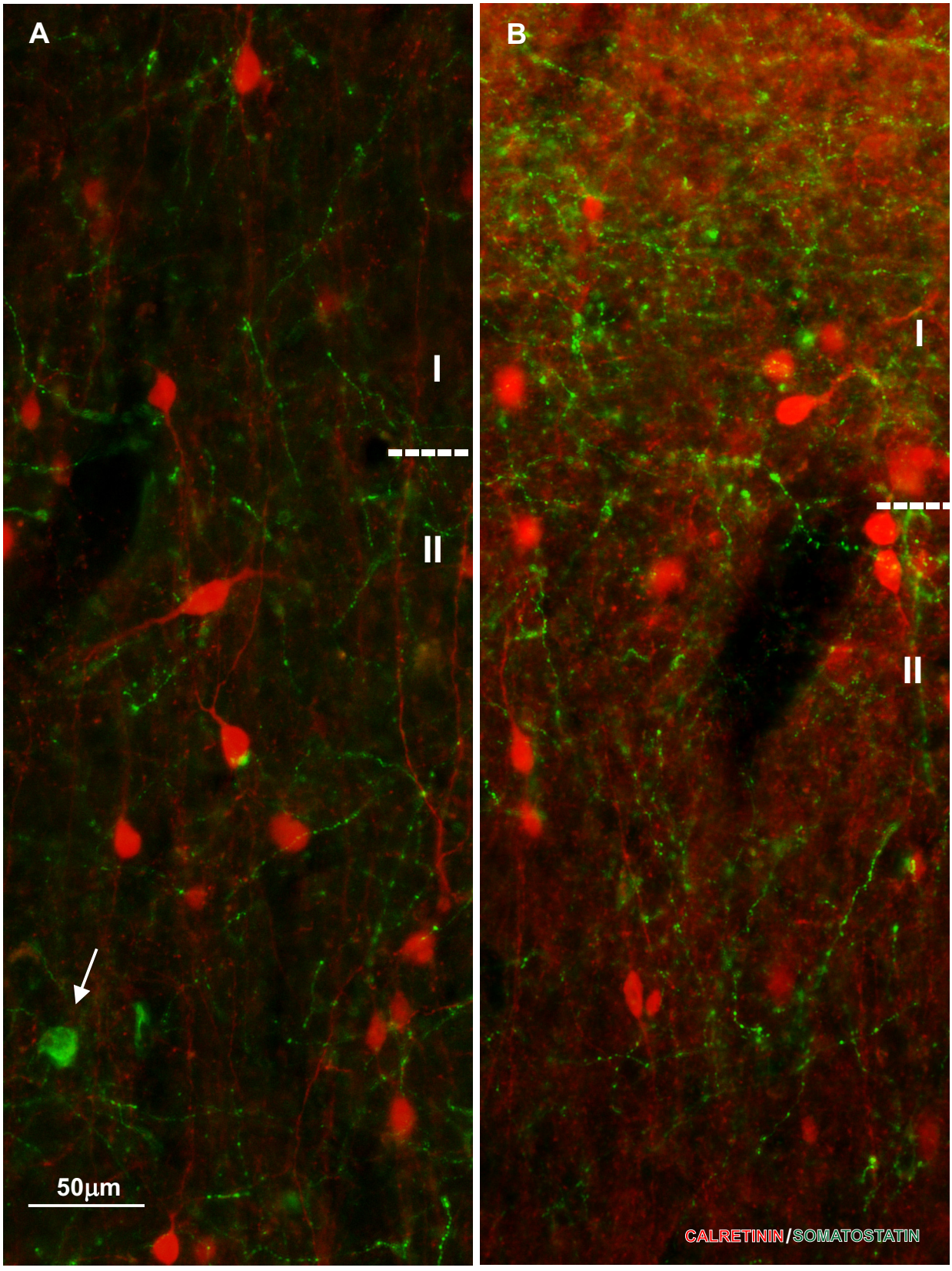


**Figure 5.32** Confocal acquisition of double labeled section with monoclonal antibody against **calretinin** (**red**) and polyclonal antibody against **somatostatin** (**green**) in layers I/II of monkey areas **9** (A) and **32** (B). In the upper cortical layers somatostatin labeled axonal plexuses are seen. Arrow points to a rare somatostatin neuron located here.

## 5.5. Simultaneous detection of VGAT/GAD65/GAD67 mRNA and calretinin in monkey and human prefrontal cortex

Simultaneous detection of calretinin and vesicular GABA transporter (VGAT) or two of the synthesizing enzymes for GABA, the glutamic acid decarboxylase 65 and 67 (GAD65 and GAD67) mRNAs were performed in order to determine whether calretinin neurons within the prefrontal cortex of monkey and human brain correspond to a subpopulation of GABAergic neurons. All calretinin neurons, observed across all cortical layers were found to express VGAT mRNA, both in monkey (Figures 5.33, 5.34, 5.35, 5.36) and the human prefrontal cortex (Figures 5.34, 5.37). Among these calretinin neurons none of them was found to express GAD65 mRNA in monkey despite the high number of GAD65 mRNA containing neurons observed (Figure 5.38). We further examined whether those neurons express the other synthesizing enzyme for GABA, GAD67 in the human prefrontal cortex. GAD67 mRNA containing neurons were distributed throughout all cortical layers (Figure 5.39). We demonstrate that almost all calretinin neurons express GAD67 mRNA in the human prefrontal cortex (Figure 5.40).

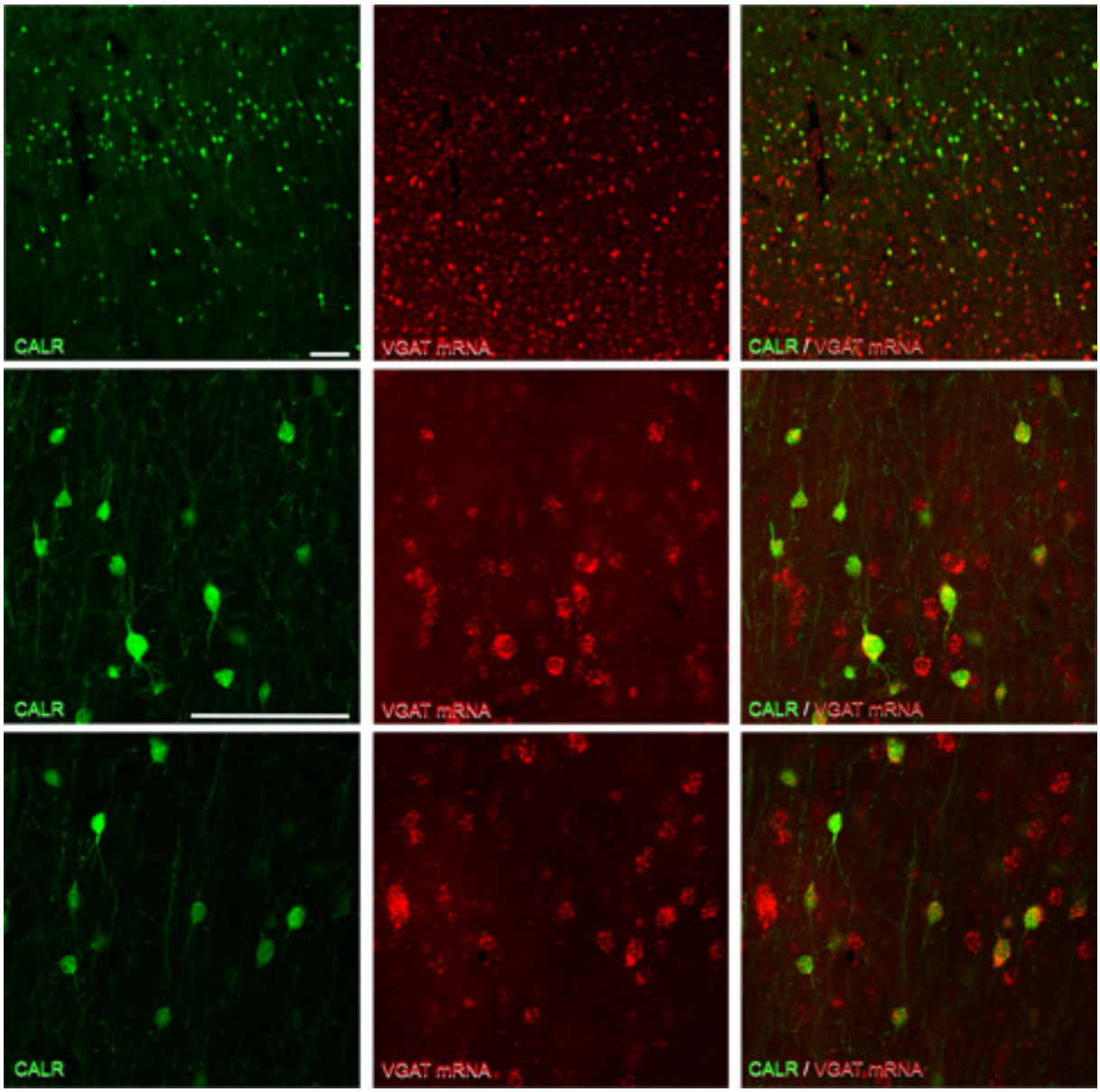


**Figure 5.33** Confocal acquisition of *RNAscope* in situ hybridization combining **VGAT** (**red**) expression with **calretinin** (**green**) immunohistochemistry in the monkey area **9** showing that all calretinin neurons express VGAT.

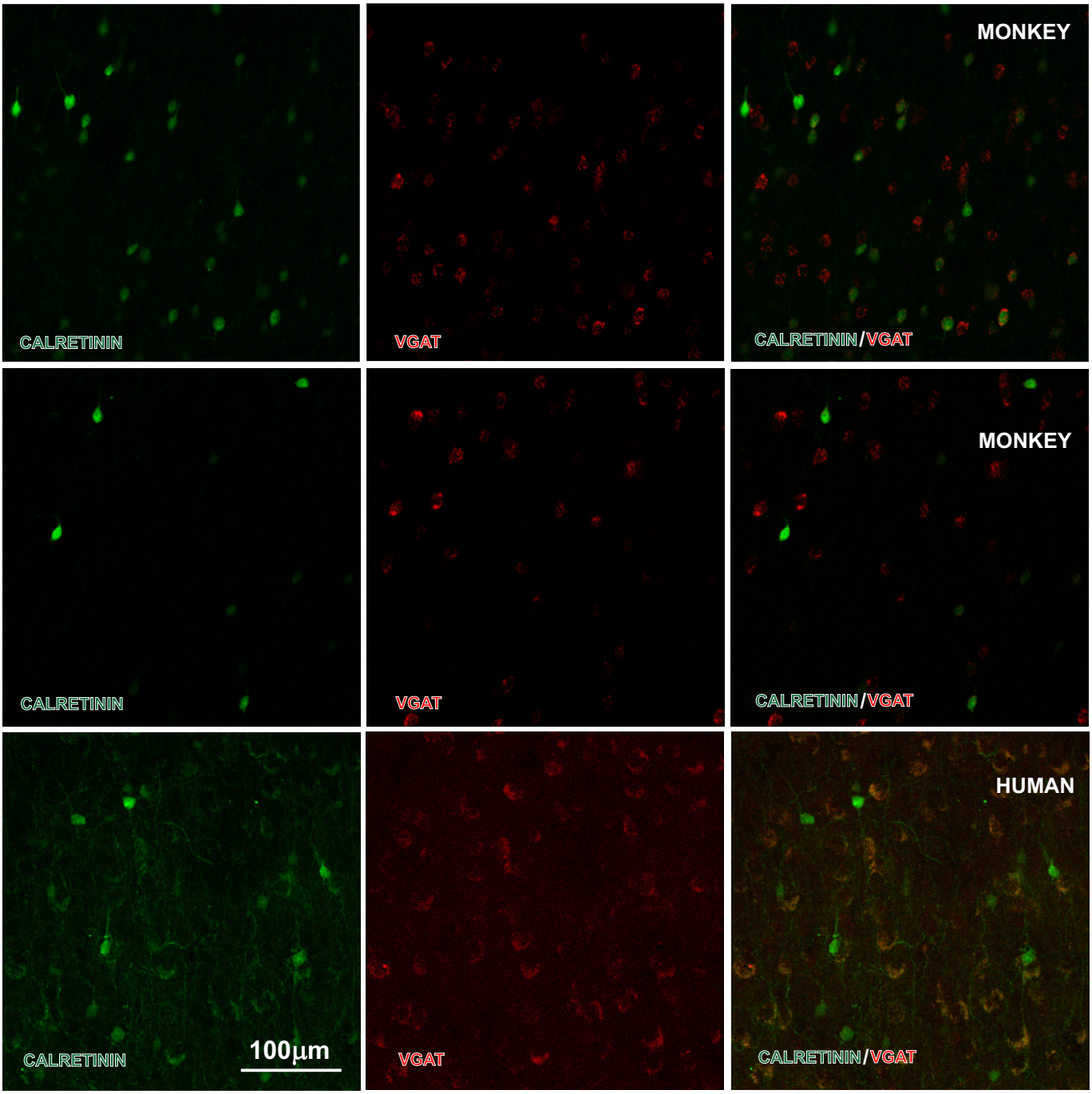


**Figure 5.34** Confocal acquisition of *RNAscope* in situ hybridization combining **VGAT** (**red**) expression with **calretinin** (**green**) immunohistochemistry in the layer II (upper row) and layer V of **monkey** and layer II of **human** area **9**. All calretinin neurons express VGAT.

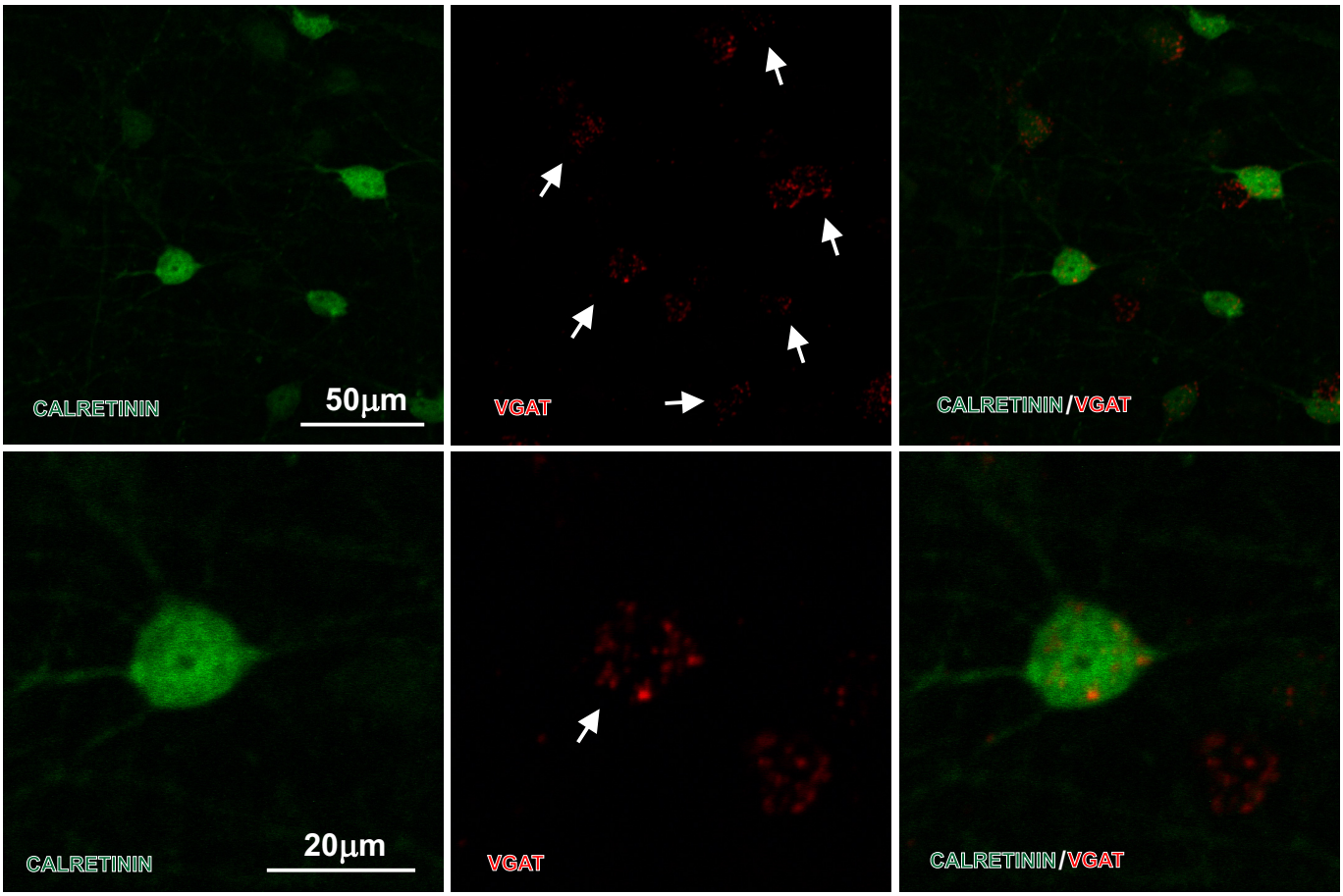


**Figure 5.35** Confocal acquisition of *RNAscope* in situ hybridization combining **VGAT** (**red**) expression with **calretinin** (**green**) immunohistochemistry in the layer II of **monkey** area **32** showing that all calretinin neurons express VGAT (arrows).

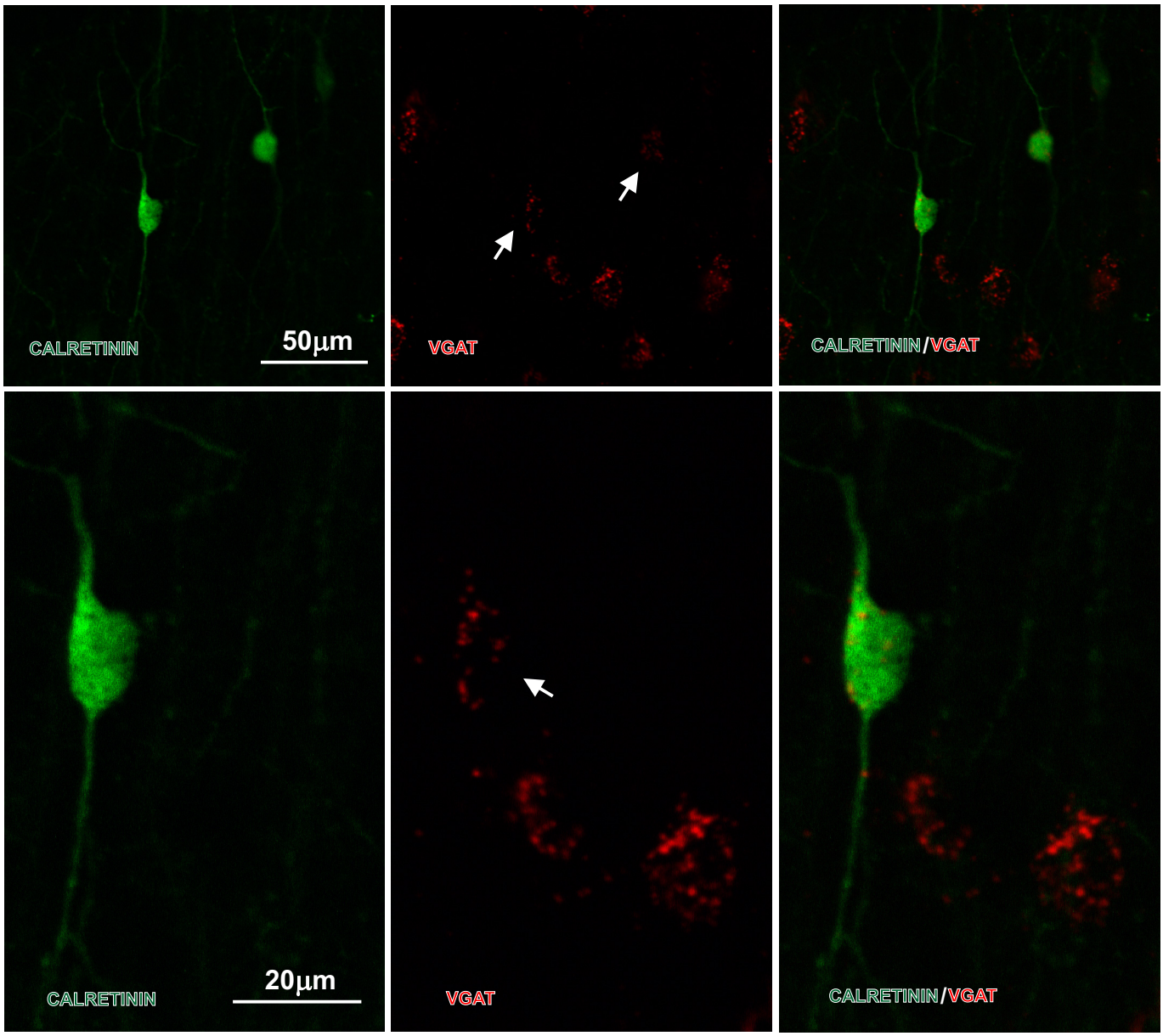


**Figure 5.36** Confocal acquisition of *RNAscope* in situ hybridization combining **VGAT** (**red**) expression with **calretinin** (**green**) immunohistochemistry in the layer III of **monkey** area **9** showing that all calretinin neurons express VGAT (arrows).

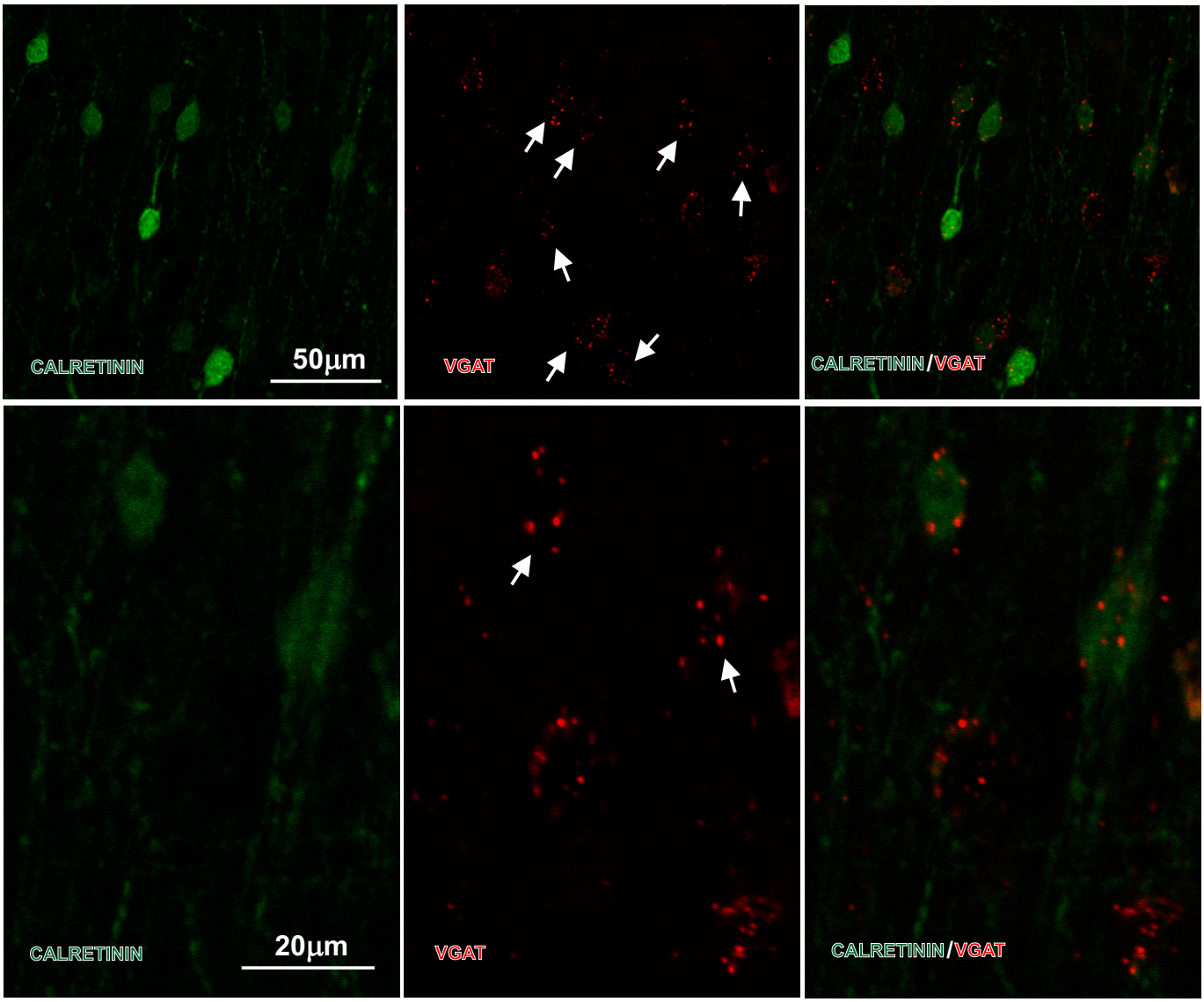


**Figure 5.37** Confocal acquisition of *RNAscope* in situ hybridization combining **VGAT** (**red**) expression with **calretinin** (**green**) immunohistochemistry in the layer II of **human** area **9** showing that all calretinin neurons express VGAT (arrows).

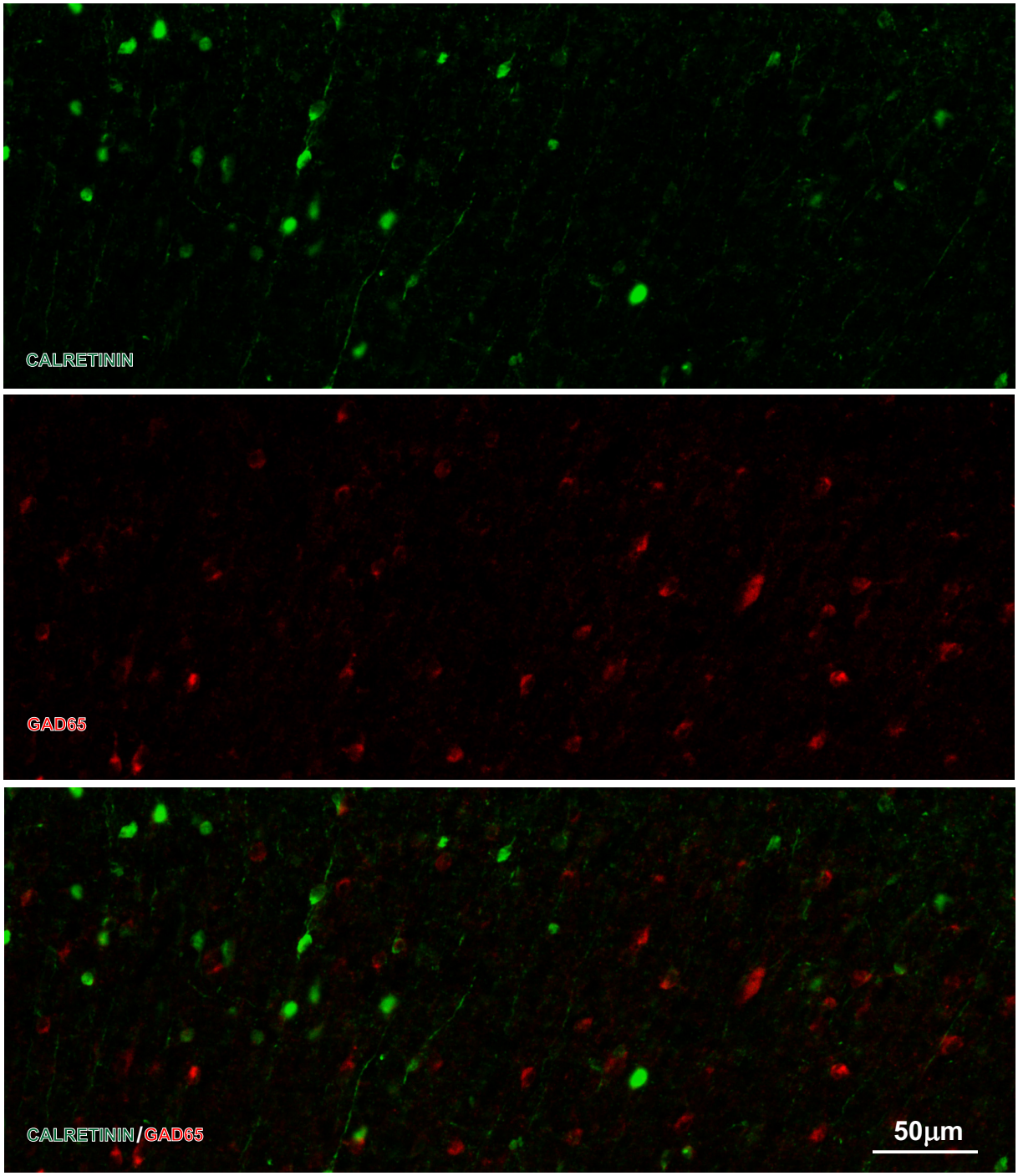


**Figure 5.38** Confocal acquisition of *RNAscope* in situ hybridization combining **GAD65** (**red**) expression with **calretinin** (**green**) immunohistochemistry in the layer II of **monkey** area **24**. It was not possible to co-localize GAD65 in calretinin neurons.

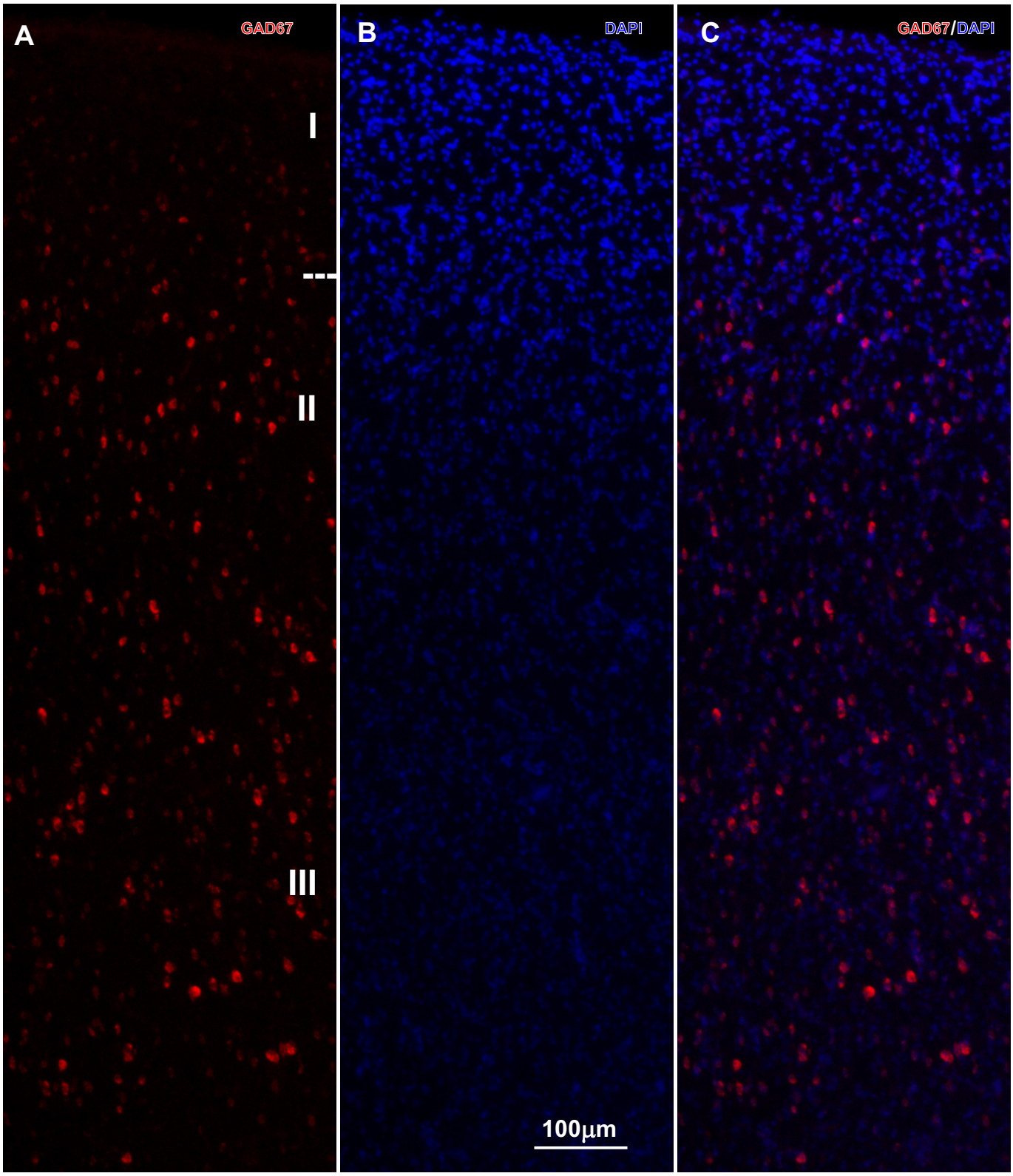


**Figure 5.39** Confocal acquisition of *RNAscope* in situ hybridization combining **GAD67** (**red**) expression with **DAPI** (**blue**) staining in the layers I-III of **human** area **32**. Data are showing that GAD67 expressing cells are uniformly distributed through layers IB-III.

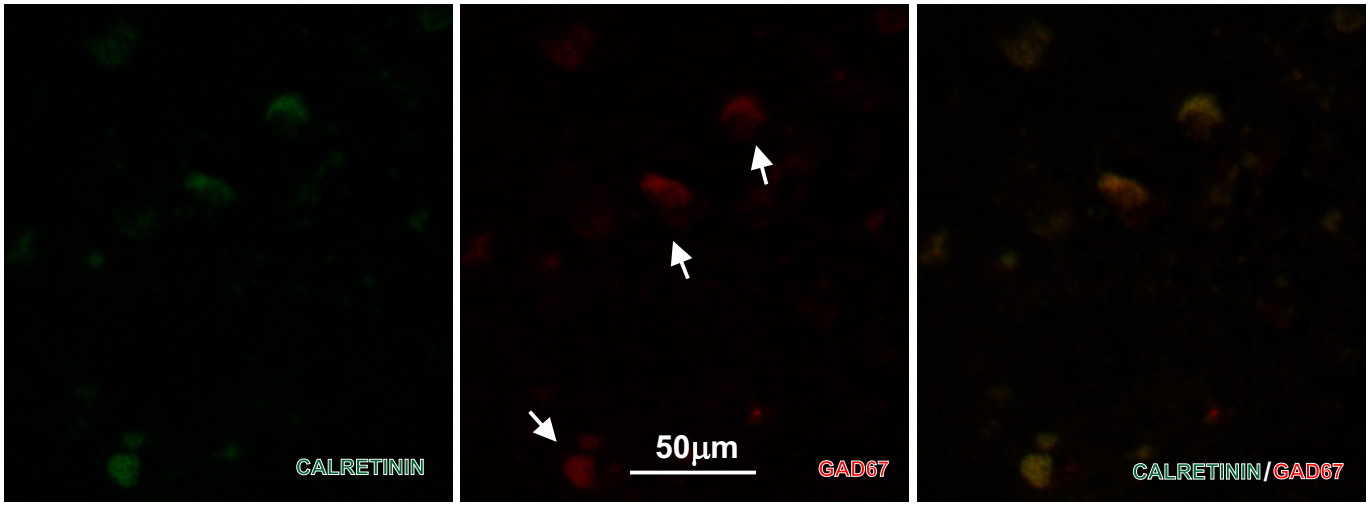


**Figure 5.40** Confocal acquisition of *RNAscope* in situ hybridization combining **GAD67** (**red**) expression with **calretinin** (**green**) immunohistochemistry in the layer III of **human** area **9** showing that calretinin neurons express GAD67 (arrows).

## 5.6. Cytoarchitectonic organization of human areas 9, 32 and 24 assessed through Nissl and NeuN labeled sections

Cytoarchitectonic organization was studied on Nissl (Figure 5.41) and NeuN (Figure 5.42) labeled sections. As in the monkey brain defining the cytoarchitecture is more reliable with NeuN than with the Nissl labeling. NeuN labeling is particularly useful in the characterization of layer I sublamination and identification of layer IV.

Sublamination of layer I in an upper neuron sparse zone, and a lower more populated zone is clear on NeuN labeled sections in all three analyzed areas as in the monkey (Figure 5.43, 5.44). The small cells composing layer I seem to be intermixed with the layer II small to medium sized pyramidal cells. Those small non-pyramidal shaped cells are grouped into island-like formations extending through lower part of layer I and layer II in all three areas (Figure 5.43). On NeuN and Nissl stained sections, no layer IV was present in area 24 (Figure 5.45). Layer IV on Nissl sections was clearly identifiable only in area 9 (Figure 5.46). At low magnification, layer IV was on NeuN sections clearly present in both areas 9 and 32, in area 32 layer IV was thick, but cells were less densely packed when compared to area 9 (Figure 5.45). At higher magnification, layer IV of area 9, was compact and composed of small triangularly shaped cells (Figure 5.45). In area 32, along the border with layer III and V, small triangular cells of layer IV intermix with large pyramidal cells of the neighboring layers.

Large pyramidal neurons of deep part of layer III (IIIc) in area 9, typically exceed the size of largest neurons in layer V. Layer IIIc large pyramidal neurons were also found in area 32, but do not exceed the size of largest neurons in layer V. Such large pyramidal neurons are not present in the layer IIIc of area 24.

Unlike in the monkey (Figures 5.4, 5.6), layer V and VI of the human area 24 contained large spindle shaped neurons (Figure 5.45). These cells are not as obvious on NeuN staining as they are on Nissl stained sections (Figure 5.42, 5.46).

More detailed descriptions of laminar organization of each area stained with NeuN, including the cell morphology, is given hereafter.

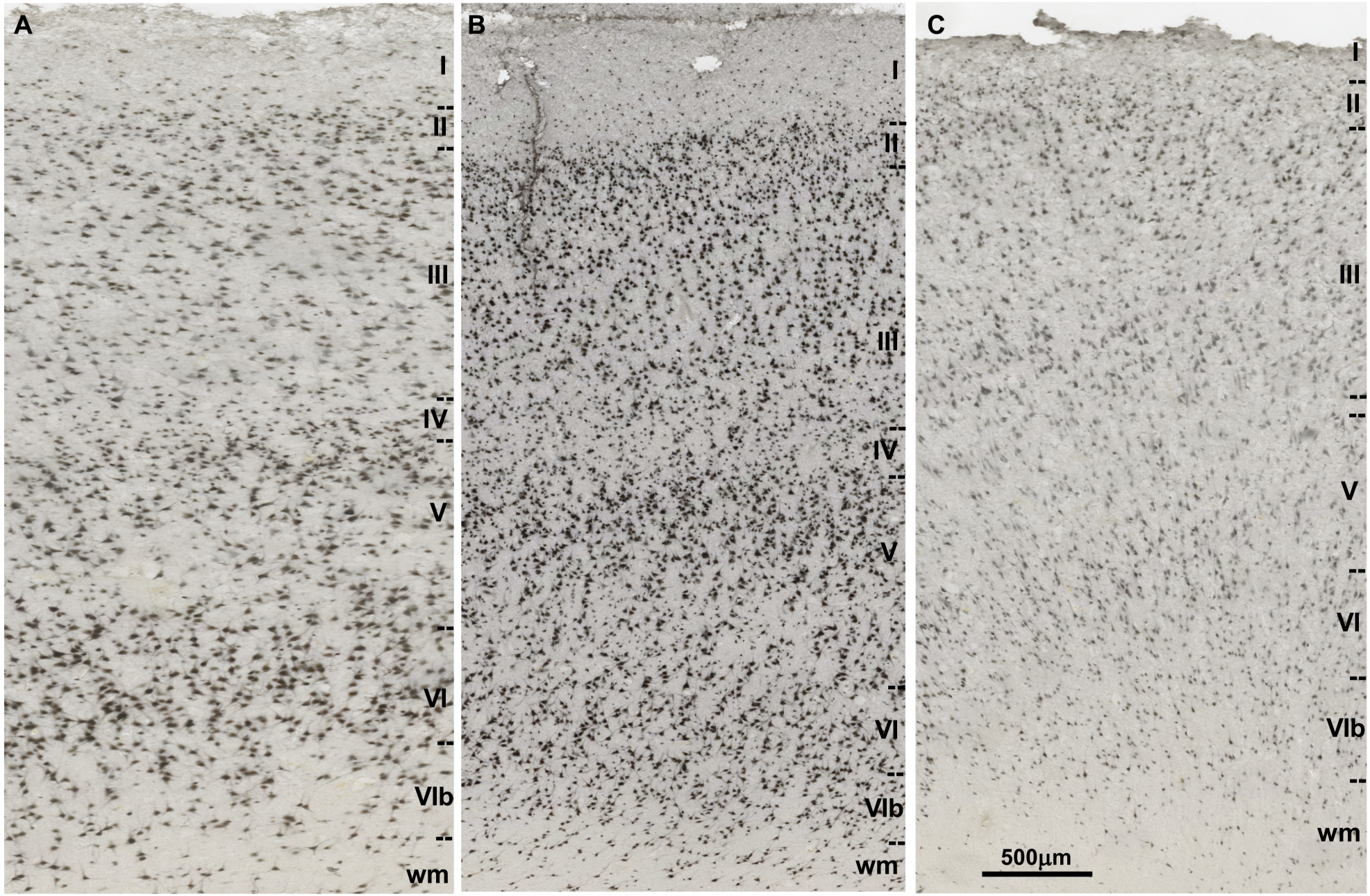


**Figure 5.41** Areas **9** (A), **32** (B) and **24** (C) in human. Immunohistochemical anti-**NeuN** staining.

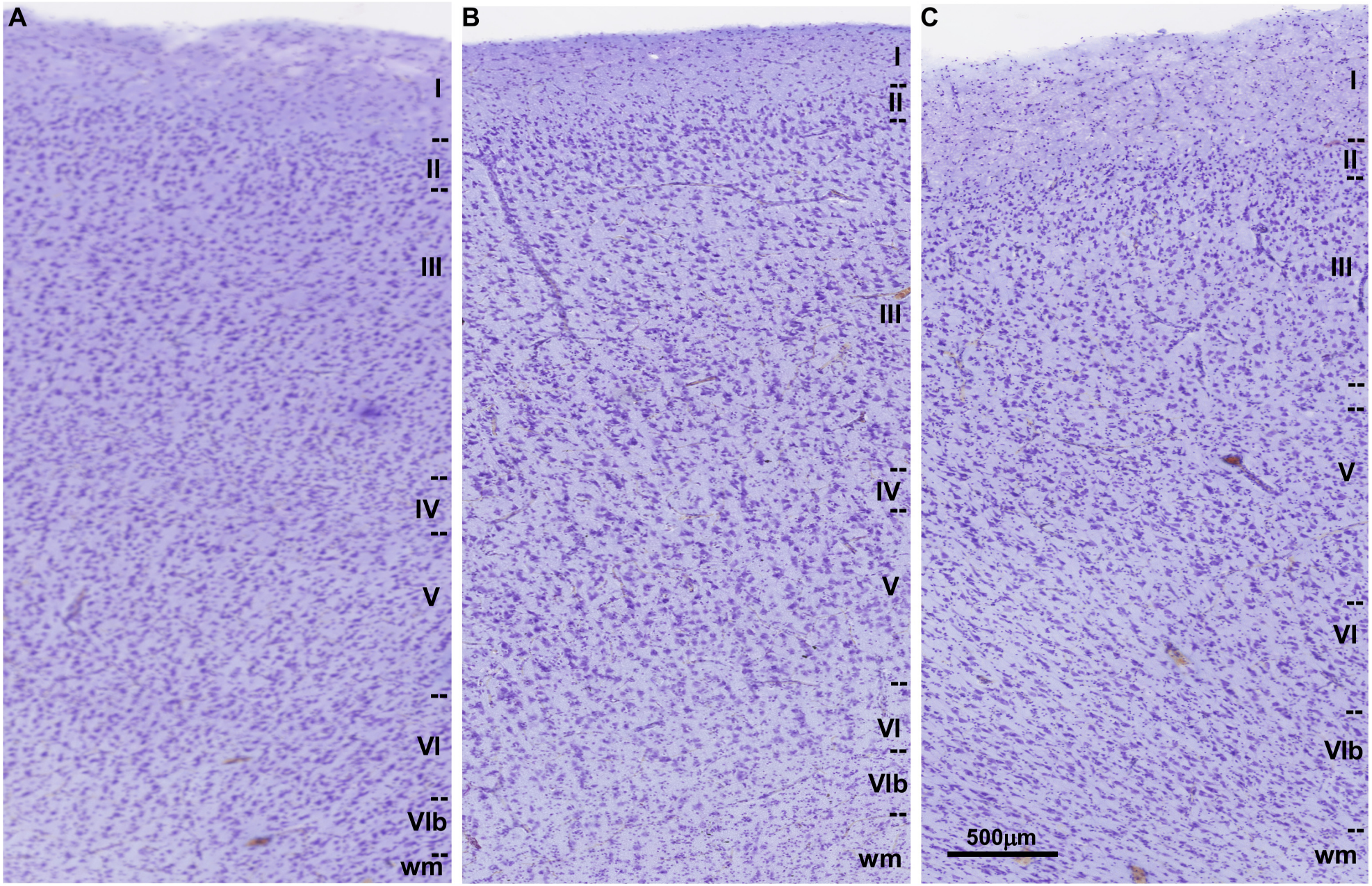


**Figure 5.42** Areas **9** (A), **32** (B) and **24** (C) in human. **Nissl** staining.

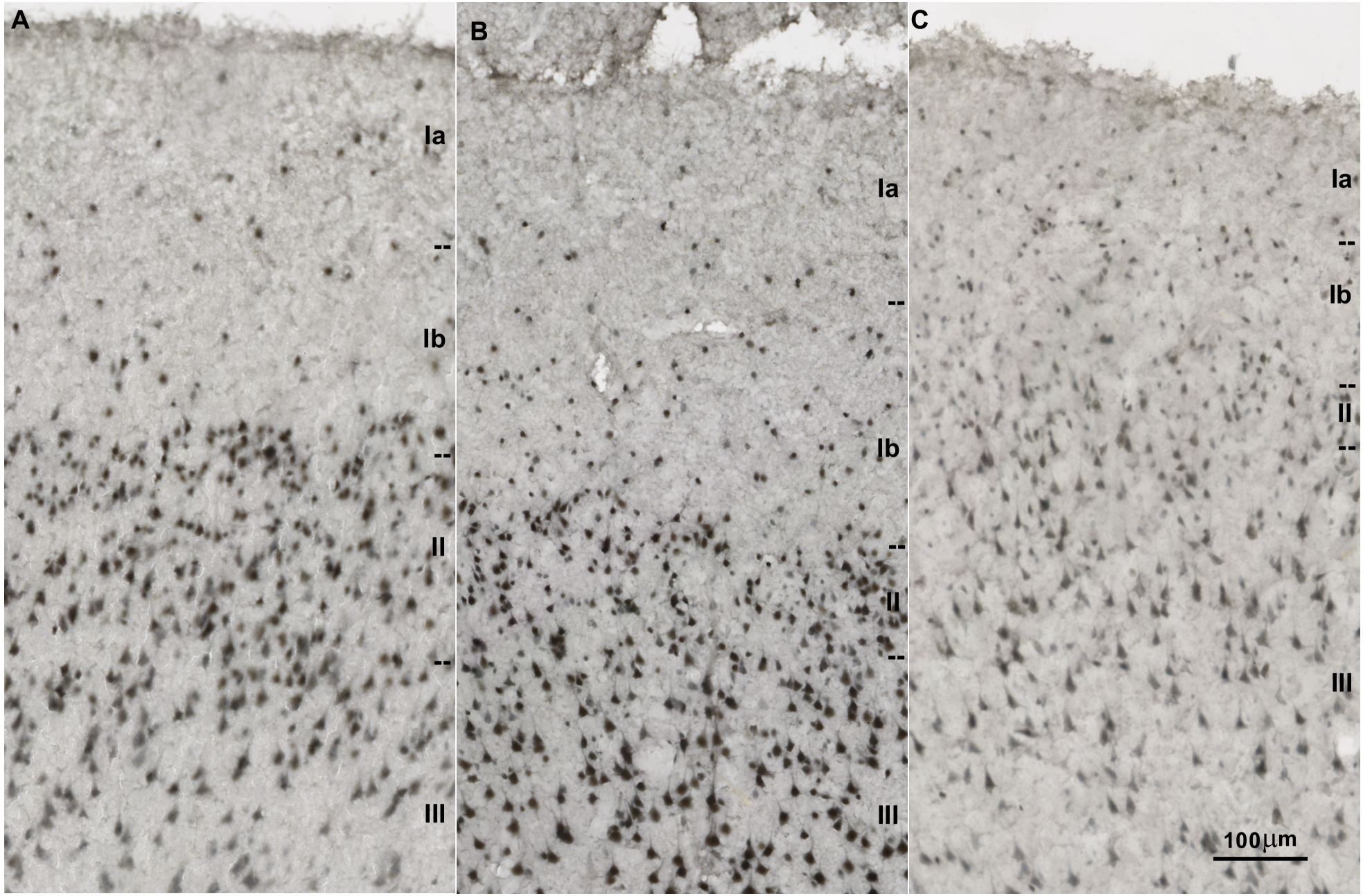


**Figure 5.43** Areas **9** (A), **32** (B) and **24** (C) in human. Immunohistochemical anti-**NeuN** staining of upper cortical layers.

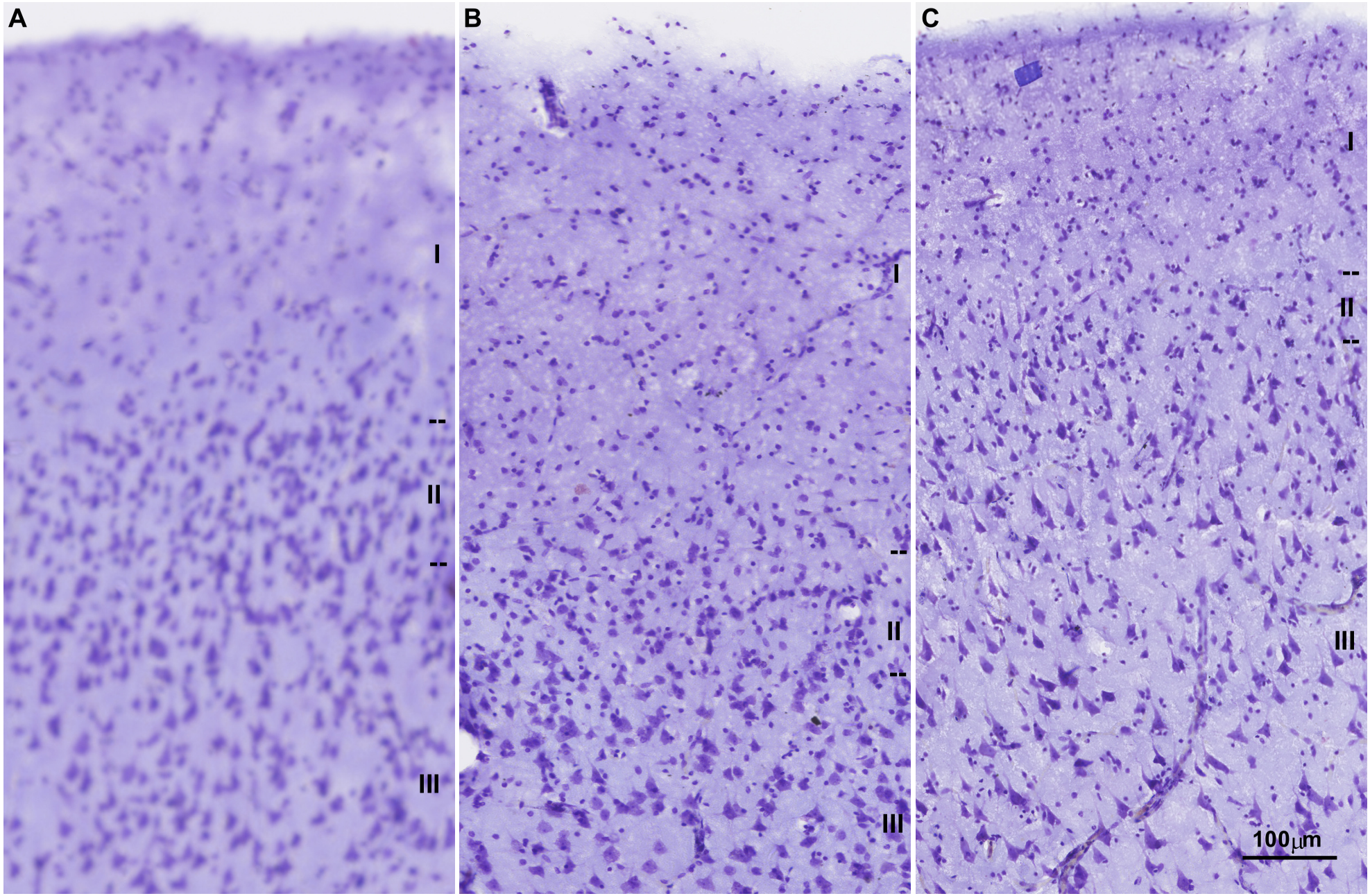


**Figure 5.44** Areas **9** (A), **32** (B) and **24** (C) in human. **Nissl** staining of upper cortical layers.

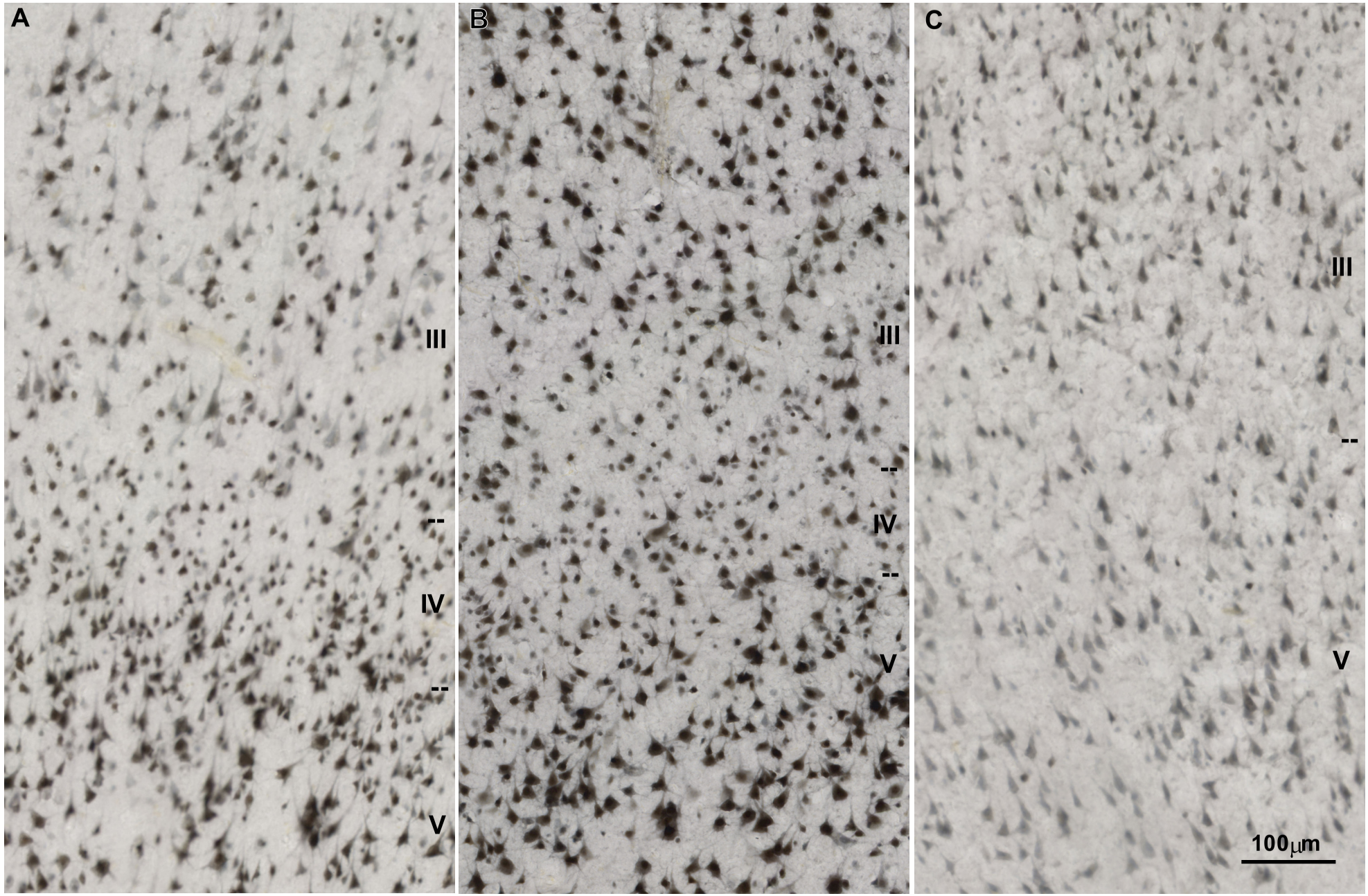


**Figure 5.45** Areas **9** (A), **32** (B) and **24** (C) in human. Immunohistochemical anti-**NeuN** staining of middle cortical layers.

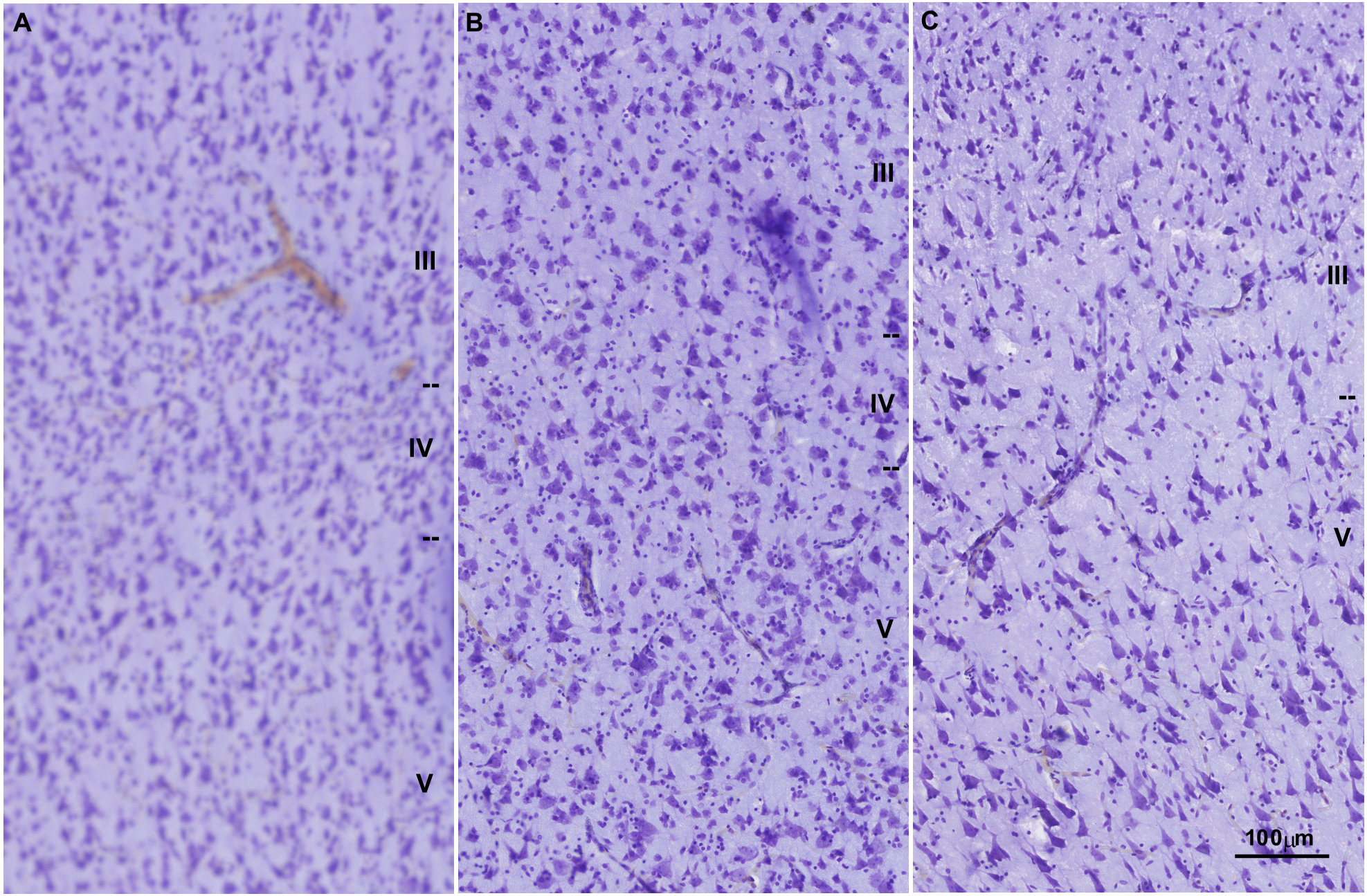


**Figure 5.46** Areas **9** (A), **32** (B) and **24** (C) in human. **Nissl** staining of middle cortical layers.

## 5.7. Laminar organization and cell morphology of human areas 9, 32 and 24 on NeuN labeled sections

**Area 9**

Area 9 is the typical neocortical area with six cortical layers and a distinct layer IIIc containing large pyramids (Figure 5.47).

Layer I can be clearly divided in two parts. An upper part with sparse cells and a lower part corresponding to a a denser neuronal zone where neurons are scattered at the border with layer II (Figure 5.43).

Layer II is composed of heavily labeled small round, oval or triangular neurons intermixed with small pyramidal cells.

Layer III has three subdivisions; the sublayer IIIa is characterized by small pyramidal cells densely packed; sublayer IIIb is composed of less densely packed but larger cells. Layer IIIc is not as dense as the upper parts but is characterized by its content in large pyramids intermixed with medium- and small-sized pyramidal cells.

Both the upper and the lower border of layer IV appear irregular because large pyramidal cells intermix with small granular cells (Figure 5.45).

Layer V is of somewhat lighter appearance than neigboring layers, especially in its lower zone. Upper part contains densely packed large pyramidal cells while layer Vb has lower neuronal density reflected in its pale appearance.

Layer VI discloses a somewhat denser arrangement of spindle (fusiform) cells oriented horizontally to the cortical surface in its upper sublayer VIa. The deeper sublayer VIb contains less cells that are also smaller in size. The border of layer VI with the underlying white matter is indistinct, characterized by a gradual transition of neurons from gray matter to white matter. The cytoarchitectonic features of area 9 in the human are very similar to those in monkey.


**Figure 5.47** Area **9** in human, immunohistochemical anti-**NeuN** staining.

**Area 32**

Area 32 is a cingulo-frontal transition cortex between typical mesocortical area 24 and typical granular neocortical area 9. Six cortical layers are present in area 32 (Figure 5.48).

Layer I is thicker than in area 9, and is, as in other areas, divided in two parts, upper zone with sparse cells and lower zone with more densely packed neurons.

Layer II is composed of heavily labeled small round, oval or triangular neurons intermixed with medium sized pyramidal cells (Figure 5.43).

Sublayers IIIa-b are very thin and neurons do not show superficial to deep increased gradient of cell body size as in area 9. Also, in area 32 layer IIIc pyramidal neurons do not vary in size as in area 9.

Layer V contains pyramidal-shaped neurons and is subdivided into two sublayers based on the cell density and the labeling intensity of neurons. In contrast to sublayer Vb, the sublayer Va contains strongly labeled neurons densely packed so this layer appears more compact. Both sublayers, Va and Vb are composed of small and medium sized pyramids that show similar size and shape through the whole layer.

Layer VI, is composed of medium sized pyramidal-shaped neurons, and perpendicularly oriented bipolar and multipolar neurons. The pyramidal-shaped neurons usually have two prominent processes. The sublayers of layer VI can be distinguished based on cell density, with a dense upper part. The decrease in neuron density is apparent in deeper layer VIb, which is a transitional zone towards the white mater.

The laminar organization and neuronal composition of area 32 in monkey and human are very similar. The most striking difference concerns layer II of area 32. Whereas in human it is clearly well developed and recognizable, in the monkey it is thin and irregular.


**Figure 5.48** Area **32** in human, immunohistochemical anti-**NeuN** staining.

**Area 24**

Area 24 in human has no recognizable layer IV and a narrow layer II, and is therefore defined as an agranular cortex (Figure 5.49).

Layer I has the typical structure as in other areas, a few neurons located in the upper sublayer and many neurons scattered in the lower part near the border with layer II (Figure 5.43). Pyramidal cells are abundant in layers II and III and comparatively sparse in layer VI. Layer III is thin and composed of small to medium sized pyramidal neurons which gradualy increase in size from superficial to deep part. Layers II and III appear almost as in continuation.

Layer V has two sublayers, its upper part is densely packed with neurons (layer Va) and contains large pyramidal neurons in the middle. The layer Vb is not as dense, and is composed of prominent lightly labeled elongated pyramidal neurons and long, perpendicular to pia, spindle-rode cells.

Layer VI, is composed predominantly of perpendicularly oriented medium sized bipolar cells and pyramidal-shaped neurons with two prominent vertically oriented processes. Multipolar neurons are frequently found in the less densely populated deep part of layer VI (VIb).

Interestingly, the laminar organization and neuronal composition of area 24 differs clearly between monkey and human. When compared to human, monkey area 24 has some distinctive features as a band of small cells dividing layers III and V, clearly visible layer II and thicker layer III. The spindle-rod shaped cells were found in the human, but not in the monkey area 24 (Figures 5.45, 5.46).


**Figure 5.49** Area **24** in human, immunohistochemical anti-**NeuN** staining.

### 5.7.1. Quantitative analysis of NeuN labeled sections

Total number of NeuN labeled neurons and total volume were estimated for each sublayer in each analyzed areas (Figure 5.50) for each animal (n= 3). The proportion and density were calculated. The mean values with SD are provided in tables (Tables 5.10, 5.11 and 5.12).

**Table 5.10** - **Proportion (%) of NeuN labeled cells** from total neuronal pool located in particular layer of human areas 9, 24 and 32 (NeuN cell number per layer / total number of NeuN cells in particular area).

| | **Area 9** | SD | **Area 32** | SD | **Area 24** | SD |
|---|---|---|---|---|---|---|
| Ia | **1.1%** | 0.4% | **1.4%** | 1.0% | **1.9%** | 0.8% |
| Ib | **3.5%** | 1.1% | **3.4%** | 2.5% | **4.7%** | 1.8% |
| II | **22.0%** | 5.4% | **20.9%** | 2.9% | **20.1%** | 2.5% |
| III | **30.2%** | 2.6% | **28.8%** | 4.0% | **32.0%** | 6.7% |
| IV | **10.5%** | 1.3% | **8.4%** | 3.4% | **Ø** | **ø** |
| Va | **12.0%** | 2.8% | **10.7%** | 2.5% | **14.5%** | 3.2% |
| Vb | **6.6%** | 1.5% | **6.6%** | 1.6% | **10.7%** | 1.8% |
| VIa | **8.1%** | 3.0% | **8.4%** | 3.2% | **8.7%** | 1.1% |
| VIb | **4.4%** | 2.5% | **8.0%** | 4.4% | **4.8%** | 1.8% |
| WM | **1.6%** | 0.7% | **3.5%** | 1.8% | **2.7%** | 0.9% |

**Table 5.11 – Proportion (%) of layer volume** in relation to total volume of human areas 9, 24 and 32 (layer volume / total areal volume).

| | **Area 9** | SD | **Area 32** | SD | **Area 24** | SD |
|---|---|---|---|---|---|---|
| Ia | **9.4%** | 0.8% | **8.6%** | 2.1% | **11.2%** | 3.0% |
| Ib | **7.6%** | 1.1% | **7.5%** | 1.7% | **10.2%** | 2.2% |
| II | **13.3%** | 2.1% | **12.9%** | 2.5% | **12.4%** | 2.2% |
| III | **33.8%** | 3.6% | **28.3%** | 4.3% | **29.4%** | 8.5% |
| IV | **5.7%** | 1.0% | **7.1%** | 1.6% | **Ø** | **ø** |
| Va | **8.4%** | 0.7% | **9.6%** | 2.3% | **11.3%** | 3.0% |
| Vb | **7.7%** | 1.8% | **7.6%** | 1.4% | **9.7%** | 3.6% |
| VIa | **7.9%** | 2.6% | **10.1%** | 3.6% | **9.2%** | 1.8% |
| VIb | **6.3%** | 3.9% | **8.4%** | 3.4% | **6.7%** | 1.5% |

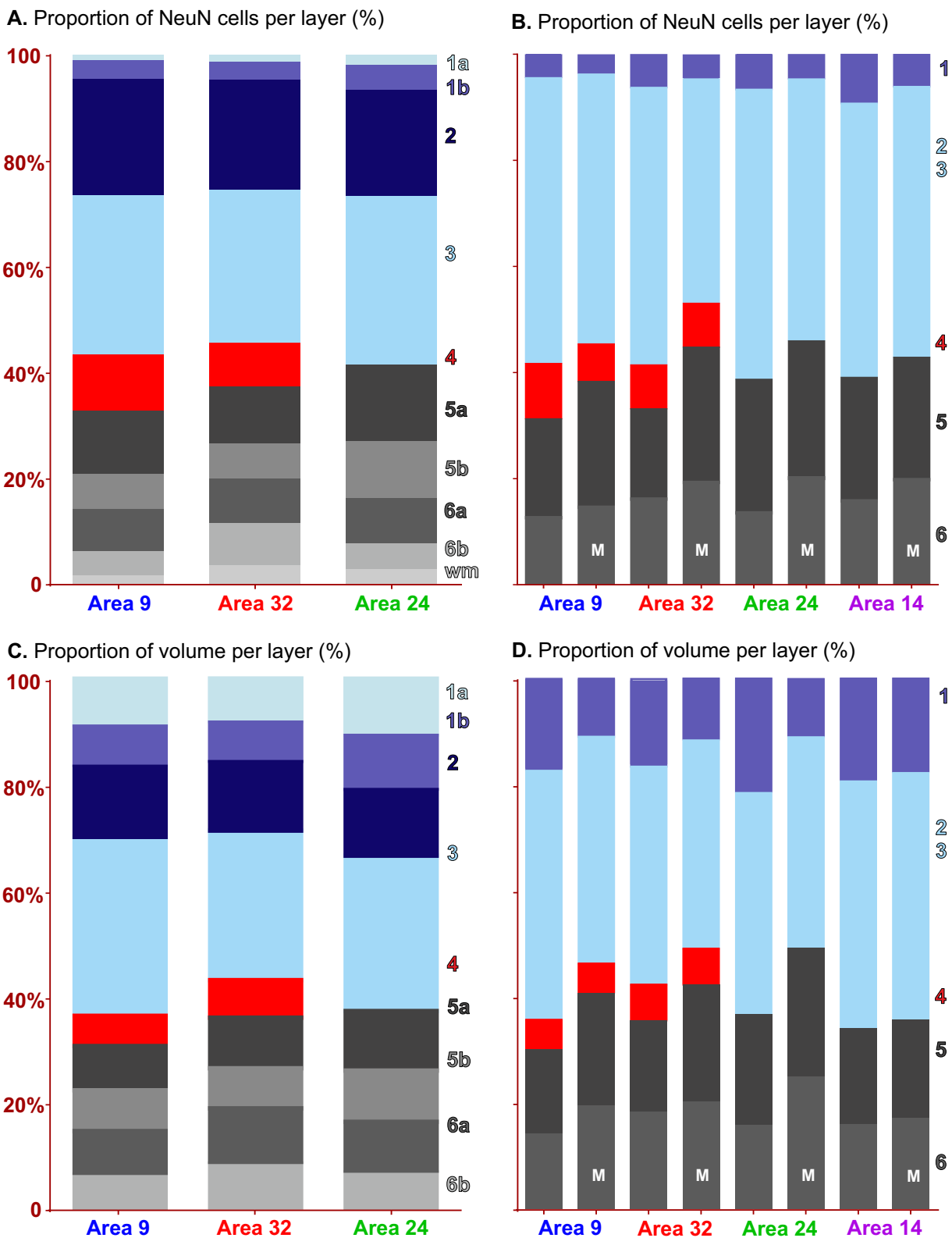


**Figure 5.50** Graphs are showing **laminar proportion of neurons** (A, B) and **layer volumes** (C, D) assessed on **NeuN** stained sections in human and monkey (M). Proportion is calculated as follows: volume and number of NeuN labeled cells in particular layer was divided by total volume and total number of NeuN labeled cells in whole area. Proportion is shown in percentage and on graphs B and D values obtained in this study are presented in the way to be comparable with data from area 14 (Džaja 2015, PhD Thesis).

The proportion of neurons for each layer is similar in all examined areas (Table 5.10; Figure 5.50A). Layer I accounts for around 5% of the total neuronal pool with 80% of neurons located in its lower half, sublayer Ib. Layers II and III contain 50% of the total neuronal pool with 20% in layer II and 30% in layer III. The proportion of neurons in the lower layers of the agranular area 24 reach 35%, and in the granular areas 30% of neurons were located there.

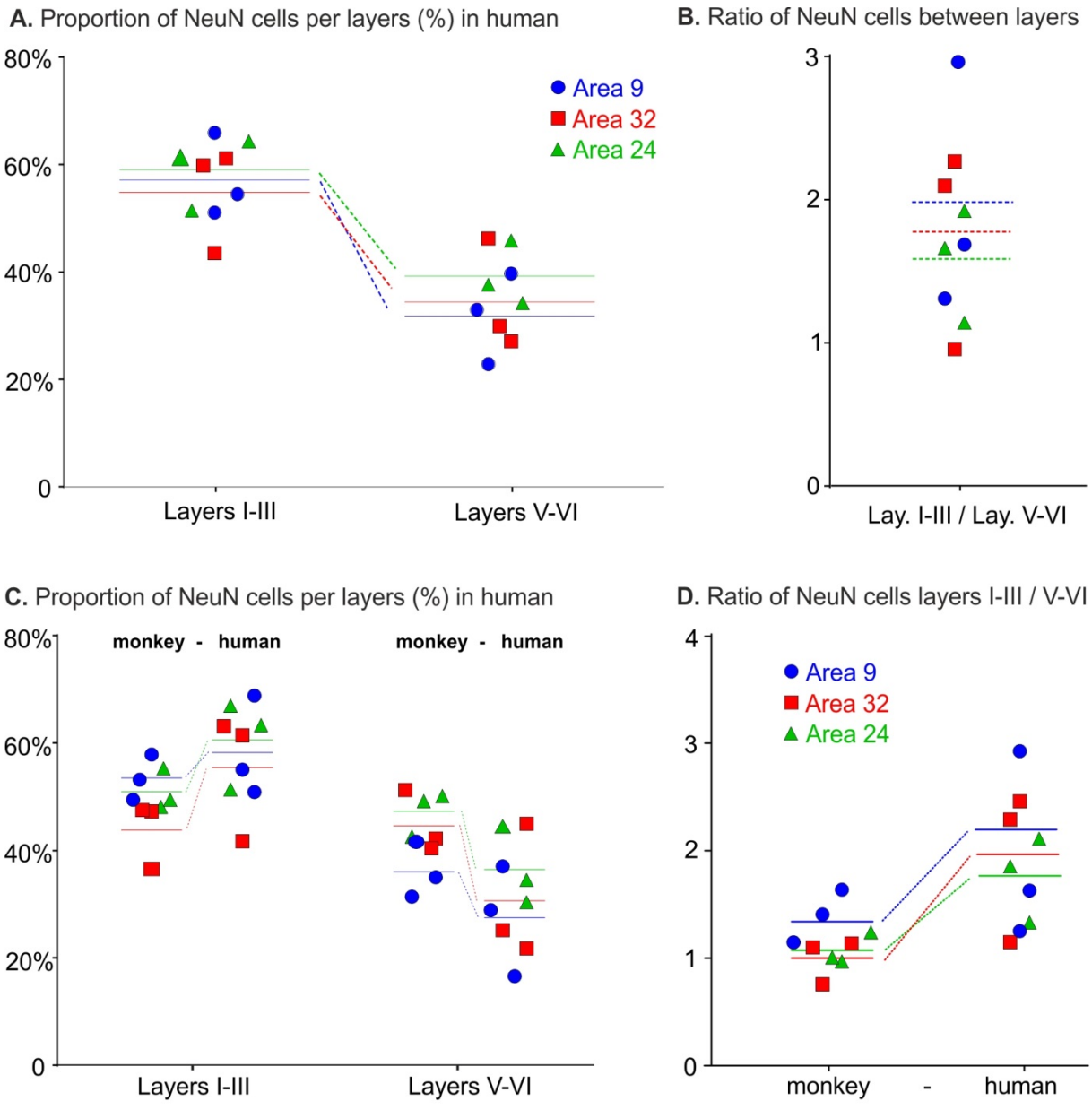


**Figure 5.51** Graphs show **proportion** from total pool of **NeuN** labeled cells located in **layers I-III** and **V-VI** (A) and **ratio** of obtained values between **layers I-III versus layers V-VI** (B) in the human. Human data are compared with monkey data (C, D).

In all three human areas analyzed, the proportion of neurons (Figure 5.51A, B) located in upper cortical layers (I-III) was 1.5-2 times higher than in lower cortical layers (V-VI). In

monkey, only area 9 had the proportion (Figure 5.51C,D) of neurons in layers I-III higher than in layers V-VI (1.4), whereas in areas 24 and 32 the neurons were almost equally (re)distributed between the upper and lower cortical layers. There is more neurons in layer I (5% in humans and up to 4% in monkey), and in both species they are mostly located in the sublayer Ib (Figure 5.50B, 5.52). The proportion of neurons located in layer I of areas 9 and 32 in human was 4.6% and 4.8%, that is slightly higher than in the corresponding monkey areas, whereas in human area 24 contains 6.6% neurons from the total pool (Tables 5.1; 5.10; Figures 5.11, 5.50).

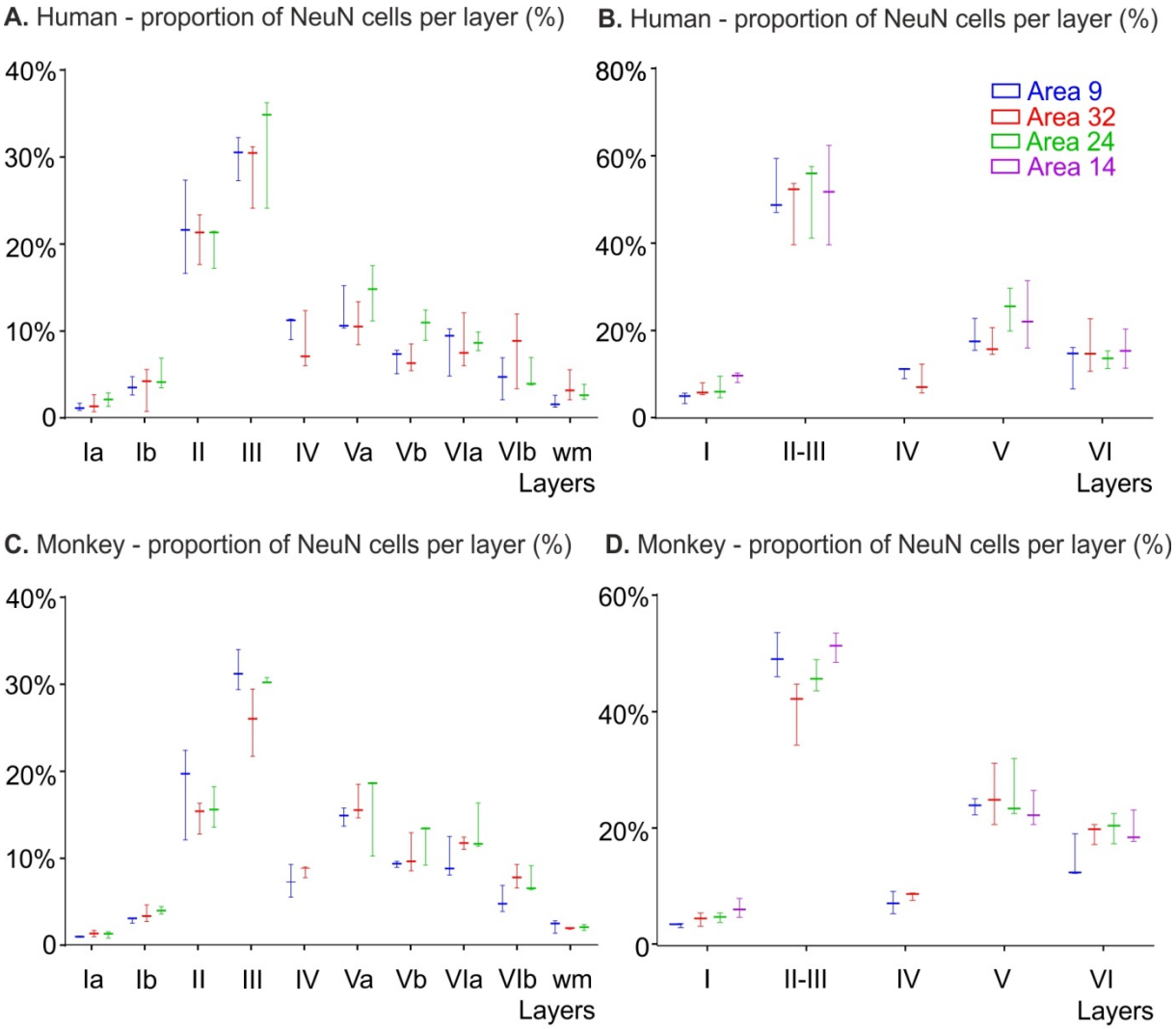


**Figure 5.52** Graphs are showing **laminar proportion of NeuN** labeled **neurons** in human (A, B) and monkey (C, D) with data from each specimen. Proportion is shown as percentage and on graphs B and D values obtained in this study are presented in the way to be comparable with data from area 14 (Džaja 2015, PhD Thesis).

Laminar distribution of neurons in human areas compared to monkey is even more obvious redistribution of neurons towards upper cortical layers. In monkey only area 9 showed the

ratio between supra- and infra-granular layers above 1 (Figure 5.51D). In comparison to monkey, the ratio increased in human for 0.5 for areas 9 and 32, and 0.7 for area 24, but individual differences should be counted (Figure 5.52). In human the individual differences in proportion of neurons located in layer I-III versus V-VI were extremely high (Figure 5.51D). Indeed, in areas 9 and 32 the layer I-III/V-VI ratio in one subject was 2.5 times higher than in another. The average ratio for area 9 in monkey is 1.4 while in humans 1.9 (1.3 -2.9); for area 32 in monkey the average value is 1 while in humans this is 1.7 (0.7-2.2); and in area 24, the average value in monkey is also 1 and in human 1.5 (1.2-1.9) (Figure 5.51). Statistical analysis comparing average value (using average value per area as raw data) between species, showed significantly higher (t-test, $p<0.03$) I-III/ V-VI ratio in human (1.8) than in monkey (1.2). This data indicate that between monkey and human there is a redistribution of neurons to supragranular (II-III) layers (Figure 5.51C).

Volume taken up by a particular layer is uniformly distributed between all three areas of prefrontal cortex (Figure 5.50C). Layer I takes up to 20% of total volume and volume of its sublayers is comparable to the volumes of infragranular sublayers (and layer IV in granular areas). Each of above mentioned layers comprises around 10% of total volume, ranging from 6% in layers IV and VIb to 11% in sublayer Va.

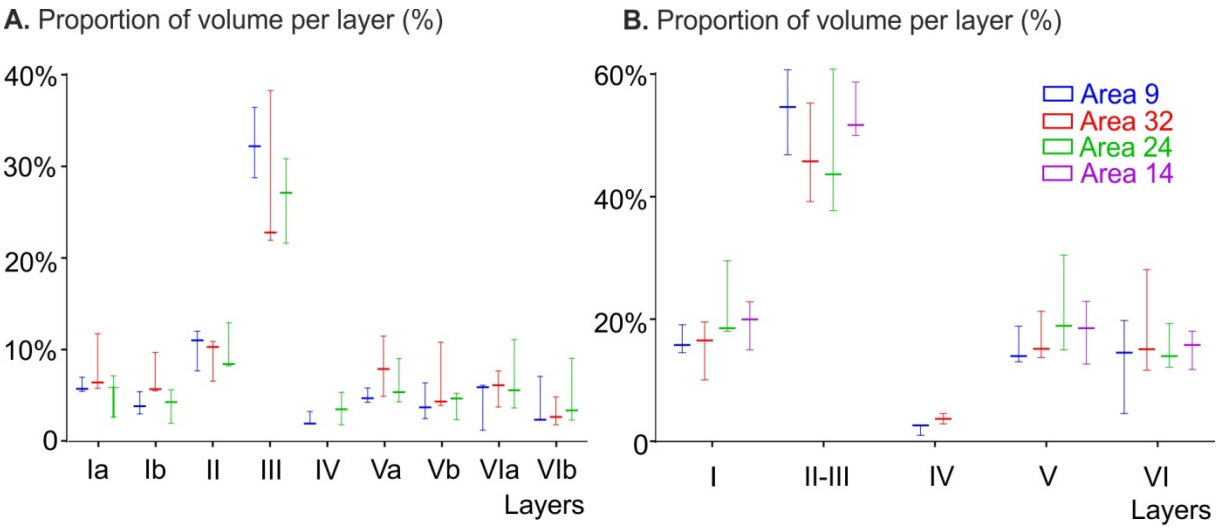


**Figure 5.53** Graphs show **proportion of volume** of particular layer in human (A). Proportion is shown as percentage and on graph B values obtained in this study are presented in the way to be comparable with data from area 14 (Džaja 2015, PhD Thesis).

When compared to monkey data (Figure 5.50D) layer I is almost doubled in volume (10% in monkey and 20% in human). The highest value in monkey was seen in area 32 (12%) and in human lowest volume was found in area 9 (15%). In human the layers I-III account for 2/3dh

of cortical volume, in contrast to monkey brain where layers I-III take around half of total volume (Tables 5.2 and 5.11; Figure 5.50).

Differences between monkey and the human cortical layers volumes are mainly caused by significant increase (t-test, $p<0,0002$) in the relative volume of layer I, which is in human around 18% (16-21%), whereas in monkey 11% (10-12%) of total cortical volume. The relative volumes of layers V-VI are in human 34% (30-36%), and in monkey 44% (41-46%), what is significantly lower (t-test, $p<0,006$). No interspecies differences in the volumes of the layer IV (6-7%) and layers II-III (41-47% in human and 39-50% in monkey) was observed. Note that in the human the volume ratio between layers II-III versus layers V-VI is also changing, being above 1 for all areas. In human area 9, the ratio is 1.55 (1.05 in monkey), and for areas 32 and 24 the ratio is 1.15 (0.8-0.9 in monkey) (Figure 5.50D).

The individual differences are much higher in the human (Figure 5.53) than in monkey brain (Figure 5.13). So, the relative volume of layer I can vary between 10-30%, and between 40-60% of layers II-III among different subjects.

**Table 5.12 - NeuN density** per layer in human areas 9, 24, 32 presents the mean value (1000 cells / $mm^3$) of each layer with standard deviation (SD) in each area. Overall neuronal densities from layers I-VI and II-VI are presented in the last two rows.

| | **Area 9** | SD | **Area 32** | SD | **Area 24** | SD |
|---|---|---|---|---|---|---|
| Ia | **3.6** | 0.3 | **6.2** | 4.5 | **5.2** | 2.7 |
| Ib | **15.6** | 3.9 | **24.8** | 3.1 | **14.7** | 7.9 |
| II | **56.4** | 19.6 | **61.6** | 23.9 | **47.4** | 17.0 |
| III | **31.5** | 14.1 | **40.0** | 19.5 | **31.7** | 7.0 |
| IV | **62.3** | 20.5 | **45.5** | 25.4 | **Ø** | **ø** |
| Va | **50.0** | 23.4 | **40.9** | 9.8 | **37.2** | 21.3 |
| Vb | **29.0** | 7.1 | **31.7** | 6.4 | **17.1** | 10.4 |
| VIa | **34.4** | 11.3 | **31.3** | 11.5 | **28.4** | 13.9 |
| VIb | **24.5** | 6.9 | **34.8** | 19.6 | **20.0** | 8.3 |
| WM | **10.9** | 5.1 | **16.3** | 5.5 | **12.0** | 8.8 |
| I-VI | **33.7** | 11.9 | **36.3** | 10.6 | **24.4** | 6.2 |
| II-VI | **38.7** | 13.7 | **40.8** | 13.1 | **28.5** | 5.5 |

Neuronal densities (Table 5.12; Figure 5.54) vary between areas. Layers I-VI in area 9 have a neuronal density of 37 000 cells per $mm^3$ and in area 24 the density is 24 000 cells per $mm^3$. Supragranular layers are most densely populated in area 32 where in layer Ib there is 24 000 cells, layer II 61 000 and in layer III 40 000 cells per $mm^3$. These values are 30-40% higher than in area 9 and 24 (Table 5.12; Figure 5.54). In almost all areas the difference between lowest and highest values vary about 2 fold between subjects. Therefore, no statistically significant interareal nor interspecies differences could be found.

We performed statistical analysis (ANOVA, SNK-test) to establish laminar differences in NeuN density. Data confirmed that layer Ia is very sparse in neurons and has significantly ($p=0.001$) lower density (5 000 NeuN stained cells per $mm^3$) than any other layer (18 300 – 55 000 NeuN stained cells per $mm^3$). Its density is below those found in underlying white matter (13 000 NeuN labeled cells per $mm^3$), therefore layer Ia can be defined as non-neuronal layer. Average density in the lower part of layer I (Ib) was 18 300 NeuN labeled cells per $mm^3$, below average values for other layers, but not statistically significant when compared to layer Vb (26 000), VIa (31 400) and VIb (26 400). The highest density (55 000 NeuN labeled cells per $mm^3$) was found in layer II and IV.

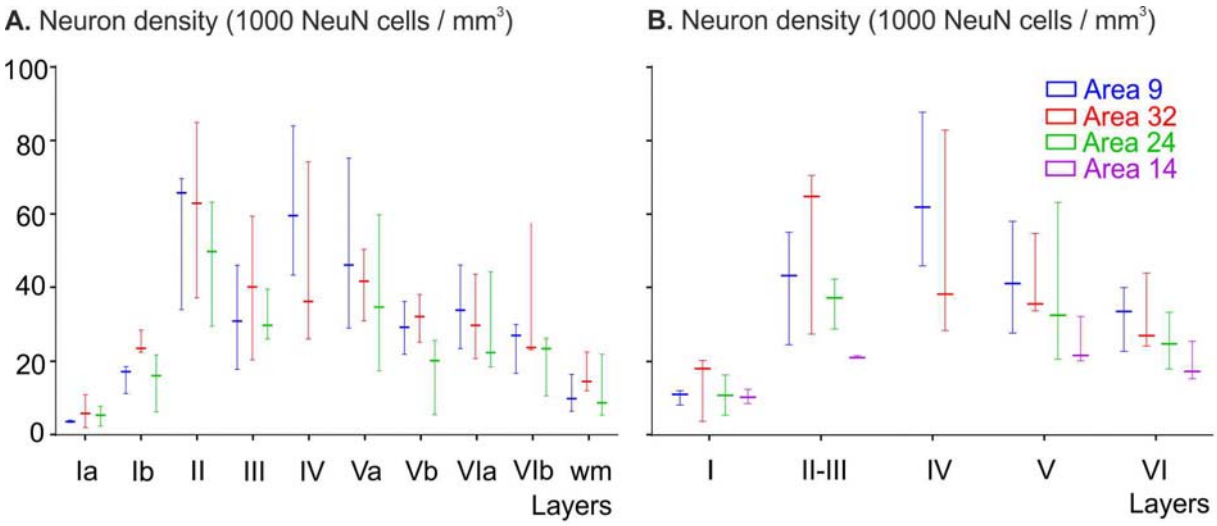


**Figure 5.54** Graphs show **neuronal density** for particular layer in human (A). Values shown on graph B are values obtained in this study and presented in the way to be comparable with data from area 14 (Džaja 2015, PhD Thesis).

Despite absence of areal differences when layers are separately analyzed, the average density (Figure 55A) for layers I-VI was 25-30% lower in area 24 (24 000 cells per $mm^3$) than in areas 9 and 32 (34 000 and 36 000 cells per $mm^3$). In area 24 all three subjects have values around average level, but in areas 9 and 32 two subjects have much higher density, whereas the third one was at the level found in area 24.

When layer densities are compared between monkey (Table 5.3; Figure 5.14) and human (Table 5.12; Figure 5.54), there is a 40% decrease in density in human areas (Figure 5.55A); with the biggest drop (50%) in density for layers Ib and II. Only the white matter density in human is higher than in monkey, showing 5 fold increase (Figure 5.55B). Despite large drop in neuronal density between these two species, this is only statistically significant in area 24 (t-test, p=0.01).

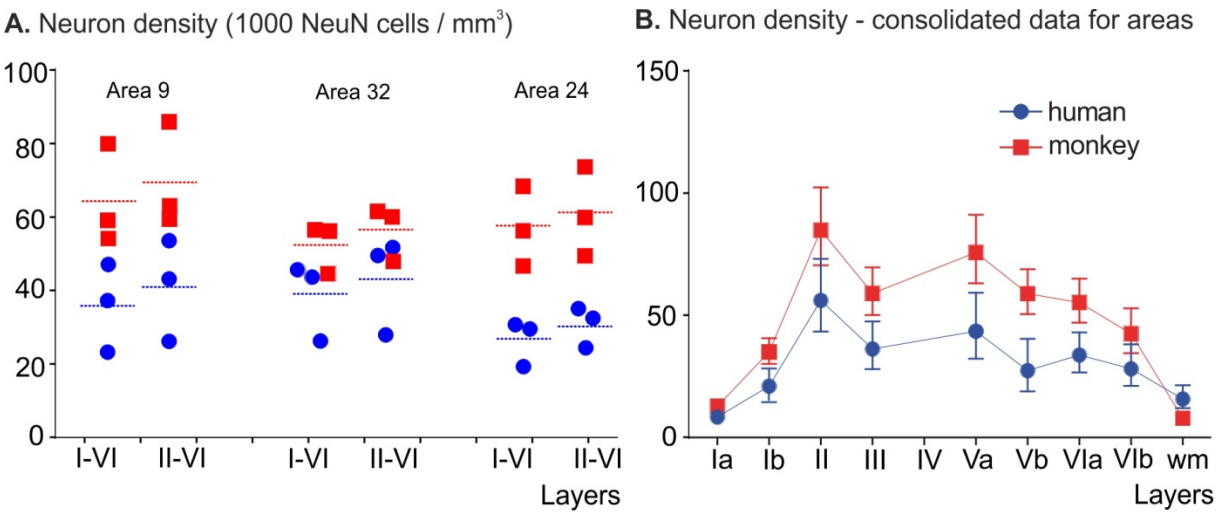


**Figure 5.55** Graphs show **neuronal density** comparing human and monkey layers I-VI and II-VI (A) and consolidated data from all areas (B).

## 5.8. Laminar distribution and morphological features of calretinin labeled neurons of human areas 9, 32 and 24

Morphology of calretinin neurons is similar in all analyzed areas. Calretinin neurons are mostly vertically oriented and are present throughout all cortical layers (Figure 5.56, 5.57, 5.58, 5.59). The laminar distribution of these neurons is similar to that observed in monkey.

In layer I calretinin neurons, are mainly located in the lower half of this layer. Most of these calretinin neurons are medium sized with vertically oriented cell bodies but horizontally oriented neurons are occasionally found, particularly in the layer I, VI and in the white matter.

Layer II contains smaller bipolar neurons that display ovoid cell bodies. These neurons are also found in the upper part of layer III. They display two vertical dendritic processes, one ascending and one descending. The lower part of layer III contains a mix of bipolar, bi-tufted and multipolar calretinin labeled neurons. A few of these neurons display a large cell body and horizontally oriented dendrites. Some, calretinin labeled cells display a pyramidal like cell body.

In layers V and VI calretinin neurons are small bipolar cells with long dendritic processes that are vertically or horizontally oriented. These dendrites occasionally reach upper layers.

Calretinin neurons in white matter are also small to medium bipolar neurons and their processes seem to branch out only below the cortical layers.

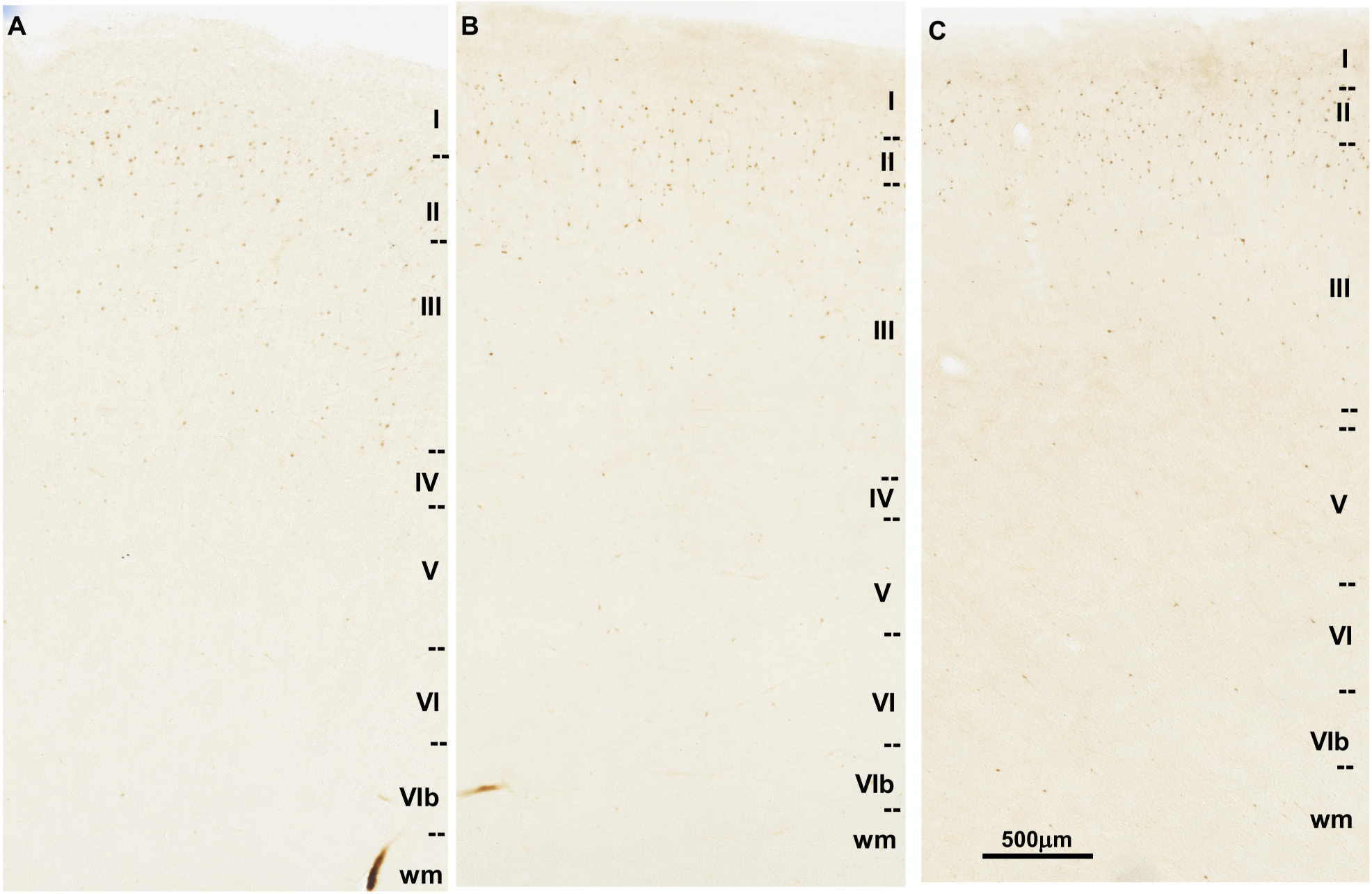


**Figure 5.56** Areas **9** (A), **32** (B) and **24** (C) in human. Immunohistochemical anti**-calretinin** (mouse monoclonal) staining.

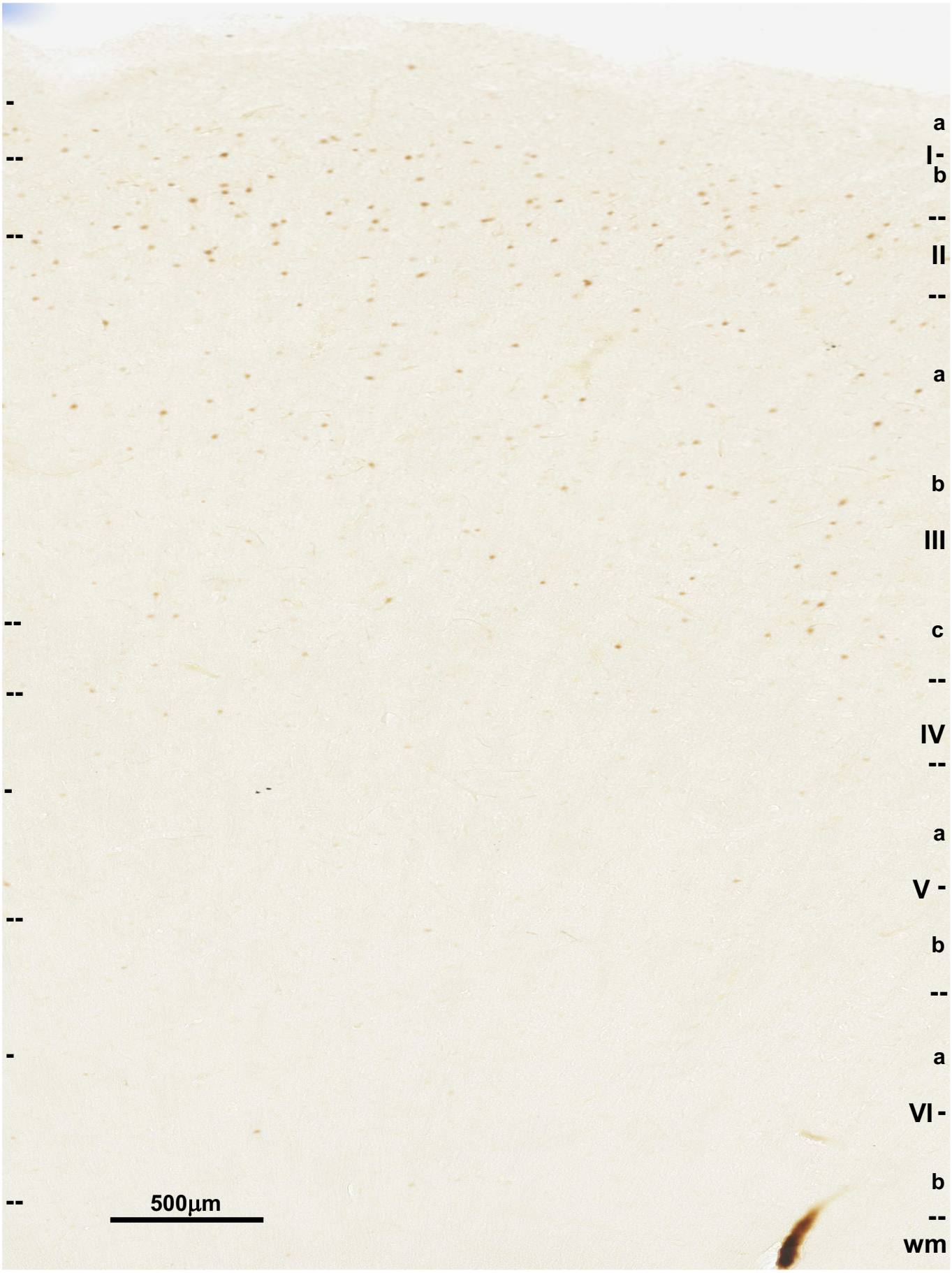


**Figure 5.57** Area **9** in human. Immunohistochemical anti-**calretinin** staining.

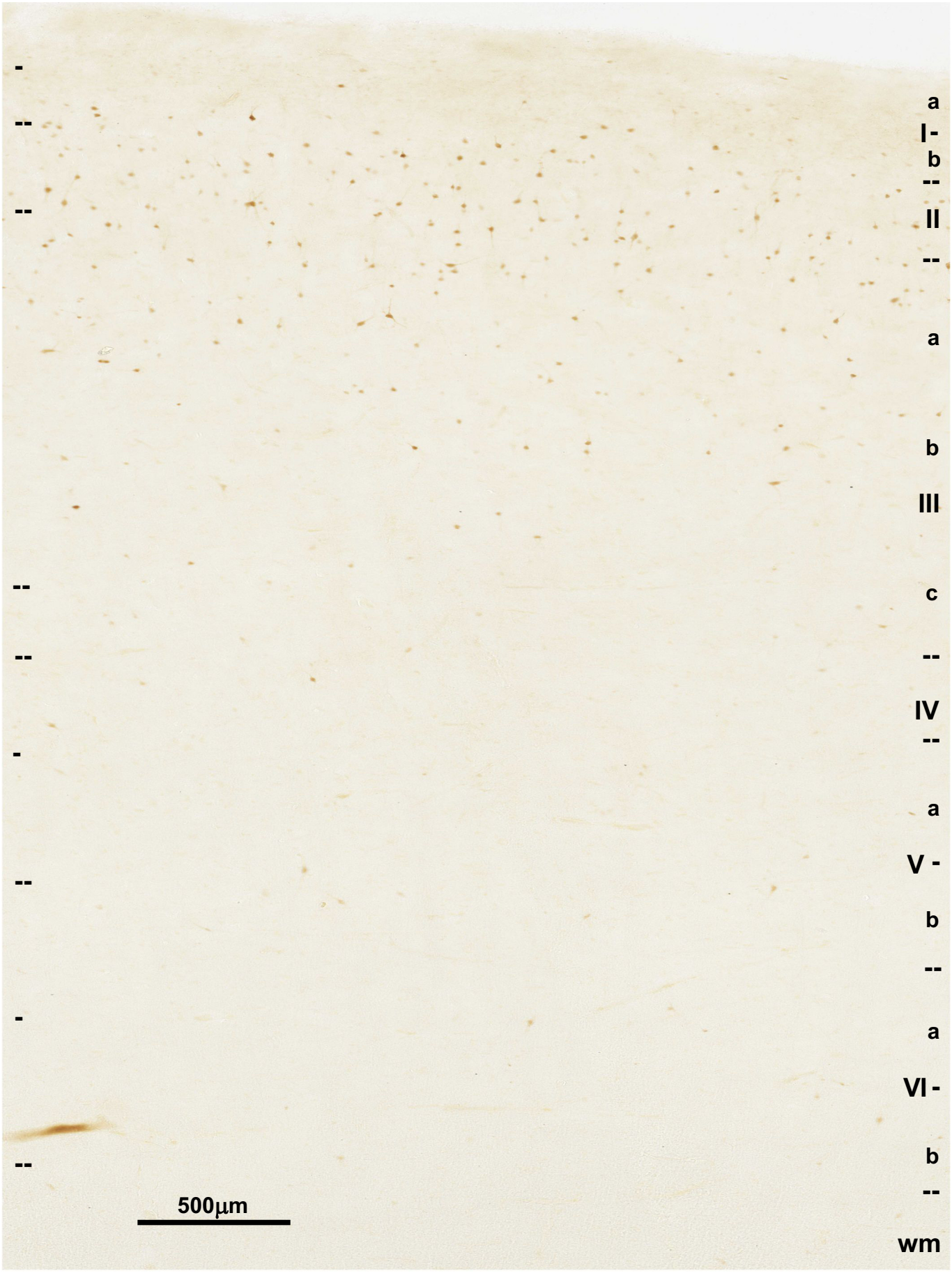


**Figure 5.58** Area **32** in human Immunohistochemical anti-**calretinin** staining.

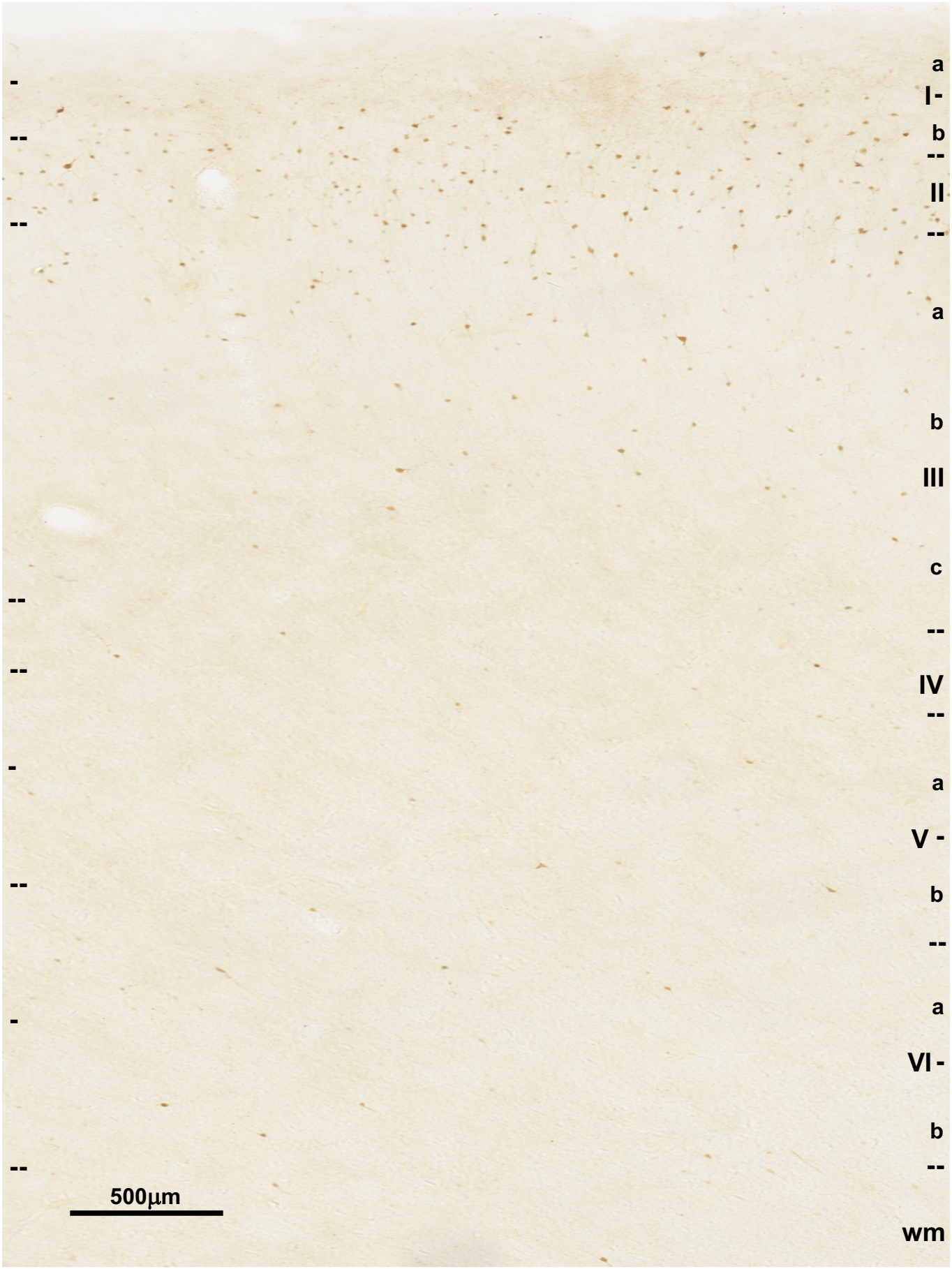


**Figure 5.59** Area **24** in human. Immunohistochemical anti-**calretinin** staining.

### 5.8.1. Quantitative analysis of calretinin neurons throughout cortical layers

Quantitative analysis did not reveal differences in laminar distribution (Table 5.13; Figure 5.60), density (Table 5.14; Figure 5.61) and proportion (Table 5.15; Figure 5.62) between the different analyzed areas. In all these areas (9, 34, 24), 75-90 % of calretinin neurons were located in upper (I-III) cortical layers, layers I and II containing the large majority of them (40-50%). Layer I contains 15% of all calretinin neurons with most of them located in the lower half. Comparison with area 14 (Džaja, 2015) revealed that there are more neurons in layer I in area 14, but the overall distribution between supragranular layers (I-II) versus infragranular (V-VI) remains consistent.

The laminar distribution of calretinin neurons observed in human is similar to that found in monkey in all cortical areas examined (Table 5.4; Figure 5.20A,B). However, the proportions of calretinin neurons in the upper cortical layers in human areas 9 and 32, are slightly higher than those in monkey.

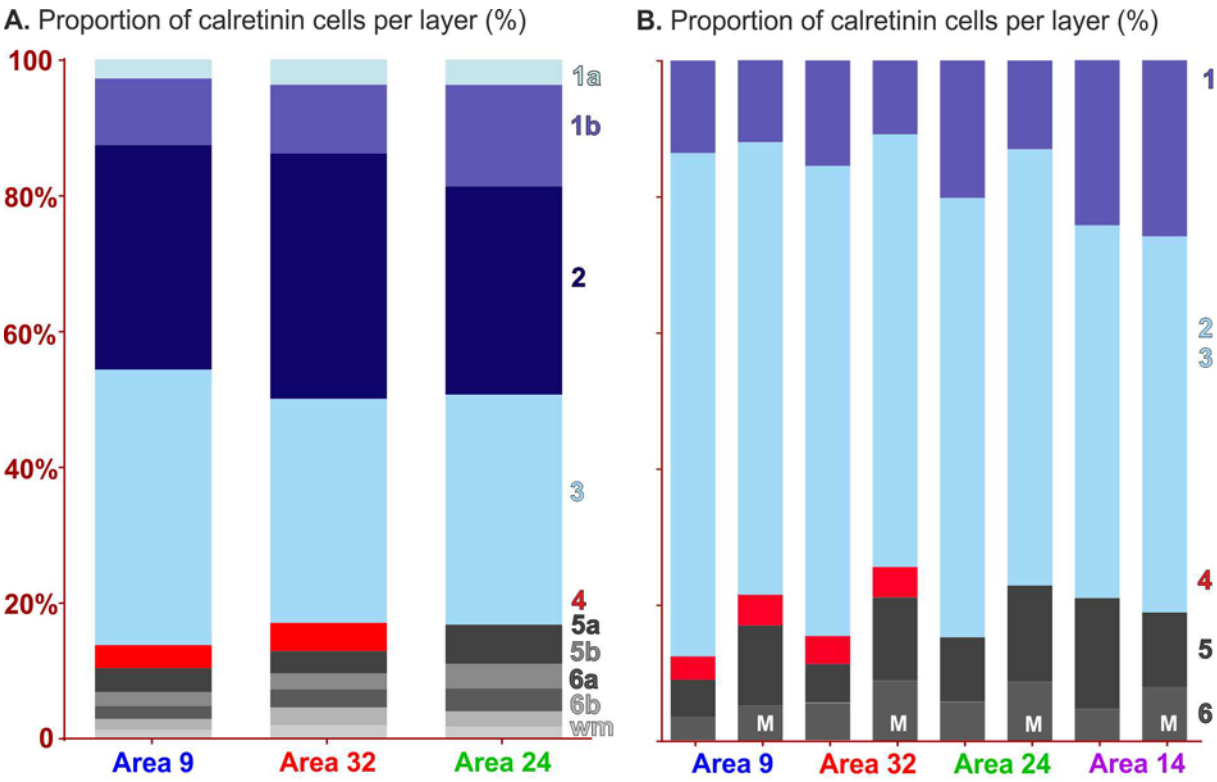


**Figure 5.60** Graphs show **laminar distribution of calretinin** immunolabeled neurons for particular layer. Values shown on graph B are values obtained in this study, for both human and monkey (M), and presented in the way to be comparable with data from area 14 (Džaja 2015, PhD Thesis).

**Table 5.13 Laminar distribution of calretinin labeled neurons** in human (relative distribution (%) per layer in areas 9, 32 and 24)

| | **Area 9** | SD | **Area 32** | SD | **Area 24** | SD |
|---|---|---|---|---|---|---|
| Ia | **2.8%** | 0.2% | **3.7%** | 1.3% | **3.8%** | 2.0% |
| Ib | **9.8%** | 2.9% | **10.1%** | 1.3% | **14.9%** | 1.1% |
| II | **33.1%** | 6.1% | **36.2%** | 4.4% | **30.7%** | 5.9% |
| III | **40.6%** | 2.3% | **33.0%** | 3.8% | **33.9%** | 4.0% |
| IV | **3.4%** | 0.7% | **4.2%** | 0.5% | **Ø** | Ø |
| Va | **3.5%** | 1.2% | **3.3%** | 0.8% | **5.8%** | 3.6% |
| Vb | **2.0%** | 1.0% | **2.4%** | 0.5% | **3.6%** | 1.9% |
| VIa | **1.9%** | 0.8% | **2.7%** | 0.6% | **3.4%** | 1.6% |
| VIb | **1.6%** | 1.0% | **2.6%** | 0.8% | **2.2%** | 0.8% |
| WM | **1.2%** | 0.5% | **1.9%** | 0.5% | **1.7%** | 0.6% |

**Table 5.14 Density of calretinin labeled neurons cells** per layer in human areas 9, 32 and 24 (1000 cells / $mm^3$). Overall calretinin densities from layers I-VI and II-VI are presented in the last two rows

| | **Area 9** | SD | **Area 32** | SD | **Area 24** | SD |
|---|---|---|---|---|---|---|
| Ia | **0.6** | 0.1 | **0.9** | 0.4 | **0.6** | 0.2 |
| Ib | **2.5** | 1.2 | **2.7** | 0.7 | **3.0** | 0.7 |
| II | **4.7** | 1.5 | **5.6** | 2.0 | **5.0** | 1.5 |
| III | **2.2** | 0.5 | **2.3** | 0.6 | **2.3** | 0.3 |
| IV | **1.0** | 0.1 | **1.1** | 0.0 | **Ø** | Ø |
| Va | **0.7** | 0.1 | **0.6** | 0.1 | **0.9** | 0.5 |
| Vb | **0.4** | 0.1 | **0.7** | 0.3 | **0.8** | 0.4 |
| VIa | **0.4** | 0.1 | **0.6** | 0.2 | **0.7** | 0.2 |
| VIb | **0.5** | 0.2 | **0.7** | 0.4 | **0.6** | 0.3 |
| WM | **0.4** | 0.3 | **0.6** | 0.3 | **0.6** | 0.2 |
| **I-VI** | **1.8** | 0.7 | **1.9** | 0.6 | **1.9** | 0.2 |
| **II-VI** | **1.9** | 0.7 | **2.0** | 0.7 | **2.0** | 0.1 |

The densities of calretinin neurons are comparable in all the three human prefrontal areas analyzed (Figure 5.62). The highest density of calretinin neurons is in layer II (4700-5600 cells per $mm^3$), followed by layer Ib and III (2200-3000 cells per $mm^3$), whereas in other layers the densities are around or below 1000 calretinin cells per $mm^3$ (Table 5.14). It should be noted that interindividual differences are high. In most layers we found differences between subjects around 2 fold (Figure 5.62A). That higher proportion of calretinin neurons is distributed to layer I especially in human area 14 (Džaja, 2015) , and calretinin density in layer I of the area 14 is higher than areas analyzed in this study (Figure 5.62B).

In monkey calretinin neurons in each layer show 3 to 4 times higher densities (Figure 5.61C, D) what is a result of decrease in NeuN density in humans.

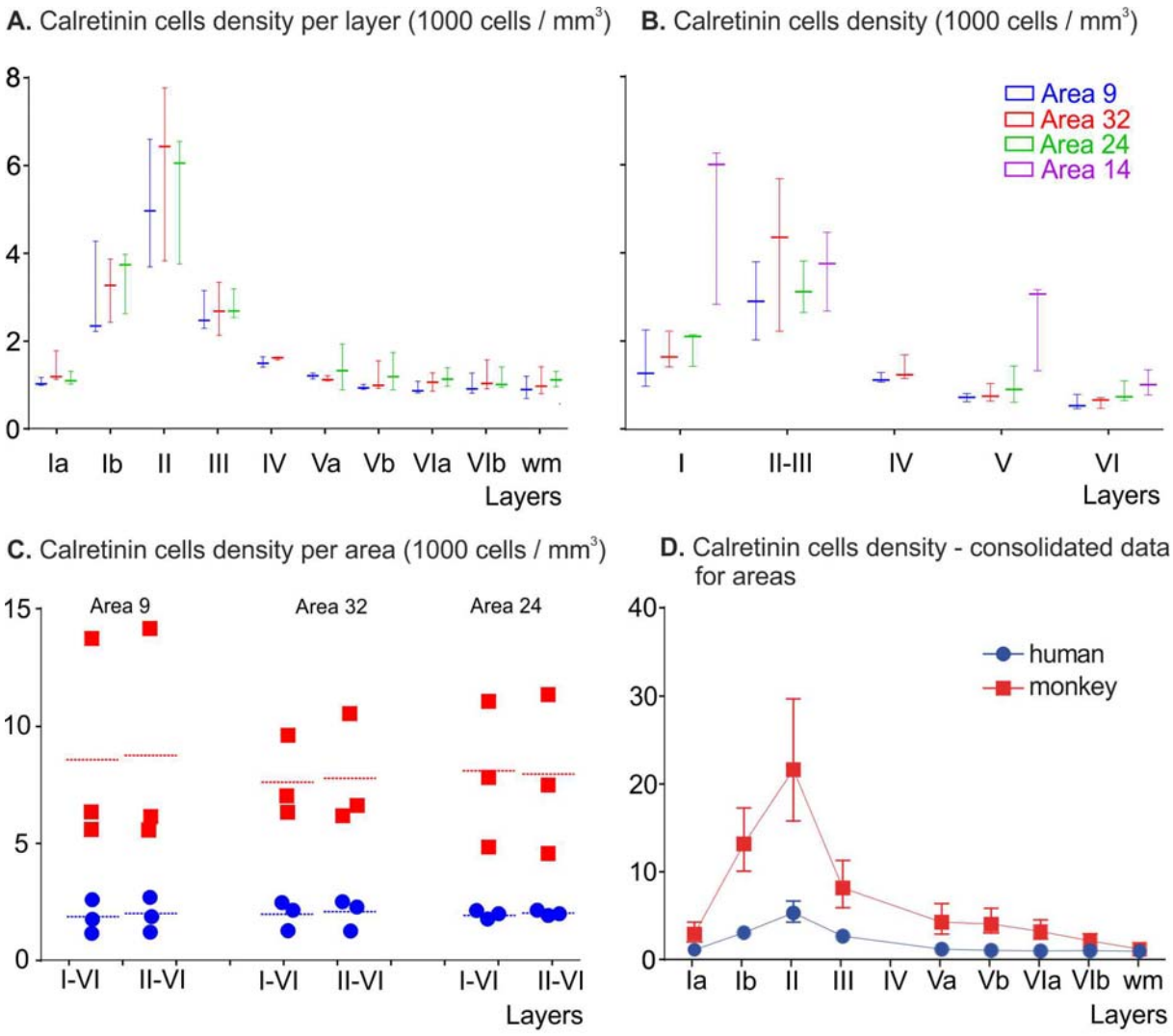


**Figure 5.61** Graphs show **density of calretinin** immunolabeled neurons for particular layer in human (A, B) and comparing human and monkey layers I-VI and II-VI (C) and consolidated data from all areas (D). Values shown on graph B are values obtained in this study and presented in the way to be comparable with data from area 14 (Džaja 2015, PhD Thesis).

The proportion of neurons expressing calretinin among total neuronal pool (NeuN stained cells) varies from 5% in area 32 to 8% in area 24 (Table 5.15). These values are lower than that observed in area 14 (Figure 5.62C), where proportion of cells expressing calretinin was 17.2% (Džaja, 2015). In all cortical areas analyzed, the proportion of calretinin labeled neurons varies between layers (Figure 5.62). In all three cortical areas examined, layer I displays the highest proportion of calretinin neurons (15-25%). In layers II and III, 6-11% of the neurons express calretinin, and less than 5% of neurons express calretinin in the other layers. However these differences between layers were not statistically significant due to large interindividual variability that reached up to 4 fold between subjects (Figure 5.62A, B).

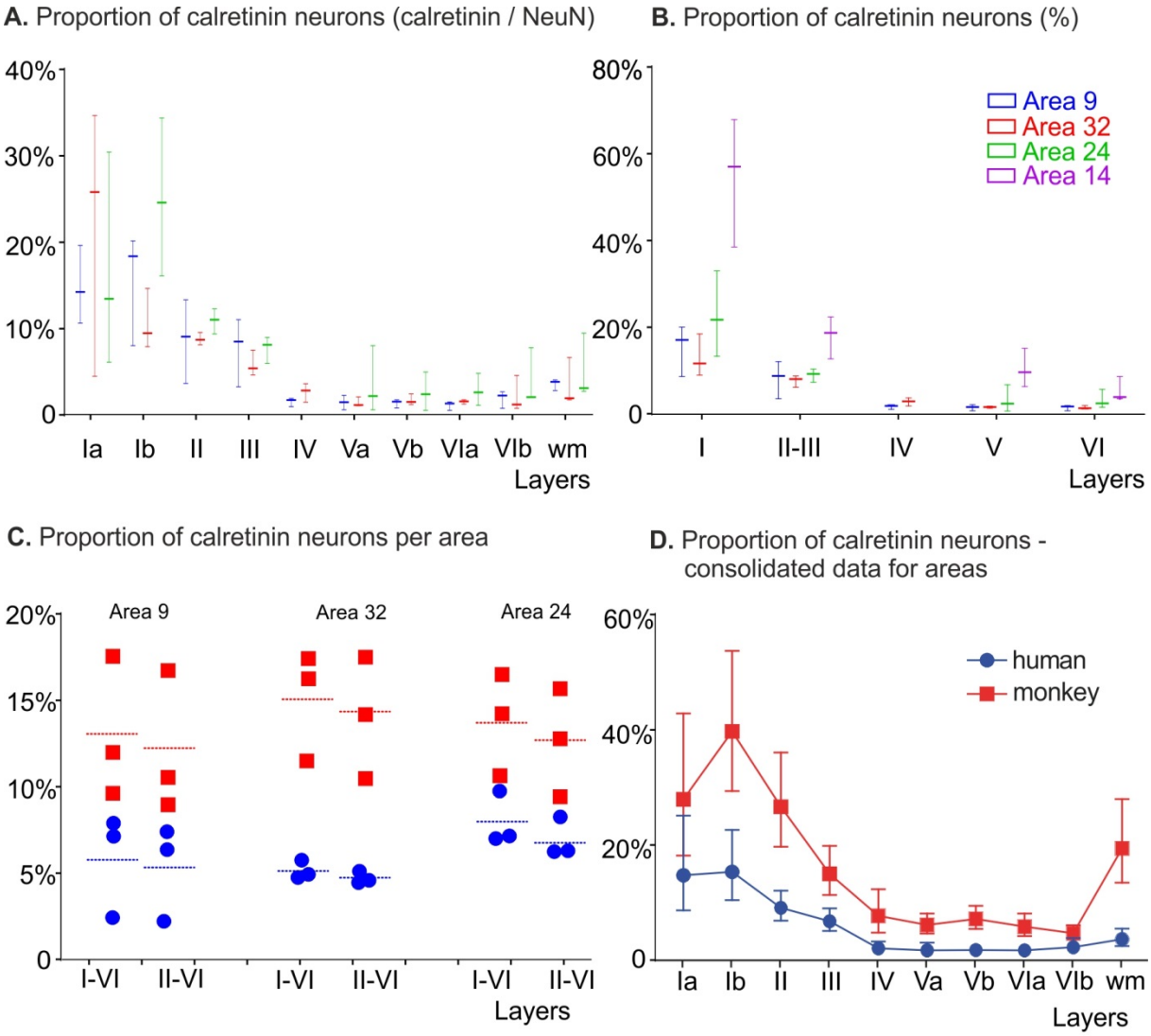


**Figure 5.62** Graphs show **proportion of calretinin** neurons (number of calretinin labeled neurons per number of NeuN labeled neurons) for particular layer in human (A, B) including comparison between human and monkey density through layers I-VI and II-VI (C), and consolidated data from all areas are also presented (D). Values shown on graph B are values obtained in this study and presented in the way to be comparable with data from area 14 (Džaja 2015, PhD Thesis).

The proportion of neurons expressing calretinin in monkey areas (13-15%) is 2 times higher than in human (5-7%). These proportions in human subjects (Tables 5.15, 5.16; Figure 5.21) rarely reach those observed in monkeys (Tables 5.6, 5.7; Figure 5.21). For example, only in one human specimen, the proportion of calretinin neurons exceeded 30% in layer I of area 24, whereas in monkeys the average proportion of neurons expressing calretinin is 30-44%. The maximal proportion found in one human area 9 was 13.6% in layer II and exceeded 10% (11.3%) in layer III. For comparison, in monkeys the average proportion of calretinin neurons is 26-34% for layer II and 14-19% for layer III.

The difference in proportion of calretinin neurons between species is statistically significant in area 32 (p=0,04) and area 24 (p=0.03), and area 9 shows the same tendency (p=0.06).

**Table 5.15 Proportion of calretinin labeled neurons** in areas 9, 24, 32 in human (number of calretinin neurons / total number (NeuN) of neurons – shown as %). Overall calretinin proportion from layers I-VI and II-VI is presented in the last two rows.

| | **Area 9** | SD | **Area 32** | SD | **Area 24** | SD |
|---|---|---|---|---|---|---|
| Ia | **15.1%** | 4.6% | **22.0%** | 15.6% | **17.0%** | 12.5% |
| Ib | **15.8%** | 6.6% | **10.9%** | 3.5% | **25.4%** | 9.2% |
| II | **8.9%** | 4.9% | **9.0%** | 0.7% | **11.1%** | 1.5% |
| III | **7.8%** | 4.0% | **6.1%** | 1.5% | **7.9%** | 1.6% |
| IV | **1.7%** | 0.5% | **2.9%** | 1.1% | **Ø** | Ø |
| Va | **1.6%** | 0.8% | **1.6%** | 0.6% | **3.8%** | 3.9% |
| Vb | **1.6%** | 0.5% | **1.9%** | 0.6% | **2.8%** | 2.2% |
| VIa | **1.3%** | 0.5% | **1.7%** | 0.3% | **3.1%** | 1.9% |
| VIb | **2.1%** | 1.0% | **2.4%** | 2.1% | **4.2%** | 3.3% |
| WM | **3.8%** | 0.7% | **3.7%** | 2.8% | **5.3%** | 3.8% |
| **I-VI** | **5.9%** | 3.0% | **5.2%** | 0.5% | **8.1%** | 1.6% |
| **II-VI** | **5.4%** | 2.8% | **4.8%** | 0.4% | **7.0%** | 1.2% |

**Table 5.16.** Proportion of calretinin **labeled neurons** in areas 9, 32 and 24 shown for each human specimen (number of calretinin neurons / total number (NeuN) of neurons – shown as %).

| layers | | **area 9** | | | **area 32** | | | **area 24** | |
|---|---|---|---|---|---|---|---|---|---|
| | H384 | H386 | H387 | H384 | H386 | H387 | H384 | H386 | H387 |
| Ia | 10,9% | 14,5% | 19,9% | 35,1% | 4,7% | 26,1% | 30,8% | 6,3% | 13,7% |
| Ib | 8,3% | 18,7% | 20,4% | 8,1% | 9,7% | 14,9% | 34,8% | 16,4% | 24,9% |
| II | 3,9% | 13,6% | 9,3% | 8,9% | 8,4% | 9,8% | 11,3% | 12,5% | 9,6% |
| III | 3,5% | 11,3% | 8,7% | 7,8% | 4,9% | 5,6% | 8,4% | 9,2% | 6,2% |
| IV | 1,1% | 2,1% | 1,9% | 3,8% | 3,0% | 1,7% | ø | ø | ø |
| Va | 0,8% | 2,5% | 1,7% | 1,3% | 2,3% | 1,3% | 8,3% | 2,4% | 0,8% |
| Vb | 1,0% | 2,0% | 1,8% | 1,7% | 1,4% | 2,6% | 5,2% | 2,6% | 0,7% |
| VIa | 0,7% | 1,5% | 1,7% | 1,5% | 2,0% | 1,8% | 5,0% | 2,8% | 1,3% |
| VIb | 1,0% | 2,4% | 2,9% | 1,4% | 1,0% | 4,8% | 8,0% | 2,2% | 2,3% |
| WM | 3,0% | 4,0% | 4,3% | 2,0% | 2,1% | 6,9% | 9,7% | 2,9% | 3,3% |
| **I-VI** | **2,5%** | **8,0%** | **7,2%** | **5,0%** | **4,8%** | **5,8%** | **9,9%** | **7,1%** | **7,2%** |
| **II-VI** | **2,2%** | **7,5%** | **6,4%** | **4,6%** | **4,5%** | **5,2%** | **8,4%** | **6,4%** | **6,3%** |

## 6. Discussion

Executive cognitive functions mediated by the prefrontal cortex have tremendously evolved in human compared to non-human primate (Aboitiz et al., 2006; Coolidge and Wynn, 2005), the human specific neuroanatomical substrate supporting such function is still an open question. One of the hypothesis relates on the selective and huge enlargement of the prefrontal cortex (or subdivisions of it) in human (Rilling, 2006; Schenker et al., 2010; Schoenemann, 2006; Semendeferi et al., 2002). However, this enlargement is actually within the expected range when reported to the allometric scaling of the entire human brain size (Donahue et al., 2018; Herculano-Houzel, 2009; Holloway et al., 2004; Sherwood, 2005; Sherwood et al., 2012).

Aside from the possible differential enlargement of areas within the prefrontal cortex, there is currently little evidence for specific histological features or organization of neuronal connections that would serve as a neurobiological basis for the unique cognitive abilities of humans. Indeed, several recent studies highlight the common features of neocortical architecture in human and non-human primates. For example, humans and chimpanzees have similar high density of axons containing serotonin, dopamine and acetylcholine innervating the prefrontal cortex (Raghanti et al., 2010; Sousa et al., 2017). Furthermore, the total number of neurons in the human neocortex accords with allometric scaling predictions from other primate brains (Azevedo et al., 2009; Sherwood et al., 2010).

Most of the studies that have analyzed the number of neurons in various cortical areas on Nissl stained sections (Gabbott & Bacon, 1996a, 1996b; Gabbott et al., 1997 a,1997b) or analyzed the prefrontal cortex as a whole (Azevedo et al., 2009; Semendeferi et al., 2002; Teffer and Semendeferi, 2012). NeuN staining does not label glial or vascular cells in contrast to Nissl staining and the advantage of using NeuN to examine cytoarchitectonic has been well documented (Atapour et al., 2018; Vogt et al., 2013). It enhances laminar differences helping us to identify layers less apparent with Nissl staining such as layer IV in area 32. Although the number of cells described in the literature is not directly comparable with our results due to previously mentioned methodological differences (NeuN versus Nissl) the overall pattern seems unchanged.

The advantage of NeuN staining is seen in the ongoing debate on the classification of, for example, area 32 in the primate frontal cortex. The literature still debates whether it has a layer IV – several Nissl studies suggest that it is agranular cortex (Carmichael et al., 2003; Öngür et al., 2003) while several other indicate the presence of layer IV, (Petrides et al., 2011; Petrides and Pandya, 1999; Triarhou, 2007; Vogt et al., 1987) as we confirmed in this study.

**Laminar distribution and neuron density**

Our study confirmed that there are no substantial differences in neuron densities between prefrontal cortical areas. On the other hand, we found some novelties regarding the laminar distribution in the primate brain. First, we showed that the number of neurons in layer I was underestimated in previous studies performed in monkey and human (Gabbott & Bacon, 1996a, 1996b; Gabbott & Bacon, 1997 a,1997b). We identified with NeuN labeling two clear, neuronal density based, subdivisions of this layer not seen on Nissl staining. We further demonstrate that at least 4% of total neuronal pool in each area examined are located in the lower part of layer I in both species. To our knowledge it is the first demonstration of such layer I organization in the primate brain. Also, the relative volume of the layer I has almost doubled through primate evolution, representing 20% of all cortical layers in human and 10% in the macaque monkey. The volumes of the other cortical layers we found are similar to that described in the literature in both species (Gabbott & Bacon, 1996a, 1996b; Gabbott et al., 1997 a,1997b). Also proportion of neurons in the layer I seems to increase from dorsal to orbitomedial (Džaja, 2015) human prefrontal cortex. We did not confirm this in the monkey prefrontal cortical areas 9, 32, and 24.

One of the main differences we observed between monkeys and human is higher number of neurons in the supragranular layers in human as compared to monkey. Despite a similar laminar distribution between monkey and human the ratio between supra- versus infra-granular layers is higher in all human subjects what is not the case in monkeys. Another consistent finding observed in both species is that the ratio of neuron numbers between supra- and infra-granular layers is the highest in area 9 followed by area 32, and the lowest in the area 24. When monkey data are compared to human the radio is always higher in human areas than in monkey. Interestingly, in monkey the highest ratio value is 1.4 in area 9, corresponding more or less to the lowest ratio value of 1.5 observed in area 24 in human. These results suggest that evolution increased the unbalance in number of neurons between the cortico-cortical projecting supragranular layers and the cortico-subcortical projecting infragranular layers.

Another major result revealed by this study is that in primate layer I contains a substantial number of neurons in contrast to rodents in which the density of neurons is comparable to that of the white matter (WM). Indeed, the neuronal density in monkey layer Ib is comparable to densities found in layer VIb in all areas (32 000 versus 44 000 neurons per $mm^3$). The layer Ia has densities that are either in area 9 comparable to density in underlying white matter (8000 neurons per mm3) or twice the value of WM neuronal density. These results suggest that between rodents and primates, mammalian evolution has provided additional neurons to the layer I.

In both human and monkey species, the layer Ia showed features which are comparable to layer I in rat including a very low density of neurons which is around 10000 neurons/mm$^3$ (Džaja, 2015) and monkey layer Ia. This density is 2-3 times lower in human layer Ia. This is mainly due to the significant increase in relative volume of layer I between monkey and human, despite an increased number of layer I neurons in human as compared to monkey. This increased volume of layer I in human versus monkey suggest further increase in connectivity of layer I in the human cortex.

During development the molecular layer can be subdivided into two portions: the upper portion (layer Ia) that contains large neurons called Cajal-Retzius cells, and the lower portion (layer Ib) with horizontally oriented fibers (Tkachenko et al., 2016). In the monkey, 1mm$^3$ of layer Ib contains about 31500 neurons, that is the number of neurons found in same volume of layer III and Va in the all analyzed areas of the human brain. In monkey the density in layer Ib was closer to density of layer VIb (40000 neurons/1mm$^3$), showing that layer Ib should not be defined as non-neuronal layer. In the human, the neuron density in layer Ib of area 9 and 24 decreases for about 50%, and in area 32 for about 15% compared to monkey values, but their density was not significantly lower than neuron density in layers Vb, VIa and VIb, confirming that in the human the layer Ib should not be defined as non-neuronal layer.

In human, the neuron densities in layer Ib were around those found in the underlying white mater (13000 cells/mm$^3$). In monkey this was not the case, and density in underlying white mater was in area 9 close to layer Ia density, in area 32 it was 2.5 times lower, and in area 24 it was 4 times lower than in layer Ia. So, in monkey the neuron density between layer VIb and underlying white mater decreases in area 9 for about 5 times, and in areas 32 and 24 for about 12-14 times, making the lower cortical border rather sharp. In human, the neuron density in underlying white mater was around two times lower than in layer VIb, and in all areas exceeded 10000 neurons/mm$^3$. These features make this zone bellow layer VIb closer in number of neurons to sublayer Ib. Therefore, in human it would be more appropriate to define zone bellow layer VI as additional cortical sublayer. Its neuron density was 2.5-3 times higher than in layer Ia, where the neuron density is supposed to be higher than in the white mater. These layers differ in their neuron numbers and densities but also in proportion of neurons expressing calretinin. The zone bellow layer VIb – the underlying white matter - had in human slightly higher proportion of calretinin neurons than layers V-VI, but below proportion found in layer III. In monkey, the proportion of calretinin neurons in this zone (14-30%) was significantly higher than in layers V-VI (4-8%), and even slightly higher than in layer III (13.5-19%). These results suggest that in human there is a novel sublayer between layer VI and white matter.

Similar conclusion could be made for monkey area 9, although not as obvious as in the human areas, the densities and calretinin proportion in layer VIb is comparable to that observed in all human areas. On the other hand, monkey areas 24 and 32 have very low neuron density and high proportion of neurons expressing calretinin suggesting that in these two cortical areas this zone is a part of white matter, and neurons found there could correspond to interstitial neurons (Judaš et al., 2010). The additional sublamination of layer VI, faintly observed on area 9 in monkey, and clearly present in all examined human areas, might be related with highly expanded subplate and its protracted developmental persistence (Judaš et al., 2013; Reep, 2000). It is also possible that in human, more subplate neurons being incorporated into adult cortical network, therefore do not undergo elimination through brain maturation.

Another main difference we observed in all cortical areas examined between monkey and human is 40% decrease in neuron density. This has also been described in a previous study performed in the orbital prefrontal cortex (Džaja, 2015). This low density of neurons compared to non-human primates and rodents is a general feature of the human cortex. It has been associated to an increased complexity of dendritic arbor of pyramidal neurons and increased connectivity (Mohan et al., 2015).

**Distribution, density and proportion of calretinin neurons**

Our data do not show major differences in the proportion of calretinin neurons between the various cortical areas examined or between humans and monkeys in keeping with previous studies (Gabbott et al., 1997 a,1997b; Gabbott and Bacon, 1996a, 1996b; Hof et al., 1999; Sherwood et al., 2010; Zaitsev et al., 2005). We further show that the percentage of calretinin and parvalbumin interneurons across areas of the frontal cortex does not differ among these two species, revealing certain fundamental characteristics of neurobiological organization shared within this branch of primate evolution (Sherwood et al., 2010).

The distribution of calretinin neurons mainly located in the upper cortical layers has already being reported by several studies in rodents, monkey and human. Although using a different approach all these studies showed that most of calretinin neurons are located in layer II in all species studied (Gabbott et al., 1997 a,1997b; Gabbott and Bacon, 1996a, 1996b; Hof et al., 1999; Sherwood et al., 2010; Zaitsev et al., 2005).

The variations in the distributions and morphologies of calretinin neurons in the medial prefrontal cortex of different species suggest functional specialization of this class of inhibitory interneurons. Many studies have reported that calretinin neurons represented 8% of the total neuron population in human medial prefrontal cortex, versus 11% in monkey and

4% in rat (Gabbott et al., 1997 a,1997b; Gabbott and Bacon, 1996a, 1996b). We obtained similar results showing that calretinin neurons represent 5% of neurons in human versus 13% in monkey in the dorsal prefrontal cortex. In monkey, depending on the region, between 13%-15% of neurons express calretinin. However, individual differences were rather high. For example, in the area 9, the proportion of neurons expressing calretinin could varies by 70% from one monkey (17.8%) to another (9.7%). Regional variation within animal were sometimes high, so in an animal where only 9.7% of neurons express calretinin in area 9, 16.5% neurons express calretinin in area 24. No consistent regional differences were observed, meaning in another animal the lowest proportion was in area 24 (11.6%) and the highest in area 32 (14.4%). In the third animal, the variations were rather low, between 16.7% and 17.8%. The reason for such variability in proportion of neurons expressing calretinin among animals is unclear. We do not believe that it could be related with difference in fixation condition since no such variability was observed with NeuN labeling. Is the relationship between the calretinin level of expression within neurons associated with physiological state of the animals at the time of fixation would be interesting to determine. Anyway taking into account this interindividual variation we estimate that in monkey, calretinin neurons indeed represent around 15% of total population in dorsal associative prefrontal areas.

Our next analyses investigated whether humans and macaque monkeys vary from each other in the proportions of interneuron subtypes across the different frontal cortical areas 9, 32 and 24. We did not find evidence for such differences. The proportion of these different interneuron population did not vary significantly between the investigated areas nor between human and monkey species. These results are in keeping with previous studies using different methodologies (Gabbott & Bacon, 1996a, 1996b; Gabbott et al., 1997 a,1997b; Gonchar et al., 2010; Sherwood et al., 2010).

Human interneuron densities were contained within the 95% prediction intervals for dorsolateral prefrontal cortex based on scaling to total neuron density in non-human anthropoids. Humans also did not differ significantly from macaques in the regional distribution of interneurons within the frontal cortex (Sherwood et al., 2010).

Regarding the proportion there is a 3-4-fold decrease in proportion in human areas. This is almost uniform across all layers, in all analyzed areas. In this study we have a methodological factor that may produce such great differences, i.e. we used a monoclonal antibody in human and polyclonal in monkey sections. The double labeling in monkey revealed that qualitatively no differences were observed on the sections labeled with monoclonal calretinin antibody compared to the one labeled with the polyclonal one. This suggests that the human monkey difference in proportion is indeed real and not the

consequence of using a different calretinin antibody. Nevertheless, this is a point that needs to be further confirmed. The fact that methodological factors affect identification of calretinin neurons is particularly important for the interpretation of the human data where monoclonal antibody is used. Monoclonal antibodies are generally not as effective in visualizing the whole population of neurons expressing particular molecule, and calretinin monoclonal antibody was additionally shown to be dependent on the level of calcium binding in neurons. This might explain why in this study in human specimens the proportion of neurons labeled with calretinin was significantly lower when compared to monkey (around 2 times lower, i.e. in average between 5.2%-8.1%). The highest proportion was observed in area 32 of one specimen (10%), but the same specimen showed also the lowest values observed, and in area 9 where only 2.5% of neurons were found to express calretinin. It should be mentioned that on double labeled sections of the monkey brain, we have not been able to identify qualitatively differences in density of calretinin neurons, but the tissue preparation protocol differs between monkey and human. In monkey brain tissue is obtained from fixation by transcardiac perfusion without delay between death and fixation, whereas human tissue was fixed by immersion with delay of 6 hours between death and fixation (Gabbott et al., 1997 a,1997b; Sherwood et al., 2010).

However, if so, the changes in calretinin proportion during primate evolution differ between orbital and dorsal part of the prefrontal cortex. In human area 14c, by using polyclonal antibody, the average proportion of neurons expressing calretinin was 17.6%, varying between 14-21% between subjects. In area 14c of monkey, 12% of neurons were found to express calretinin, varying between 9-15% in particular animal (Džaja, 2015). These results compared to ours suggest that an increase in calretinin neurons could occur in specific cortical region such as the area 14c orbito-prefrontal cortex but not all cortical regions (dorsal prefrontal areas) through primate evolution.

A possible explanation for smaller proportion of calretinin neurons in the human brain is that the number of inhibitory calretinin neurons attained in the primate evolution is enough to maintain the optimal function of the cortical networks (Trevelyan and Watkinson, 2005). Thus, although the number of neurons in the upper layers is increased the number of inhibitory controls remains the same. This suggests that evolutionary expansion in proportion of calretinin neuron in the primate brain that occurs between rodents and monkeys (Džaja et al., 2014) is enough for optimal human information processing (Sherwood et al., 2010).

**Molecular profile of calretinin neurons in primate brain**

The GABAergic phenotype of calretinin neurons was confirmed in rodent neocortex (Gonchar et al., 2007; Gonchar and Burkhalter, 1997; Uematsu et al., 2008). On the other hand, in monkey and human neocortex, it was shown that about 25% of calretinin neurons do express GABA (Melchitzky et al., 2005; Rio and Defelipe, 1996). This question of GABAergic profile of calretinin neurons was addressed in this study. We confirmed the GABAergic profile showing that all these neurons in the primate brain express mRNAs for the vesicular GABA transporter (VGAT) and one of the synthesizing enzyme for GABA, the glutamic acid decarboxylase 67 (GAD67) as did a study by Rocco et al. where it was shown that calretinin neuron *boutons* always express GAD67 (Rocco et al., 2016), but occasionally GAD65, that is also in line with results from this study.

## 7. Conclusion

Our results highlight some differences in the organization of the prefrontal cortex between monkey and human as well as major specific features of primate brain as compared to rodents. Results of this study give ground for the future research on the pathogenesis of different brain dysfunctions. Firstly, we showed that in the primate brain cortical calretinin neurons are GABAergic inhibitory neurons what raises the possibility of finding novel therapeutic targets in diseases such as epilepsy. Secondly, the data we obtained on the positioning of neurons inside the prefrontal cortex areas that are involved in higher cognitive functioning are crucial for the research that could reveal the pathophysiology of complex neuropsychiatric disorders in humans, as autism or schizophrenia.

**A. Major findings regarding calretinin neuron subpopulation:**

1. Calretinin neurons express VGAT in the primate brain.
2. Calretinin neurons do not overlap with parvalbumin, calbindin and somatostatin.
    a. Calbindin, parvalbumin and somatostatin neurons altogether are as numerous as calretinin subpopulation.
3. In the dorsal prefrontal areas up to 15% of all neurons express calretinin.
4. Upper cortical layers consist of 75% calretinin neurons.
    a. In the layers II and III they represent at least 1/3 of total neuron population.
5. Increase in the number of calretinin neurons is changing the laminar organization of layers I and VI, leading to the formation of layer Ib as specific feature of the primate brain.

**B. Major findings regarding laminar organization:**

1. Human areas show a 40% decrease in neuron density compared to monkey.
2. Primate prefrontal cortical areas show a neuronal redistribution in favor of supragranular layers (I-III) (ratio I-II/V-VI above 1).
    a. Only area 9 in the monkey has more neurons in the supragranular layers whereas areas 32 and 24 do not show this feature.
    b. All human prefrontal cortical areas show neuronal organization in favor of supragranular layers, with the highest ratio in area 9 followed by areas 32 and 24
3. The primate sublamination in the prefrontal cortex suggests two new sublayers, in the layer I and bellow layer VIb.
    a. Layer I is clearly divided in upper neuron sparse part and a lower part with neuron density corresponding to those found in other sublayers.
    b. Zone bellow sublayer VIb has higher neuron density than in surrounding white matter and sublayer Ia in monkey area 9 and in all human prefrontal cortical areas analyzed.

## 8. Abstract in Croatian

**KALRETININSKI NEURONI U PREFRONTALNOM KORTEKSU PRIMATA**, Dora Sedmak, 2019.

**Sažetak**

Pojava složenih moždanih funkcija u čovjeka mora biti odraz reorganizacije u strukturi neuralnih mreža kore velikog mozga. Promjene u sinaptičkoj arhitekturi primata su temelj razvoja viših kognitivnih funkcija, a narušena arhitektonika dovodi do neuroloških i psihijatrijskih poremećaja. Pretpostavlja se kako u evoluciji primata do najvećih promjena u strukturi neuralne mreže dolazi upravo u prefrontalnoj kori velikog mozga. Cilj ovog istraživanja je provesti sustavnu kvantitativnu analizu proporcije, distribucije i molekularnog fenotipa kalretininskih neurona kroz funkcionalno različita polja prefrontalnoga korteksa (Brodmanova polja 9, 32 i 24) u majmuna i čovjeka te utvrditi postoje li obilježja specifična za polje ili vrstu.

U mozgu primata kalretininski neuroni čine 15% ukupnog broja neurona i većinom su smješteni u površnijim kortikalnim slojevima (40% u sloju II, 70% u sloju I). Pokazano je da svi kalretininski neuroni eksprimiraju VGAT mRNA što izravno potvrđuje njihov GABAergički fenotip. Dvostruko bojanje je pokazalo da su kalretininski neuroni brojniji od ostalih glavnih subpopulacija interneurona. Ovi podatci ukazuju da su GABAergički neuroni u slojevima I i II u asocijativnim područjima u primata jednako brojni kao i glutamatergički neuroni. Ne postoji razlika u njihovoj proporciji između majmuna i čovjeka niti između različitih moždanih polja unutar iste vrste.

Može se zaključiti kako je tijekom evolucije primata došlo do reorganizacije laminarne strukture, tako da je veći broj neurona smješten u gornjim slojevima moždane kore koji su izvor kortiko-kortikalnih projekcija. Tendencija ovim promjenama vidljiva je između vrsta i između različitih polja unutar vrste, pa tako hijerarhijski viša područja imaju veći broj neurona u površnijim slojevima.

## 9. Abstract in English

Calretinin neurons in the primate prefrontal cortex, Dora Sedmak, MD; 2019

Neuronal circuitries of the cerebral cortex are the main biological substrates for mental abilities found in mammals. Diversity of primate synaptic architecture enable appearance of complex cognition and their disorganization leads to many neurological and behavioral disturbances. Substantial reorganization of cortical network occurring during primate evolution is necessary to achieve complex information processing. We performed systematic quantitative analysis in prefrontal cortical areas 9, 32 and 24 of monkey and human to determine the proportion, distribution and neurotransmitter phenotype of calretinin neurons, whose proportion dramatically increases when primates are compared to rodents.

In primate brain up to 15% of neurons express calretinin and they are mostly positioned in upper cortical layers (up to 40% in layer II, and up to 70% in layer I). VGAT mRNA was found in all calretinin neurons, which directly confirmed their GABAergic phenotype. Double labeling showed that calretinin neurons are more numerous than other subpopulation of interneurons. This data suggest that GABAergic neurons in layer I and II of the primate associative areas outnumber the principal glutamatergic neurons. There were no areal differences in laminar distribution of calretinin neurons in the primate brain, but we found spatial reorganization inside the cortical lamina favoring the upper cortico-cortical layers and affecting higher order neocortical areas in monkey and all of human prefrontal cortical areas.

## 10. List of references


1. Aboitiz, F., García, R. R., Bosman, C., and Brunetti, E. (2006). Cortical memory mechanisms and language origins. Brain Lang. 98, 40–56. doi:10.1016/j.bandl.2006.01.006.
2. Allman, J. M., Hakeem, A., Erwin, J. M., Nimchinsky, E., and Hof, P. (2006). The Anterior Cingulate Cortex. Ann. N. Y. Acad. Sci. 935, 107–117. doi:10.1111/j.1749-6632.2001.tb03476.x.
3. Ansen-Wilson, L. J., and Lipinski, R. J. (2017). Gene-environment interactions in cortical interneuron development and dysfunction: A review of preclinical studies. Neurotoxicology 58, 120–129. doi:10.1016/j.neuro.2016.12.002.
4. Atapour, N., Majka, P., Wolkowicz, I. H., Malamanova, D., Worthy, K. H., and Rosa, M. G. P. (2018). Neuronal Distribution Across the Cerebral Cortex of the Marmoset Monkey (Callithrix jacchus). Cereb. Cortex, doi:10.1093/cercor/bhy263.
5. Azevedo, F. A. C., Carvalho, L. R. B., Grinberg, L. T., Farfel, J. M., Ferretti, R. E. L., Leite, R. E. P., et al. (2009). Equal numbers of neuronal and nonneuronal cells make the human brain an isometrically scaled-up primate brain. J. Comp. Neurol. 513, 532–541. doi:10.1002/cne.21974.
6. Barbas, H. (2000). Connections underlying the synthesis of cognition, memory, and emotion in primate prefrontal cortices. Brain Res. Bull. 52, 319–330. doi:10.1016/S0361-9230(99)00245-2.
7. Barbas, H. (2015). General Cortical and Special Prefrontal Connections: Principles from Structure to Function. Annu. Rev. Neurosci. 38, 269–289. doi:10.1146/annurev-neuro-071714-033936.
8. Barinka, F., Druga, R., and Druga, R. (2010a). Calretinin Expression in the Mammalian Neocortex: A Review. Physiol. Res 59, 665–677. Available at: www.biomed.cas.cz/physiolres [Accessed July 17, 2018].
9. Barinka, F., Druga, R., Marusic, P., Krsek, P., and Zamecnik, J. (2010b). Calretinin immunoreactivity in focal cortical dysplasias and in non-malformed epileptic cortex. Epilepsy Res. 88, 76–86. doi:10.1016/j.eplepsyres.2009.09.021.
10. Barinka, F., Maglóczky, Z., and Zecevic, N. (2015). Editorial: At the top of the interneuronal pyramid—calretinin expressing cortical interneurons. Front. Neuroanat. 9, 108. doi:10.3389/fnana.2015.00108.
11. Barton, R. A., and Venditti, C. (2013). Human frontal lobes are not relatively large. Proc. Natl. Acad. Sci. USA 110, 9001–9006. doi:10.1073/pnas.1215723110.
12. Beasley, C. L., Zhang, Z. J., Patten, I., and Reynolds, G. P. (2002). Selective deficits in prefrontal cortical GABAergic neurons in schizophrenia defined by the presence of calcium-binding proteins. Biol. Psychiatry 52, 708–715.
13. Benes, F., and Berretta, S. (2001). GABAergic Interneurons Implications for Understanding Schizophrenia and Bipolar Disorder. Neuropsychopharmacology 25, 1–27. doi:10.1016/S0893-133X(01)00225-1.
14. Billwiller, F., Castillo, L., Elseedy, H., Ivanov, A. I., Scapula, J., Ghestem, A., et al. (2019). The GABA-Glutamate supramammillary–dorsal Dentate Gyrus pathway controls theta and gamma oscillations in the DG during paradoxical sleep. bioRxiv. doi:10.1101/584862.
15. Bok, S. T. (1929). Der Einflu\ der in den Furchen und Windungen auftretenden Krümmungen der Gro\hirnrinde auf die Rindenarchitektur. Zeitschrift für die gesamte Neurol. und Psychiatr. 121, 682–750. doi:10.1007/BF02864437.

16. Brisch, R., Bielau, H., Saniotis, A., Wolf, R., Bogerts, B., Krell, D., et al. (2015). Calretinin and parvalbumin in schizophrenia and affective disorders: a mini-review, a perspective on the evolutionary role of calretinin in schizophrenia, and a preliminary post-mortem study of calretinin in the septal nuclei. Front. Cell. Neurosci. 9, 1–13. doi:10.3389/fncel.2015.00393.

17. Bu, J., Sathyendra, V., Nagykery, N., and Geula, C. (2003). Age-related changes in calbindin-D28k, calretinin, and parvalbumin-immunoreactive neurons in the human cerebral cortex. Exp. Neurol. 182, 220–231. doi:10.1016/S0014-4886(03)00094-3.

18. Burkhalter, A. H. (2008). Many specialists for suppressing cortical excitation. Front. Neurosci. 2, 155–167. doi:10.3389/neuro.01.026.2008.

19. Buxhoeveden, D. P. (2012). Minicolumn size and human cortex. Prog. Brain. Res. 195, 219-235. doi:10.1016/B978-0-444-53860-4.00010-6.

20. Buzsaki, G., and Draguhn, A. (2004). Neuronal Oscillations in Cortical Networks. Science 304, 1926–1929. doi:10.1126/science.1099745.

21. Caputi, A., Rozov, A., Blatow, M., and Monyer, H. (2009). Two Calretinin-Positive GABAergic Cell Types in Layer 2/3 of the Mouse Neocortex Provide Different Forms of Inhibition. Cereb. Cortex 19, 1345–1359. doi:10.1093/cercor/bhn175.

22. Carmichael, S. T., and Price, J. L. (1994). Architectonic Subdivision of the Orbital and Medial Prefrontal Cortex in the Macaque Monkey. J. Comp. Neurol. 346, 366-402.

23. Carmichael, S. T., Price, J. L., Öngür, D., Ferry, A. T., and Price, J. L. (2003). Architectonic subdivision of the human orbital and medial prefrontal cortex. J. Comp. Neurol. 460, 425–449. doi:10.1002/cne.10609.

24. Casanova, M. F., Buxhoeveden, D., and Gomez, J. (2003). Disruption in the Inhibitory Architecture of the Cell Minicolumn: Implications for Autisim. Neurosci. 9, 496–507. doi:10.1177/1073858403253552.

25. Chahrour, M., and Zoghbi, H. Y. (2007). The Story of Rett Syndrome: From Clinic to Neurobiology. Neuron 56, 422–437. doi:10.1016/j.neuron.2007.10.001.

26. Charvet, C. J., and Finlay, B. L. (2012). Embracing covariation in brain evolution : Large brains, extended development , and flexible primate social systems. Prog. Brain Res. 195, 71-87. doi:10.1016/B978-0-444-53860-4.00004-0.

27. Conde, F., Lund, J., Jacobowitz, D. M., Baimbridge, K. G., and Lewis, D. A. (1994). Local Circuit Neurons Immunoreactive for Calretinin , Calbindin D-28k or Parvalbumin in Monkey Prefrontal Cortex : Distribution and Morphology. 116, 95–116.

28. Conover, W., and Iman, R. (1981). Rank Transformations as a Bridge Between Parametric and Nonparametric Statistics. Am. Stat. 35, 124–129. doi:10.1080/00031305.1981.10479327.

29. Coolidge, F. L., and Wynn, T. (2005). Working Memory, its Executive Functions, and the Emergence of Modern Thinking. Cambridge Archaeol. J. 15, 5–26. doi:10.1017/S0959774305000016.

30. Cotter, D., Mackay, D., Chana, G., Beasley, C., Landau, S., and Everall, I. P. (2002). Reduced Neuronal Size and Glial Cell Density in Area 9 of the Dorsolateral Prefrontal Cortex in Subjects with Major Depressive Disorder. 9, 386–394.

31. Deacon, T. W. (1997). The symbolic species : the co-evolution of language and the brain. BMJ. 319, 715.

32. DeFelipe, J. (1997). Types of neurons, synaptic connections and chemical characteristics of cells immunoreactive for calbindin-D28K, parvalbumin and calretinin in the neocortex. J. Chem. Neuroanat. 14, 1–19.

33. DeFelipe, J., Alonso-Nanclares, L., and Arellano, J. I. (2002). Microstructure of the neocortex: comparative aspects. J. Neurocytol. 31, 299–316.

34. DeFelipe, J., López-Cruz, P. L., Benavides-Piccione, R., Bielza, C., Larrañaga, P., Anderson, S., et al. (2013). New insights into the classification and nomenclature of cortical GABAergic interneurons. Nat. Rev. Neurosci. 14, 202–16. doi:10.1038/nrn3444.

35. DelRio, M. R., and Defelipe, J. (1996). Colocalization of Calbindin D-28k , Calretinin , and GABA Immunoreactivities in Neurons of the Human Temporal Cortex. J. Comp. Neurol. 482, 472–482. doi: 10.1002/(SICI)1096-9861(19960603)369:3<472::AID-CNE11>3.0.CO;2-K.

36. Donahue, C. J., Glasser, M. F., Preuss, T. M., Rilling, J. K., and Van Essen, D. C. (2018). Quantitative assessment of prefrontal cortex in humans relative to nonhuman primates. Proc. Natl. Acad. Sci. USA 115, E5183–E5192. doi:10.1073/pnas.1721653115.

37. Duncan, J., Emslie, H., Williams, P., Johnson, R., and Freer, C. (1996). Intelligence and the Frontal Lobe: The Organization of Goal-Directed Behavior. Cogn. Psychol. 30, 257–303. doi:10.1006/COGP.1996.0008.

38. Džaja, D. (2015). Morphological and chemical characteristics of calretinin neurons in the primate neocortex. (Morfološka i kemijska obilježja kalretininskih neurona u neokorteksu primata.) [dissertation thesis]. [Zagreb (CRO)]: University of Zagreb.

39. Džaja, D., Hladnik, A., Bičanić, I., Baković, M., and Petanjek, Z. (2014). Neocortical calretinin neurons in primates: increase in proportion and microcircuitry structure. Front. Neuroanat. 8, 103. doi:10.3389/fnana.2014.00103.

40. Esclapez, M., Tillakaratne, N. J., Kaufman, D. L., Tobin, A. J., and Houser, C. R. (1994). Comparative localization of two forms of glutamic acid decarboxylase and their mRNAs in rat brain supports the concept of functional differences between the forms. J. Neurosci. 14, 1834–1855.

41. Etkin, A., Egner, T., and Kalisch, R. (2011). Emotional processing in anterior cingulate and medial prefrontal cortex. Trends Cogn. Sci. 15, 85–93. doi:10.1016/j.tics.2010.11.004.

42. Eyles, D. W., McGrath, J. J., and Reynolds, G. P. (2002). Neuronal calcium-binding proteins and schizophrenia. Schizophr. Res. 57, 27–34.

43. Fajardo, C., Escobar, M. I., Buriticá, E., Arteaga, G., Umbarila, J., Casanova, M. F., et al. (2008). Von Economo neurons are present in the dorsolateral (dysgranular) prefrontal cortex of humans. Neurosci. Lett. 435, 215–218. doi:10.1016/j.neulet.2008.02.048.

44. Favorov, O. V, and Kelly, D. G. Minicolumnar organization within somatosensory cortical segregates: I. Development of afferent connections. Cereb. Cortex 4, 408–427. Available at: http://www.ncbi.nlm.nih.gov/pubmed/7950312 [Accessed August 3, 2018].

45. Ferrer, I., Tuñón, T., Serrano, M. T., Casas, R., Alcántara, S., Zújar, M. J., et al. (1993). Calbindin D-28k and parvalbumin immunoreactivity in the frontal cortex in patients with frontal lobe dementia of non-Alzheimer type associated with amyotrophic lateral sclerosis. J. Neurol. Neurosurg. Psychiatry 56, 257–261.

46. Forbes, C. E., and Grafman, J. (2010). The Role of the Human Prefrontal Cortex in Social Cognition and Moral Judgment. Annu. Rev. Neurosci. 33, 299–324. doi:10.1146/annurev-neuro-060909-153230.

47. Friocourt, G., and Parnavelas, J. G. (2011). Identification of Arx targets unveils new candidates for controlling cortical interneuron migration and differentiation. Front. Cell. Neurosci. 5, 28. doi:10.3389/fncel.2011.00028.

48. Fung, S. J., Webster, M. J., Sivagnanasundaram, S., Duncan, C., Elashoff, M., and Weickert, C. S. (2010). Expression of Interneuron Markers in the Dorsolateral Prefrontal Cortex of the Developing Human and in Schizophrenia. Am. J. Psychiatry 167, 1479–1488. doi:10.1176/appi.ajp.2010.09060784.

49. Fuster, J. M. (1980). The Prefrontal Cortex. London; Burlington, NJ; San Diego: Academic Press. doi: 10.1016/B978-0-12-373644-4.00002-5.

50. Gabbott, P. L. A. A., and Bacon, S. J. (1996a). Local Circuit Neurons in the Medial Prefrontal Cortex ( Areas 24a , b , c , 25 and 32 ) in the Monkey: I. Cell Morphology and Morphometrics. J. Comp. Neurol. 608, 567–608. doi:10.1002/(SICI)1096-9861(19960122)364:4<567::AID CNE1>3.0.CO;2-1.

51. Gabbott, P. L. A., and Bacon, S. J. (1996b). Local circuit neurons in the medial prefrontal cortex (areas 24a,b,c, 25 and 32) in the monkey:Quantitative Areal and Laminar Distributions. J.Comp.Neurol. 364, 567–636.

52. Gabbott, P. L. A., and Bacon, S. J. (1997a). Vasoactive intestinal polypeptide containing neurones in monkey medial prefrontal cortex (mPFC): Colocalisation with calretinin. Brain Res. 744, 179–184. doi:10.1016/S0006-8993(96)01232-2.

53. Gabbott, P. L. A., Jays, P. R. L., and Bacon, S. J. (1997b). Calretinin neurons in human medial prefrontal cortex (areas 24a,b,c, 32, and 25). J. Comp. Neurol. 381, 389–410. doi:10.1002/(SICI)1096-9861(19970519)381:4<389::AID-CNE1>3.0.CO;2-Z.

54. Gabi, M., Neves, K., Masseron, C., Ribeiro, P. F. M., Ventura-Antunes, L., Torres, L., et al. (2016). No relative expansion of the number of prefrontal neurons in primate and human evolution. Proc. Natl. Acad. Sci. 113, 9617–9622. doi:10.1073/pnas.1610178113.

55. Gallagher, H. L., and Frith, C. D. (2003). Functional imaging of “theory of mind.” Trends Cogn. Sci. 7, 77–83.

56. Goel, V., and Grafman, J. (1995). Are the frontal lobes implicated in "planning" functions? Interpreting data from the Tower of Hanoi. Neuropsychologia 33, 623–642.

57. Goldman-Rakic, P. S. (1991). Chapter 16 Cellular and circuit basis of working memory in prefrontal cortex of nonhuman primates. Prog. Brain Res. 85, 325–336. doi:10.1016/S0079-6123(08)62688-6.

58. Gonchar, Y., and Burkhalter, A. (1997). Three distinct families of GABAergic neurons in rat visual cortex. Cereb. Cortex 7, 347–358.

59. Gonchar, Y., Burkhalter, A., Wang, Q., Burkhalter, A., Zaitsev, A. V., Gonzalez-Burgos, G., et al. (2010). Calretinin expression in the mammalian neocortex: A review. Physiol. Res. 59, 665–677. doi:10.1093/cercor/bhh218.

60. Gonchar, Y., Wang, Q., and Burkhalter, A. (2007). Multiple distinct subtypes of GABAergic neurons in mouse visual cortex identified by triple immunostaining. Front. Neuroanat. 1, 3. doi:10.3389/neuro.05.003.2007.

61. Hattori, R., Kuchibhotla, K. V., Froemke, R. C., and Komiyama, T. (2017). Functions and dysfunctions of neocortical inhibitory neuron subtypes. Nat. Neurosci. 20, 1199–1208. doi:10.1038/nn.4619.

62. Hendry, S. H., Schwark, H. D., Jones, E. G., and Yan, J. (1987). Numbers and proportions of GABA-immunoreactive neurons in different areas of monkey cerebral cortex. J. Neurosci. 7, 1503–1519.

63. Herculano-Houzel, S. (2009). The human brain in numbers: a linearly scaled-up primate brain. Front. Hum. Neurosci. 3, 31. doi:10.3389/neuro.09.031.2009.

64. Herculano-Houzel, S. (2012). The remarkable, yet not extraordinary, human brain as a scaled-up primate brain and its associated cost. Proc. Natl. Acad. Sci. 109, 10661–10668. doi:10.1073/pnas.1201895109.

65. Herculano-Houzel, S., Collins, C. E., Wong, P., and Kaas, J. H. (2007). Cellular scaling rules for primate brains. Proc. Natl. Acad. Sci. USA 104, 3562-3567

66. Herculano-Houzel, S., Collins, C. E., Wong, P., Kaas, J. H., and Lent, R. (2008). The basic nonuniformity of the cerebral cortex. Proc. Natl. Acad. Sci. USA 105, 12593–12598. doi:10.1073/pnas.0805417105.

67. Hladnik, A., Džaja, D., Darmopil, S., Jovanov-Milošević, N., and Petanjek, Z. (2014). Spatio-temporal extension in site of origin for cortical calretinin neurons in primates. Front. Neuroanat. 8, 50. doi:10.3389/fnana.2014.00050.

68. Hof, P. R., Glezer, I. I., and Flagg, R. A. (1999). Cellular distribution of the calcium-binding proteins parvalbumin , calbindin , and calretinin in the neocortex of mammals: phylogenetic and developmental patterns. J Chem Neuroanat. 16, 77–116.

69. Hof, P. R., Nimchinsky, E. A., Celio, M. R., Bouras, C., and Morrison, J. H. (1993a). Calretinin-immunoreactive neocortical interneurons are unaffected in Alzheimer's disease. Neurosci. Lett. 152, 145–148. doi:10.1016/0304-3940(93)90504-E.

70. Hof, P. R., Archin, N., Osmand, A. P., Dougherty, J.H., Wells, C., Bouras, C., and Morrison, J. H. (1993b). Posterior cortical atrophy in Alzheimer's disease: analysis of a new case and re-evaluation of a historical report. Acta Neuropathol. 86, 215-223.

71. Holloway, R. L., Broadfield, D. C., and Yuan, M. S. (2004). The Human Fossil Record, Brain Endocasts—The Paleoneurological Evidence, Volume 3. John Wiley & Sons, Inc. USA doi:10.1002/0471663573.

72. Hoshi, E. (2006). Functional specialization within the dorsolateral prefrontal cortex: A review of anatomical and physiological studies of non-human primates. Neurosci. Res. 54, 73–84. doi:10.1016/j.neures.2005.10.013.

73. Hsu, S. M., and Raine, L. (1981). Protein A, avidin, and biotin in immunohistochemistry. J. Histochem. Cytochem. 29, 1349–1353. doi:10.1177/29.11.6172466.

74. Hu, H., Gan, J., and Jonas, P. (2014). Fast-spiking, parvalbumin+ GABAergic interneurons: From cellular design to microcircuit function. Science 345, 1255263–1255263. doi:10.1126/science.1255263.

75. Jerison, H. J. (1985). Animal intelligence as encephalization. Philos. Trans. R. Soc. Lond. B. Biol. Sci. 308, 21–35.

76. Judaš, M., Sedmak, G., and Kostović, I. (2013). The significance of the subplate for evolution and developmental plasticity of the human brain. Front. Hum. Neurosci. 7, 423. doi:10.3389/fnhum.2013.00423.

77. Judaš, M., Sedmak, G., Pletikos, M., and Jovanov-Milošević, N. (2010). Populations of subplate and interstitial neurons in fetal and adult human telencephalon. J. Anat. 217, 381-399. doi:10.1111/j.1469-7580.2010.01284.x.

78. Kawaguchi, Y., and Kubota, Y. (1997). GABAergic cell subtypes and their synaptic connections in rat frontal cortex. Cereb. Cortex 7, 476–486.

79. Kuchukhidze, G., Wieselthaler-Hölzl, A., Drexel, M., Unterberger, I., Luef, G., Ortler, M., et al. (2015). Calcium-binding proteins in focal cortical dysplasia. Epilepsia 56, 1207–1216. doi:10.1111/epi.13053.

80. Lefebvre, L. (2012). Primate encephalization. Prog Brain Res. 195, 393-412. doi:10.1016/B978-0-444-53860-4.00019-2.

81. Lewis, D. A., Hashimoto, T., and Volk, D. W. (2005). Cortical inhibitory neurons and schizophrenia. Nature 6, 312–324. doi:10.1038/nrn1648.

82. Lund, J. S., and Lewis, D. A. (1993). Local circuit neurons of developing and mature macaque prefrontal cortex: Golgi and immunocytochemical characteristics. J. Comp. Neurol. 328, 282–312. doi:10.1002/cne.903280209.

83. Luscher, B., Shen, Q., and Sahir, N. (2010). The GABAergic deficit hypothesis of major depressive disorder. Mol. Psychiatry 16, 383–406. doi:10.1038/mp.2010.120.

84. Ma, T., Wang, C., Wang, L., Zhou, X., Tian, M., Zhang, Q., et al. (2013). Subcortical origins of human and monkey neocortical interneurons. Nat. Neurosci. 16, 1–12. doi:10.1038/nn.3536.

85. Mai, J. K., Paxinos, G., and Voss, T. (2008). Atlas of the human brain. London; Burlington, NJ; San Diego: Academic Press.

86. Marín, O. (2012). Interneuron dysfunction in psychiatric disorders. Nat. Rev. Neurosci. 13, 107–120. doi:10.1038/nrn3155.

87. Marklund, P., Fransson, P., Cabeza, R., Petersson, K. M., Ingvar, M., and Nyberg, L. (2007). Sustained and transient neural modulations in prefrontal cortex related to declarative long-term memory, working memory, and attention. Cortex. 43, 22–37.

88. Markram, H., Toledo-Rodriguez, M., Wang, Y., Gupta, A., Silberberg, G., and Wu, C. (2004). Interneurons of the neocortical inhibitory system. Nat. Rev. Neurosci. 5, 793–807. doi:10.1038/nrn1519.

89. Melchitzky, D. S., Eggan, S. M., and Lewis, D. A. (2005). Synaptic targets of calretinin-containing axon terminals in macaque monkey prefrontal cortex. Neuroscience 130, 185–195. doi:10.1016/j.neuroscience.2004.08.046.

90. Mohan, H., Verhoog, M. B., Doreswamy, K. K., Eyal, G., Aardse, R., Lodder, B. N., et al. (2015). Dendritic and Axonal Architecture of Individual Pyramidal Neurons across Layers of Adult Human Neocortex. Cereb. Cortex 25, 4839–4853. doi:10.1093/cercor/bhv188.

91. Molyneaux, B. J., Arlotta, P., Menezes, J. R. L., and Macklis, J. D. (2007). Neuronal subtype specification in the cerebral cortex. Nat. Rev. Neurosci. 8, 427–437. doi:10.1038/nrn2151.

92. Mountcastle, V. B. (1997). The columnar organization of the neocortex. Brain 120, 701–722.

93. Öngür, D., Ferry, A. T., and Price, J. L. (2003). Architectonic subdivision of the human orbital and medial prefrontal cortex. J. Comp. Neurol. 460, 425–449. doi:10.1002/cne.10609.

94. Opris, I., and Casanova, M. F. (2014). Prefrontal cortical minicolumn : from executive control to disrupted cognitive processing. doi:10.1093/brain/awt359.

95. Passingham, R. E., and Smaers, J. B. (2014). Is the Prefrontal Cortex Especially Enlarged in the Human Brain? Allometric Relations and Remapping Factors. Brain. Behav. Evol. 84, 156–166. doi:10.1159/000365183.

96. Paxinos, G., Huang, X. F., and Toga, A. W. (2000). The rhesus monkey brain in stereotaxic coordinates. London; Burlington, NJ; San Diego: Academic Press.

97. Petilla Interneuron Nomenclature Group, Ascoli, G. A., Alonso-Nanclares, L., Anderson, S. A., Barrionuevo, G., Benavides-Piccione, R., et al. (2008). Petilla terminology: nomenclature of features of GABAergic interneurons of the cerebral cortex. Nat. Rev. Neurosci. 9, 557–568. doi:10.1038/nrn2402.

98. Petrides, M., and Pandya, D. N. (1999). Dorsolateral prefrontal cortex: comparative cytoarchitectonic analysis in the human and the macaque brain and corticocortical connection patterns. Eur. J. Neurosci. 11, 1011–1036.

99. Petrides, M., Tomaiuolo, F., Yeterian, E. H., and Pandya, D. N. (2011). Special issue : Review The prefrontal cortex : Comparative architectonic organization in the human and the macaque monkey brains. Cortex 48, 46–57. doi:10.1016/j.cortex.2011.07.002.

100. Pugliese, M., Carrasco, J. L., Geloso, M. C., Mascort, J., Michetti, F., and Mahy, N. (2004). Gamma-aminobutyric acidergic interneuron vulnerability to aging in canine prefrontal cortex. J. Neurosci. Res. 77, 913–920. doi:10.1002/jnr.20223.

101. Raghanti, M. A., Spocter, M. A., Butti, C., Hof, P. R., and Sherwood, C. C. (2010). A comparative perspective on minicolumns and inhibitory GABAergic interneurons in the neocortex. Front. Neuroanat. 4, 3. doi:10.3389/neuro.05.003.2010.

102. Raghanti, M. A., Stimpson, C. D., Sciences, B., and Kent, P. O. B. (2008). Cortical dopaminergic innervation among humans, chimpanzees and macaque monkeys: A comparative study. Neuroscience 155, 203–220. doi:10.1016/j.neuroscience.2008.05.008.

103. Rajkowska, G., and Goldman-Rakic, P. S. (1995a). Cytoarchitectonic Definition of Prefrontal Areas in the Normal Human Cortex: II. Variability in Locations of Areas 9 and 46 and Relationship to the Talairach Coordinate System. Cereb. Cortex 5, 323–337.

104. Rajkowska, G., and Goldman-Rakic, P. S. (1995b). Rajkowska & Goldman-Rakic 1995 Cytoarchitectonic definition of prefrontal areas in the normal human cortex I. Remapping of aread 9 and 46 using quantitative criteria. Cereb. Cortex 5, 307–322.

105. Rajkowska, G., O'Dwyer, G., Teleki, Z., Stockmeier, C. A., and Miguel-Hidalgo, J. J. (2007). GABAergic Neurons Immunoreactive for Calcium Binding Proteins are Reduced in the Prefrontal Cortex in Major Depression. Neuropsychopharmacology 32, 471–482. doi:10.1038/sj.npp.1301234.

106. Rakic, P. (2009). Evolution of the neocortex: a perspective from developmental biology. Nat. Rev. Neurosci. 10, 724–735. doi:10.1038/nrn2719.

107. Reep, R. L. (2000). Cortical Layer VII and Persistent Subplate Cells in Mammalian Brains. Brain. Behav. Evol. 56, 212–234. doi:10.1159/000047206.

108. Rilling, J. K. (2006). Human and nonhuman primate brains: Are they allometrically scaled versions of the same design? Evol. Anthropol. Issues, News, Rev. 15, 65–77. doi:10.1002/evan.20095.

109. Rocco, B. R., Sweet, R. A., Lewis, D. A., and Fish, K. N. (2016). GABA-Synthesizing Enzymes in Calbindin and Calretinin Neurons in Monkey Prefrontal Cortex. Cereb. Cortex 26, 2191–2204. doi:10.1093/cercor/bhv051.

110. Rockel, A. J., Hiorns, R. W., and Powell, T. P. (1980). The basic uniformity in structure of the neocortex. Brain 103, 221–244.

111. Rogers, J., Khan, M., and Ellis, J. (1990). Calretinin and other CaBPs in the nervous system. Adv. Exp. Med. Biol. 269, 195–203.

112. Roth, G., and Dicke, U. (2012). Evolution of the brain and intelligence in primates. 1st ed. Elsevier B.V. doi:10.1016/B978-0-444-53860-4.00020-9.

113. Rudy, B., Fishell, G., Lee, S., and Hjerling-Leffler, J. (2011). Three groups of interneurons account for nearly 100% of neocortical GABAergic neurons. Dev. Neurobiol. 71, 45–61. doi:10.1002/dneu.20853.

114. Sarnat, H. B., Nochlin, D., and Born, D. E. (1998). Neuronal nuclear antigen (NeuN): a marker of neuronal maturation in early human fetal nervous system. Brain Dev. 20, 88–94.

115. Schenker, N. M., Hopkins, W. D., Spocter, M. A., Garrison, A. R., Stimpson, C. D., Erwin, J. M., et al. (2010). Broca's Area Homologue in Chimpanzees (Pan troglodytes): Probabilistic Mapping, Asymmetry, and Comparison to Humans. Cereb. Cortex 20, 730–742. doi:10.1093/cercor/bhp138.

116. Schoenemann, P. T. (2006). Evolution of the Size and Functional Areas of the Human Brain. Annu. Rev. Anthropol. 35, 379–406. doi:10.1146/annurev.anthro.35.081705.123210.

117. Semendeferi, K., Lu, A., Schenker, N., and Damasio, H. (2002). Humans and great apes share a large frontal cortex. Nat. Neurosci. 5, 272–276. doi:10.1038/nn814.

118. Shepherd, G. M. (2004). The synaptic organization of the brain. New York, NY: Oxford University Press.

119. Sherwood, C. C. (2005). Comparative anatomy of the facial motor nucleus in mammals, with an analysis of neuron numbers in primates. Anat. Rec. Part A Discov. Mol. Cell. Evol. Biol. 287A, 1067–1079. doi:10.1002/ar.a.20259.

120. Sherwood, C. C., Bauernfeind, A. L., Bianchi, S., Raghanti, M. A., and Hof, P. R. (2012). Human brain evolution writ large and small. Prog Brain Res. 195, 237-254. doi:10.1016/B978-0-444-53860-4.00011-8.

121. Sherwood, C. C., Raghanti, M. A., Stimpson, C. D., Spocter, M. A., Uddin, M., Boddy, A. M., et al. (2010). Inhibitory interneurons of the human prefrontal cortex display conserved evolution of the phenotype and related genes. Proc. R. Soc. B Biol. Sci. 277, 1011–1020. doi:10.1098/rspb.2009.1831.

122. Smaers, J. B., Steele, J., Case, C. R., Cowper, A., Amunts, K., and Zilles, K. (2011). Primate Prefrontal Cortex Evolution: Human Brains Are the Extreme of a Lateralized Ape Trend. Brain. Behav. Evol. 77, 67–78. doi:10.1159/000323671.

123. Somogyi, P., Tamás, G., Lujan, R., and Buhl, E. H. (1998). Salient features of synaptic organisation in the cerebral cortex. Brain Res. Brain Res. Rev. 26, 113–35.

124. Sousa, A. M. M., Zhu, Y., Raghanti, M. A., Kitchen, R. R., Onorati, M., Tebbenkamp, A. T. N., et al. (2017). Molecular and cellular reorganization of neural circuits in the human lineage. Science 358, 1027-1032 doi:10.1126/science.aan3456.

125. Soussi, T. (2010). The history of p53. EMBO Rep. 11, 822–826. doi:10.1038/embor.2010.159.

126. Striedter, G. F. (2005). Principles of brain evolution. New York, NY: Oxford University Press.

127. Takano, T. (2015). Interneuron Dysfunction in Syndromic Autism: Recent Advances. Dev. Neurosci. 37, 467–475. doi:10.1159/000434638.

128. Talairach, J., and Szikla, G. (1980). Application of stereotactic concepts to the surgery of epilepsy. Acta Neurochir. Suppl. (Wien). 30, 35–54.

129. Teffer, K., and Semendeferi, K. (2012). Human prefrontal cortex. Evolution, development, and pathology. Prog. Brain Res. 195, 191–218. doi:10.1016/B978-0-444-53860-4.00009-X.

130. Tkachenko, L. A., Zykin, P. A., Nasyrov, R. A., and Krasnoshchekova, E. I. (2016). Distinctive Features of the Human Marginal Zone and Cajal–Retzius Cells: Comparison of Morphological and Immunocytochemical Features at Midgestation. Front. Neuroanat. 10, 1–12. doi:10.3389/fnana.2016.00026.

131. Toledo-Rodriguez, M., Blumenfeld, B., Wu, C., Luo, J., Attali, B., Goodman, P., et al. (2004). Correlation Maps Allow Neuronal Electrical Properties to be Predicted from Single-cell Gene Expression Profiles in Rat Neocortex. Cereb. Cortex 14, 1310–1327. doi:10.1093/cercor/bhh092.

132. Tremblay, R., Lee, S., and Rudy, B. (2016). GABAergic Interneurons in the Neocortex: From Cellular Properties to Circuits. Neuron 91, 260–92. doi:10.1016/j.neuron.2016.06.033.

133. Trevelyan, A. J., and Watkinson, O. (2005). Does inhibition balance excitation in neocortex? Prog. Biophys. Mol. Biol. 87, 109–143. doi:10.1016/j.pbiomolbio.2004.06.008.

134. Triarhou, L. C. (2007). A proposed number system for the 107 cortical areas of Economo and Koskinas, and Brodmann area correlations. Stereotact. Funct. Neurosurg. 85, 204–215. doi:10.1159/000103259.

135. Uematsu, M., Hirai, Y., Karube, F., Ebihara, S., Kato, M., Abe, K., et al. (2008). Quantitative chemical composition of cortical GABAergic neurons revealed in transgenic venus-expressing rats. Cereb. Cortex 18, 315–330. doi:10.1093/cercor/bhm056.

136. Uylings, H. B. M., Groenewegen, H. J., and Kolb, B. (2003). Do rats have a prefrontal cortex? Behav. Brain Res. 146, 3–17. doi:10.1016/J.BBR.2003.09.028.

137. Uylings, H. B., and van Eden, C. G. (1990). Qualitative and quantitative comparison of the prefrontal cortex in rat and in primates, including humans. Prog. Brain Res. 85, 31–62.

138. Vogt, B. A., Hof, P. R., Zilles, K., Vogt, L. J., Herold, C., and Palomero-Gallagher, N. (2013). Cingulate area 32 homologies in mouse, rat, macaque and human: Cytoarchitecture and receptor architecture. J. Comp. Neurol. 521, 4189–4204. doi:10.1002/cne.23409.

139. Vogt, B. A., Nimchinsky, E. A., Vogt, L. J., and Hof, P. R. (1995). Human Cingulate Cortex : Surface Features , Flat Maps and Cytoarchitecture 506, 490–506.

140. Vogt, B. A., Pandya, D. N., and Rosene, D. L. (1987). Cingulate Cortex of the Rhesus Monkey: I . Cytoarchitecture and Thalamic Afferents. J Comp Neurol. 262, 256-270.

141. Wang, F., Flanagan, J., Su, N., Wang, L.-C., Bui, S., Nielson, A., et al. (2012). RNAscope. J. Mol. Diagnostics 14, 22–29. doi:10.1016/j.jmoldx.2011.08.002.

142. Wang, X., Gallegos, D. A., Pogorelov, V. M., O'Hare, J. K., Calakos, N., Wetsel, W. C., et al. (2018). Parvalbumin Interneurons of the Mouse Nucleus Accumbens are Required For Amphetamine-Induced Locomotor Sensitization and Conditioned Place Preference. Neuropsychopharmacology 43, 953–963. doi:10.1038/npp.2017.178.

143. West, M. J., Slomianka, L., and Gundersen, H. J. G. (1991). Unbiased stereological estimation of the total number of neurons in the subdivisions of the rat hippocampus using the optical fractionator. Anat. Rec. 231, 482–497. doi:10.1002/ar.1092310411.

144. Woo, T. U., Whitehead, R. E., Melchitzky, D. S., and Lewis, D. A. (1998). A subclass of prefrontal gamma-aminobutyric acid axon terminals are selectively altered in schizophrenia. Proc. Natl. Acad. Sci. USA 95, 5341–5346.

145. Yáñez, I. B., Muñoz, A., Contreras, J., Gonzalez, J., Rodriguez-Veiga, E., and DeFelipe, J. (2005). Double bouquet cell in the human cerebral cortex and a comparison with other mammals. J. Comp. Neurol. 486, 344–360. doi:10.1002/cne.20533.

146. Zaitsev, A. V., Gonzalez-Burgos, G., Povysheva, N. V., Kröner, S., Lewis, D. A., and Krimer, L. S. (2005). Localization of calcium-binding proteins in physiologically and morphologically characterized interneurons of monkey dorsolateral prefrontal cortex. Cereb. Cortex 15, 1178–1186. doi:10.1093/cercor/bhh218.

## 11. Curriculum vitae

Dora (Mandić) Sedmak was born on 6th July 1989 in Zagreb. She graduated in 2014 at University of Zagreb School of Medicine. After internship in Clinical hospital Merkur she worked as a general practitioner in Zagreb. In 2015 she started working at Department of Anatomy and Clinical anatomy, University of Zagreb School of Medicine as a research and teaching assistant. She teaches anatomy at School of Medicine, Dentistry and Faculty of food technology and biotechnology. Her scientific work started during her graduate studies at Croatian Institute for Brain Research where she was involved in MRI post processing studies on the development of the human brain during perinatal period. She started her PhD studies in 2014 at SCM and as a part of Croatian Science Foundation project led by Professor Petanjek. Her PhD Thesis Calretinin neurons in the primate prefrontal cortex was accepted in 2016 with Zdravko Petanjek, MD, PhD and Monique Esclapez, PhD as her mentors. As a part of her scientific training she was at INSERM UMR 1106, Institute de Neurosciences des Systèmes, Aix-Marseille University, Marseille France (Laboratory for GABAergic networks); and Department of Neuroscience Yale University School of Medicine, Kavli Institute for Neuroscience, New Haven USA (Sestan Lab).

She was awarded French government scholarship for training at INSERM in 2015 and a FENS travel grant in 2017. As student she was chair of Student Society for Neuroscience and a founder and editor in chief of their journal for which she was awarded with Rectors award.

She is a member of Croatian medical chamber, Croatian Society for Neuroscience and Society for anatomy, embryology and histology. She is fluent in English and German and basics of Croatian sign language. She published 4 papers in *Current Content*, 8 abstracts at international meetings and one chapter in textbook.